Summary Report of Mission Acceleration Measurements for STS-87

Launched November 19, 1997

November 23, 1998

Melissa J. B. Rogers
National Center for
Microgravity Research
Cleveland, Ohio

Kenneth Hrovat
Tal-Cut Company
North Olmsted, Ohio

Kevin McPherson
NASA Lewis Research Center
Cleveland, Ohio

Timothy Reckart
Tal-Cut Company
North Olmsted, Ohio

Richard DeLombard
NASA Lewis Research Center
Cleveland, Ohio

Abstract

Two accelerometer systems, the Orbital Acceleration Research Experiment and the Space Acceleration Measurement System, were used to measure and record the microgravity environment of the Orbiter Columbia during the STS-87 mission in November-December 1997. Data from two separate Space Acceleration Measurement System units were telemetered to the ground during the mission and data plots were displayed for investigators of the Fourth United States Microgravity Payload experiments in near real-time using the World Wide Web. Plots generated using Orbital Acceleration Research Experiment data (telemetered to the ground using a tape delay) were provided to the investigators using the World Wide Web approximately twelve hours after data recording.

Disturbances in the microgravity environment as recorded by these instruments are grouped by source type: Orbiter systems, on-board activities, payload operations, and unknown sources. The environment related to the Ku-band antenna dither, Orbiter structural modes, attitude deadband collapses, water dump operations, crew sleep, and crew exercise was comparable to the effects of these sources on previous Orbiter missions. Disturbances related to operations of the Isothermal Dendritic Growth Experiment and Space Acceleration Measurement Systems that were not observed on previous missions are detailed. The effects of Orbiter cabin and airlock depressurization and extravehicular activities are also reported for the first time. A set of data plots representing the entire mission is included in the CD-ROM version of this report.

Acronyms and Abbreviations

AADSF	Advanced Automated Directional Solidification Furnace
AZ	azimuth
CHeX	Confined Helium Experiment
CUE	Collaborative Ukranian Experiments
DAP	Digital Auto Pilot
EDFT	Extravehicular Activity Demonstration Flight Test
EL	elevation
ELF	Enclosed Laminar Flames
EVA	extravehicular activity
g_{RMS}	root-mean-square acceleration
IDGE	Isothermal Dendritic Growth Experiment
LHP/NaSBE	Looped Heat Pipe and Sodium Sulphur Battery Experiment
MAWS	Microgravity Analysis Workstation
MEPHISTO	Materials for the Study of Interesting Phenomena of Solidification on Earth and in Orbit
MET	Mission Elapsed Time
MEWS	Mission Evaluation Workstation System
MPESS	Mission Peculiar Experiment Support Structure
MSID	Measurement Stimulus Identifier
OARE	Orbital Acceleration Research Experiment
PAO	Public Affairs Office
PCIS	Passive Cycle Isolation System
PEP	Particle Engulfment and Pushing by a Solid/Liquid Interface
PIMS	Principal Investigator Microgravity Services
PRCS	Primary Reaction Control System
PSD	power spectral density
QTH	Quasi-Steady Three-Dimensional Histogram
RMS	root-mean-square
RSS	root-sum-of-squares
SAMS	Space Acceleration Measurement System
SIMPLEX	Shuttle Ionospheric Modification with Pulsed Local Exhaust
SOLSE	Shuttle Ozone Limb Sounding Experiment
TGDF	Turbulent Gas-Jet Diffusion Flames
TSH	Triaxial Sensor Head
USMP-4	Fourth United States Microgravity Payload
VM	vector magnitude
VRCS	Vernier Reaction Control System
WCI	Wetting Characteristics of Immiscibles
WWW	World Wide Web
X_b, Y_b, Z_b	Orbiter body coordinate system axes
X_O, Y_O, Z_O	Orbiter structural coordinate system axes

Table of Contents

List of Figures

List of Tables

Acknowledgements

The authors would like to thank several persons for providing information and support that added significantly to this report. Brian Matisak, currently with CST, Inc., Huntsville, Alabama, was the Lead Payload Activities Coordinator for the USMP-4 payload, and provided the as-flown scenario chart and a wealth of information used during data interpretation. The rest of the PAC team, Teri Mears and Wayne Wright, were helpful in tracking down activity times during the mission. Diane Malarik and Richard Abramczyk of the IDGE experiment team provided information about the experiment fans. Various aspects of the quasi-steady environment of Columbia were discussed with Larry French and the rest of the Microgravity Analysis Workstation team during the mission. The Marshall Space Flight Center data reduction team worked closely with the PIMS team to provide data in the format requested.

After the mission, Johnson Space Center personnel provided information needed for the interpretation of SAMS and OARE data from STS-87. Richard LaBrode, an Instrumentation and Communication Officer with United Space Alliance during the mission and Martin O'Hare, Ku-Band Subsystem Engineer with Boeing North American, provided information about the operations of the Ku-band antenna. Carmelo Asuncion, Orbiter ECLSS Engineer with Boeing North American, and Brenda Eliason, Rockwell International, answered questions about cabin depressurization for extravehicular activities.

1. Introduction

The STS-87 mission launched on the Space Shuttle Orbiter Columbia at 1997/323/19:46:00 Greenwich Mean Time, which corresponds to Eastern Standard Time 14:46 on 19 November 1997. Wheel stop upon landing was at 1997/339/12:21:02 Greenwich Mean Time. In addition to Greenwich Mean Time, the timing convention typically used on Orbiter missions is Mission Elapsed Time (MET). This timing system provides a measure of time elapsed since launch in days/hours:minutes:seconds. For STS-87, wheel stop occurred at MET 015/16:35:02. The payloads manifested on this mission include the microgravity experiments of the Fourth United States Microgravity Payload (USMP-4): three materials science experiments growing semiconductor crystals in the Advanced Automated Directional Solidification Furnace (AADSF); a fundamental physics investigation called the Confined Helium Experiment (CHeX); a study geared towards an improved understanding of the growth of metals, the Isothermal Dendritic Growth Experiment (IDGE); a semiconductor crystal growth experiment in the French furnace MEPHISTO; combustion science studies of Enclosed Laminar Flames (ELF); materials science investigations into Particle Engulfment and Pushing by a Solid/Liquid Interface (PEP) and the Wetting Characteristics of Immiscibles (WCI); and two accelerometer systems, the Orbital Acceleration Research Experiment (OARE) and the Space Acceleration Measurement System (SAMS).

One common characteristic of these experiments is that various effects of gravity make it difficult, if not impossible, to achieve usable results when performing the experiments on Earth's surface. Therefore, the investigators have taken advantage of the microgravity environment afforded by being in low-Earth orbit to perform their research. Interpretation of the experiment results both during the mission and upon post-mission analyses of data and samples requires an understanding of the microgravity environment in which the experiments were conducted.

This report provides the experiment teams with a post-mission interpretation of the accelerometer data collected during the mission. The data files, processed into engineering units, are available on the Internet; see Appendix A for data access instructions. It is such accelerometer data, combined with an assessment of mission and experiment activities, that permits a characterization of the microgravity environment that existed on Columbia during the mission. The text herein gives details about some characteristics of the environment that were noted during the mission and during post-mission data analysis. For example, the disturbances studied include the Ku-band antenna 17 Hz dither; the effect of changing the Orbiter attitude deadband limits; the effects of different bicycle ergometer configurations; the environment related to different Orbiter attitudes; and the effect of IDGE experiment fans and SAMS computer hard drives. The enclosed CD-ROM contains the text of this report, plots of accelerometer data collected during STS-87, and previous reports discussing the environment experienced by the second and third USMP payloads [1,2]. The data plots give an overview of the environment during the majority of the mission. The plots, which are included on the CD-ROM as Appendices B, C, D, E, and supplementary spectrograms plotted out to the Nyquist frequencies for all SAMS sensor heads collecting data during the mission, are also useful for identifying times when specific disturbances were apparent.

2. Mission Configuration

In addition to USMP-4, several other payloads were included on the STS-87 flight, see Table 1. The Extravehicular Activity Demonstration Flight Test (EDFT) and the Spartan satellite deploy and retrieval were of particular interest to the USMP-4 investigators because there was a possibility that these activities would impact the timeline assigned to USMP-4, thus also impacting the microgravity environment. The AADSF, CHeX, IDGE, MEPHISTO, and SAMS USMP-4 experiments were located in the payload bay of Columbia on two Mission Peculiar Experiment Support Structures (MPESS). The Spartan satellite and the equipment for the EDFT were also located in the payload bay, as were several experiments on a Hitchhiker platform. Figure 1 is a schematic of the payload bay which gives an indication of the approximate locations of the USMP-4 experiments. The OARE was attached to the keel bridge of Columbia, underneath the other USMP-4 experiments, see Figure 2. Within the middeck, the crew performed the USMP-4 investigations ELF, PEP, and WCI in the Middeck Glovebox Facility. The plant growth investigations of the Collaborative Ukrainian Experiment were also conducted within the middeck. The crew exercised on a bicycle ergometer located in the flight deck, attached to the floor so that the long axis of the bicycle was aligned with the Orbiter X_O-axis. The STS-87 crew members are listed in Table 2.

Table 1. STS-87 Payloads

Payloads	Location
Fourth United States Microgravity Payload (USMP-4)	Payload Bay
Extravehicular Activity Demonstration Flight Test (EDFT-05)	Payload Bay
Spartan 201-04	Payload Bay
Middeck Glovebox	Middeck
Looped Heat Pipe and Sodium Sulphur Battery Experiment (LHP/NaSBE)	Hitchhiker-Payload Bay
Turbulent Gas-Jet Diffusion Flames (TGDF)	Gas Canister-Payload Bay
Shuttle Ozone Limb Sounding Experiment (SOLSE)	Payload Bay
GAS G-036	Payload Bay
Collaborative Ukranian Experiments (CUE)	Middeck
AERCam/Sprint	Freeflyer
Shuttle Ionospheric Modification with Pulsed Local Exhaust (SIMPLEX)	Middeck

Table 2. STS-87 Crew

Crewmember	Position
Kevin R. Kregel	Commander
Steven W. Lindsey	Pilot
Kalpana Chawla	Mission Specialist 1
Winston E. Scott	Mission Specialist 2
Takao Doi	Mission Specialist 3
Leonid K. Kadenyuk	Payload Specialist 1

Several of the payload bay USMP-4 experiments were started at the beginning of the mission. The remaining experiments were initiated when the primary microgravity time started at approximately MET 005/12:00. During the designated microgravity period, the crew and Orbiter control teams attempted to maintain a quiet microgravity environment. Prior to that time, the Spartan satellite deploy and retrieval and EDFT activities occurred. The Spartan satellite was deployed using the Orbiter Remote Manipulator System, with initial grapple of the satellite at MET 001/23:46. A deploy situation resulting in an uncontrolled tumbling of the satellite resulted in replanning of the mission timeline. The satellite was captured and returned to the payload bay by two crew members during an extravehicular activity (EVA) at about MET 005/07:40. A portion of the EDFT was run following the satellite stow until about MET 005/11. IDGE, Middeck Glovebox microgravity investigations, CUE operations, and Hitchhiker experiments were performed throughout the mission. A redeployment of the Spartan and additional EDFT activities occurred late in the mission. Times for several activities that were of interest to the microgravity scientists are listed in Table 3. Appendix F, available on the report CD-ROM, is a copy of the logbook kept by the Principal Investigator Microgravity Services (PIMS) team during the mission. Numerous events of interest are indicated there. Figure 3 gives an overview of the timing of major mission events.

3. Acceleration Measurement Program Support of USMP-4

The Microgravity Research Program's Acceleration Measurement Program is based at the NASA Lewis Research Center. This program provides microgravity investigators with accelerometer systems, acceleration data analysis, and carrier microgravity environment characterization.

3.1 Accelerometer Systems on USMP-4

Two types of accelerometer systems were included in the USMP-4 contingent to provide the experiments with a characterization of the microgravity environment of Columbia during the STS-87 mission. Two SAMS units were located on the MPESS. These units recorded and downlinked in near real-time acceleration data in the 0.01 Hz to 100 Hz range in support of the AADSF, MEPHISTO, CHeX, and IDGE experiments. This frequency range is mostly affected by vibrations

due to the operation of Orbiter and experiment apparatus and by crew activity. More information about the SAMS is available in the literature [1-7] and details about the specific configuration of the two SAMS units on STS-87 are provided in Table 4. SAMS Unit G, Triaxial Sensor Head (TSH) C was activated during the mission, but set to a scientifically insignificant data sampling rate because of data downlink restrictions. The SAMS data are reported here in terms of the Orbiter structural coordinate system and the reference frame used is such that a forward thrust of the Orbiter is recorded as a negative X_0 acceleration.

Table 3. Activities of Interest to Microgravity Scientists

EVENT	MSID	MET	GMT
PAYLOAD BAY DOOR OPEN	V37X3300Y V37X3305Y	000/01:29:42 000/01:31:02	323:21:15:42 323:21:17:02
SPARTAN GRAPPLE	V54X2027J	001/23:46:13	325:19:32:13
SPARTAN UNBERTH	V54X8131E	002/00:19:45	325:20:05:45
SPARTAN RELEASE	V54X2027J	002/01:18:37	325:21:04:37
SPARTAN RE-GRAPPLE	V54X2034J	002/01:24:37	325:21:10:37
STARBOARD RADIATOR DEPLOY	V37X3510E	003/09:51:42	327:05:37:42
CABIN DEPRESSURIZATION (END)	V64P2405A	004/09:34:42	328:05:20:42
STARBOARD RADIATOR STOW	V37X3548E	005/00:54:28	328:20:40:28
ORBITAL MANEUVERING SYSTEM 3 IGNITION	V43H4655C V43H5655C	N/A 005/01:33:33	N/A 328:21:19:33
ORBITAL MANEUVERING SYSTEM 3 CUTOFF	V43H4655C V43H5655C	N/A 005/01:33:48	N/A 328:21:19:48
ORBITAL MANEUVERING SYSTEM IGNITION	V43H4655C V43H5655C	005/03:04:38 N/A	328:22:50:38 N/A
ORBITAL MANEUVERING SYSTEM CUTOFF	V43H4655C V43H5655C	005/03:04:50 N/A	328:22:50:50 N/A
AIRLOCK DEPRESSURIZATION (END)	V64P0101A	005/03:56:25	328:23:42:25
CABIN REPRESSURIZATION (START)	V64P2405A	005/04:15:54	329:00:01:54
SPARTAN GRAPPLE	V54X2027J	005/06:52:50	329:02:38:50
SPARTAN BERTH	V54X8135E	005/07:37:09	329:03:23:09
SPARTAN LATCH	V54X8144E	005/07:37:09	329:03:23:09
SPARTAN UNGRAPPLE	V54X2027J	005/07:40:24	329:03:26:24
AIRLOCK REPRESSURIZATION (START)	V64PO101A	005/11:59:40	329:07:45:40
PORTSIDE RADIATOR DEPLOY	V37X3501E	007/03:43:57	330:23:29:57
PORTSIDE RADIATOR STOW	V37X3505E	010/07:48:56	334:03:34:56
STARBOARD RADIATOR DEPLOY	V37X3511E	010/20:38:42	334:16:24:42
PORTSIDE RADIATOR DEPLOY	V37X3500E	012/14:35:06	336:10:21:06
CABIN DEPRESSURIZATION (END)	V61P2405A	012/19:31:30	336:15:17:30
STARBOARD RADIATOR STOW	V37X3563E	012/19:44:18	336:15:30:18
PORTSIDE RADIATOR STOW	V37X3543E	012/19:44:55	336:15:30:55
SPARTAN GRAPPLE	V54X2027J	013/08:56:53	337:04:42:53
SPARTAN UNBERTH	V54X8131E	013/09:10:19	337:04:56:19
SPARTAN BERTH	V54X8136E	013/13:25:27	337:09:11:27
SPARTAN LATCH	V54X8144E	013/13:26:02	337:09:12:02
SPARTAN UNGRAPPLE	V54X2027J	013/13:28:54	337:09:14:54
CABIN REPRESSURIZATION (START)	V64P2405A	013/13:24:49	337:09:10:49
AIRLOCK DEPRESSURIZATION (END)	V64P0101A	013/13:25:05	337:09:11:05
AIRLOCK REPRESSURIZATION (START)	V64P0101A	013/18:22:24	337:14:08:24
FLIGHT CONTROL SYSTEM CHECKOUT -AUXILIARY POWER UNIT START	V46P0320A	014/14:05:24	338:09:51:24
AUXILIARY POWER UNIT STOP	V46P0320A	014/14:17:21	338:10:03:21
PAYLOAD BAY DOOR CLOSE	V37X3307Y V37X3302Y	015/12:53:10 015/12:56:16	339:08:39:10 339:08:42:16
AUXILIARY POWER UNIT ACTIVATION	V46P0220A V46P0120A V46P0320A	015/15:30:35 015/15:49:26 015/15:49:33	339:11:16:35 339:11:35:26 339:11:35:33
DEORBIT BURN	V43H4655C V43H5655C	015/15:35:28 015/15:35:28	339:11:21:28 339:11:21:28
DEORBIT BURN CUTOFF	V43H4655C V43H5655C	015/15:38:00 015/15:38:00	339:11:24:00 339:11:24:00

Table 4. STS-87 SAMS Sensor Head Orientations and Locations

Unit F TSH A		Sample Rate: 50 samples/second
Serial no.: 047-1		
Location: Forward MPESS carrier (near AADSF)		Frequency: 10 Hz
ORIENTATION		**LOCATION**
Orbiter Structural Axis	**Sensor Axis**	**Structural Axis**
X_O	$-Y_H$	X_O = 987.69 in
Y_O	$+Z_H$	Y_O = 3.94 in
Z_O	$-X_H$	Z_O = 416.76 in

Unit F TSH B		Sample Rate: 125 samples/second
Serial no.: 047-3		
Location: Forward MPESS carrier (near MEPHISTO)		Frequency: 25 Hz
ORIENTATION		**LOCATION**
Orbiter Structural Axis	**Sensor Axis**	**Structural Axis**
X_O	$-Y_H$	X_O = 987.69 in
Y_O	$+Z_H$	Y_O = -4.31 in
Z_O	$-X_H$	Z_O = 416.76 in

Unit G TSH A		Sample Rate: 50 samples/second
Serial no.: 821-46		
Location: Rear MPESS carrier (inside IDGE)		Frequency: 5 Hz
ORIENTATION		**LOCATION**
Orbiter Structural Axis	**Sensor Axis**	**Structural Axis**
X_O	$+Z_H$	X_O = 1083.77 in
Y_O	$-.7071X_H + .7071Y_H$	Y_O = -37.08 in
Z_O	$-.7071X_H - .7071Y_H$	Z_O = 442.82 in

Unit G TSH B		Sample Rate: 250 samples/second
Serial no.: 821-45		
Location: Rear carrier (inside CHeX)		Frequency: 100 Hz
ORIENTATION		**LOCATION**
Orbiter Structural Axis	**Sensor Axis**	**Structural Axis**
X_O	$+.5446X_H + .8387Z_H$	X_O = 1069.52 in
Y_O	$+Y_H$	Y_O = 29.52 in
Z_O	$-.8387X_H + .5446Z_H$	Z_O = 442.51 in

During post-mission analyses for MEPHISTO in which long series of SAMS Unit F, TSH A data were processed, it became evident that this TSH's acceleration data erroneously tracked the sensor temperature data. This problem is most evident in the lowest frequency regime of the data. Throughout the mission, the Orbiter was commanded to a number of different attitudes, which resulted in different temperature profiles. For those with large temperature variations (over the course of an orbit), the acceleration data manifests this problem most noticeably. For other periods of relatively small temperature swings, the problem is less obvious. The analyses performed for this report were done before this problem was noticed, but the analysis results were subsequently examined to assure that this problem was properly accounted for.

The OARE measures the quasi-steady acceleration environment of the Orbiter Columbia. The OARE was mounted to the floor of Columbia's cargo bay on a keel bridge, close to the Orbiter center of mass in the Orbiter X_0 - and Y_0 -axes. The location and orientation of the sensor with respect to the Orbiter structural coordinate system are given in Table 5. The quasi-steady microgravity environment is affected by aerodynamic drag on the Orbiter, gravity gradient effects, rotational motion of the Orbiter about its center of mass, maneuvering of the Orbiter, venting of water and air from the Orbiter, and crew activity. More information about OARE is available in references [8-11]. On STS-87, the OARE was configured such that data were recorded on-board the Orbiter and sent down to the ground periodically. The data are reported in terms of the Orbiter body coordinate system with a frame of reference fixed to the Orbiter, such that a forward thrust of the Orbiter (for example, during an Orbital Maneuvering System burn) is recorded as a negative X_b-axis acceleration because a free particle would appear to translate in the negative X_b-axis direction relative to the Orbiter.

The OARE was designed to measure quasi-steady accelerations from below $1x10^{-8}$ g up to $2.5x10^{-3}$ g. The OARE consists of an electrostatically suspended proof mass sensor, an in-flight calibration subsystem, and a microprocessor which is used for in-flight experiment control, processing, and storage of flight data. In support of USMP-4 experiments, the sensor output acceleration signal was filtered with a Bessel filter with a cutoff frequency of 1 Hz. The output signal was digitized at 10 samples per second and was processed and digitally filtered with an adaptive trimmean filter prior to electronic storage.

Table 5. STS-87 OARE Sensor Head Orientation and Location

OARE Sensor		Sample Rate: 10 samples/second
Location: Orbiter Cargo Bay Keel Bridge		Frequency: 0 to 1 Hz
ORIENTATION		**LOCATION**
Orbiter Structural Axis	**Sensor Axis**	**Structural Axis**
X_O	$-X_{OARE}$	X_O = 1153.3 in
Y_O	Z_{OARE}	Y_O = -1.3 in
Z_O	Y_{OARE}	Z_O = 317.8 in

OARE data are available from MET 00/00:11 through sensor saturation at MET 015/14:34 during Orbiter re-entry. Appendix A describes how these data can be accessed through the Internet.

3.2 Accelerometer Data Flow During STS-87

The PIMS team is tasked to characterize the microgravity environment of spacecraft and other carriers used by NASA Microgravity Research Program investigators. Prior to flight, PIMS talked to USMP-4 project scientists and principal investigators in an effort to understand the nature of acceleration data support required for real-time, near real-time, and post-mission analysis. These inquiries resulted in identification of the accelerometer systems, the frequency characteristics of the SAMS sensor heads, the real-time plot formats, and near real-time plot formats to be used in support of the USMP-4 experiments. A combination of each of these items would allow the best correlation between acceleration events and experiment science data.

Real-time support of the science teams was accomplished exclusively using SAMS data. Throughout the mission, PIMS received real-time downlink data from both SAMS units, converted the raw SAMS telemetry frame to engineering unit data, and generated data plots in the format requested pre-mission by the USMP-4 principal investigators. Periodic updates to the plotted images were made available approximately every two minutes through the PIMS USMP-4 World Wide Web (WWW) page.

The plot types developed by PIMS for Unit G, TSH B real-time data were driven specifically by the CHeX experiment team. Throughout the entire USMP-4 segment of the mission, the CHeX team requested plots of real-time acceleration versus time, interval maximum absolute value acceleration versus time, power spectral density, color spectrograms, and g_{RMS} versus time (for three frequency bands specified by CHeX). The plot types displayed using the Unit F, TSH A real-time data were acceleration versus time and color spectrograms. PIMS selected these plots as a compromise among varied plot type requests for the Unit F, TSH A data.

The unprocessed OARE data were recorded on the Orbiter payload tape recorder and telemetered to the ground approximately 8-10 hours after the measurement. Because the OARE data on USMP-4 were not available in real-time, payload recorder dumps containing the OARE data were processed by Marshall Space Flight Center's Data Reduction group for subsequent processing by PIMS computers located at the NASA Lewis Research Center's Telescience Support Center. The results of OARE data analysis were made available to the USMP-4 teams via the PIMS WWW page approximately ten to twelve hours after the actual measurement time had transpired. The plot types developed by PIMS using OARE data were limited to trimmean filtered acceleration versus time as measured at the OARE location and mathematically mapped to the following locations within the Orbiter: Orbiter center of mass, AADSF experiment location, and IDGE experiment location. See Table 6 for the structural coordinates used for these locations.

The AADSF experiment team requested processing of an additional set of data depicting the quasi-steady acceleration environment. This data set was from the Microgravity Analysis Workstation (MAWS). The MAWS model is used to predict the quasi-steady acceleration environment at any

point in the Orbiter. The AADSF experiment team requested comparison plots of the MAWS predictions of the quasi-steady acceleration environment at the AADSF experiment location with the OARE data mapped to the AADSF experiment location. These comparison plots were generated in support of the three AADSF experiment runs.

Table 6. Structural Coordinates of Experiment Locations

OARE Mapping Location	Orbiter Structural Coordinate (inches)		
	X_o -axis	Y_o -axis	Z_o -axis
AADSF	1008.00	0.00	439.25
IDGE	1078.62	-42.04	434.32
Orbiter Center of Mass	1091.85	-0.09	373.47

3.3 Roadmap to Accelerometer Data Plots

Several different types of data displays are provided in this report. The analysis techniques used to create the plots and generate data values provided in several tables are discussed at length in [12,13]. Because some readers may not be familiar with some of the plot types and also because there are some unusual features on some of the displays, we provide here some guidance for interpreting the plots in this report.

Line plots have clearly marked axis labels, typically time or frequency on the abscissa and acceleration levels in units of g (9.8 m/s^2), μg ($1x10^{-6}$ g), g_{RMS} (root-mean-square of acceleration level), or g^2/Hz (power spectral density, PSD) on the ordinate. Spectrograms, presented in color throughout this report and in the appendices, represent a series of PSD calculations performed on successive sections of data and are arranged such that the PSD information is oriented vertically on the page with time increasing from left to right and frequency increasing from bottom to top. Each time-frequency bin is assigned a color corresponding to the base 10 logarithm of the PSD magnitude.

4. Microgravity Environment of Columbia on STS-87

In addition to the real-time accelerometer data displays that PIMS provided during the mission, the PIMS team also provided data analysis and interpretation during the mission in an “off-line” fashion. When experiment team members needed information about the STS-87 microgravity environment some time after a particular occurrence, the PIMS team used archived data to fulfill the request. During the mission, the PIMS team received close to 100 different requests. This section provides details on the effects that specific events had on the microgravity environment of Columbia. The data analysis in several examples (for instance Deadband Collapse and EVA Operations) was initiated by user requests during the mission.

4.1 Orbiter Systems

4.1.1 Ku-Band Antenna

The Ku-band antenna is located on the forward starboard sill of the Orbiter's cargo bay. On orbit, this antenna is used primarily for communications between the Orbiter and the ground via the Tracking and Data Relay Satellite System. In order to maintain line-of-sight, the Ku-band antenna must slew to compensate for motion of the Orbiter with respect to these communications satellites. The Ku-band antenna is mounted on gimbals, which allow for this tracking; however, the antenna must be dithered at 17 Hz to prevent stiction of the gimbal mechanism. Reaction torque forces at the base of this assembly introduce a strong 17 Hz oscillatory disturbance into the acceleration environment of the Orbiter, along with various contributions from its 2nd through at least its 6th harmonics. Focusing analysis on a narrow spectral region (0.2 Hz wide) centered on the dither frequency, we can track the root-mean-square (RMS) acceleration for the frequency band from 16.93 to 17.13 Hz. Figures 4 and 5 depict 56-hour periods for this type of analysis performed on SAMS Unit F, TSH B data for the USMP-3 and USMP-4 payloads, respectively. For both of these missions, SAMS Unit F, TSH B was mounted on the forward MPESS at the Orbiter structural coordinates shown in Table 7.

Table 7. SAMS Unit F, TSH B Sensor Locations for USMP-3 and USMP-4 With Respect to Orbiter Structural Coordinate System

Mission	Sensor Location (inches)		
	X_o	Y_o	Z_o
STS-75/USMP-3	1048.37	-4.37	418.13
STS-87/USMP-4	987.69	-4.31	416.76

The vertical dashed lines at the 47-hour mark in Figures 4 and 5 indicate the Ku-band antenna stowage time, which brings antenna dithering to an end. More details on the stowage operation are given later in this section. Table 8 aims to quantify the measured disparity between "dither on" and "dither off" periods. The values given represent the average RMS acceleration values for the times shown.

Table 8. Ku-Band Antenna Dither RMS Acceleration ($16.93 < f < 17.13$ Hz)

MET	Mission	Dither	RMS Acceleration (μg_{RMS})
012/00:00 - 013/00:00	STS-75/USMP-3	ON	143
014/00:00 - 014/08:00	STS-75/USMP-3	OFF	9
012/21:20 - 013/21:20	STS-87/USMP-4	ON	197
014/21:20 - 015/05:20	STS-87/USMP-4	OFF	8

While the ambient Orbiter environment for this small frequency range was measured to be under 10 μg_{RMS}, the antenna dithering added over 100 μg_{RMS} for both USMP-3 and USMP-4 missions. The Euclidean distance between the two Orbiter cargo bay positions enumerated in Table 7 is approximately 5 feet, but transmission of the dither frequency vibrations for the different structural paths to these locations is uncertain. Table 8 suggests a couple of possibilities: the USMP-3 location was less responsive to the 17 Hz disturbance than the USMP-4 location, and/or the dithering intensity was somewhat greater on the latter mission. Note that acceleration measurements recorded in the Spacelab module during STS-65/IML-2 averaged around 100 μg_{RMS} for this same 0.2 Hz wide frequency band. This would suggest, not surprisingly, that transmission of the Ku-band dither excitation is damped by the structure of the Spacelab module. Speculation that a Spacelab module structural mode exists around 17 Hz is not supported by these observations.

While the dither intensity does typically vary with time throughout most missions, there are certain times when the intensity decreases or the dither is turned off altogether. Expected off times take place during gimbal flips. When the Ku-band antenna is actively tracking a satellite and the line-of-sight causes one of its two gimbals to reach their physical limit, the system will do what is commonly called a gimbal flip. Further details on this are given in Section 5.4 of [2]. During the gimbal flip, the antenna will quickly slew (20 degrees per second) until the dish is again pointing in the correct direction on the other side of the physical stop. During fast slew operations, the 17 Hz dither is disabled. Figure 6 shows a Ku-band antenna gimbal flip. This overlay plot shows SAMS Unit F, TSH B Y_0-axis acceleration data (blue trace, left ordinate scale) and Johnson Space Center Mission Evaluation Workstation System (MEWS) data for the Ku-band antenna's alpha gimbal angle (red trace, right ordinate scale), both as a function of time. It is clear from this plot and Table 9, that when the antenna is slewing quickly (where the slope of the red trace is large), the dither disturbance is non-existent. Also, note that when the alpha gimbal angle stays relatively constant at about 0 degrees for several seconds just before the 3-minute mark in Figure 6, the dither intensity dips considerably (compare first two rows of Table 9).

Table 9. PSD Levels for Selected Times Relative to Figure 6

SAMS Unit F, TSH B	
Offset Time (minutes)	**PSD Level at 17 Hz (g^2/Hz)**
1.45 - 1.60	1.02×10^{-7}
2.82 - 3.02	2.80×10^{-8}
3.05 - 3.22	2.14×10^{-11}*
3.28 - 3.33	4.54×10^{-8}
4.20 - 4.35	1.36×10^{-7}

* ambient level, no distinct spectral peak observed on PSD

Prior to de-orbit, the Ku-band antenna must be moved into its stowed position so that the payload bay doors can be closed for re-entry. Table 10 details timing of the events for this stow procedure. The spectrogram of Figure 7 captures the antenna stow event for the USMP-4 mission. Note that this spectrogram is plotted out to the Nyquist frequency of the data, therefore the spectra are attenuated above 25 Hz, the cutoff frequency for this TSH. From this figure, we see the spectral peak at the dither frequency (the red horizontal streak at 17 Hz) cease just before the 8-minute mark. The same goes for its 2nd and 3rd harmonics, the spectral peaks at 34 and 51 Hz, respectively. These are the horizontal streaks labeled H2 and H3 in the figure. We attribute the other spectral components, that are labeled with an A, to aliasing. The three arrows near the lower left portion of this figure mark one final item of interest on this spectrogram. These are times when the antenna briefly stopped dithering for the purpose of fast slewing. This is evidenced by the large slope of the red trace on Figure 8 at these times. This plot is similar to Figure 6, except that the blue trace here (left ordinate scale) is acceleration magnitude, instead of the Y_0-axis acceleration, for SAMS Unit F, TSH B. The crew performs a cable repositioning procedure (gimbal flip) prior to stowing the antenna. This is seen around the 4-minute mark [14]. The dither stop time, as seen on this plot just before the 8-minute mark, occurred at MET 014/20:17:52. Mean acceleration magnitude for dither-on times in Figure 8 was 264 μg, compared to about 83 μg for the dither-off times. The highest acceleration magnitudes recorded in the time frame of Figure 8 were in excess of 1 milli-g, and occurred over a span of about 8 seconds just before dithering ceased. When the crew takes the "KU ANT" switch to the "STOW" position, the system moves to prescribed stow angles. Next, the system drives the locking pins, and then performs a "wiggle" test to verify that the pins are seated properly and that the antenna is in a locked position. This would account for the large accelerations observed just before the 8-minute mark of Figure 8 [15].

Table 10. Timeline for Ku-Band Antenna Stow Procedure

Time Relative to MET 014/20:10:00 (mm:ss)	Mission Event
00:00	Start of STOW event
02:36	Ku-Band in RADAR mode
02:55	Start slew to AZ = 0, EL = 0
03:15	At AZ = 0, EL = 0 (Alpha = 0, Beta = 0)
03:25	Slew up for 14 sec. (Cable positioning procedure)
03:39	Cable positioning complete
04:08	Slew to AZ = -123, EL = -27 (Alpha = 124.4, Beta = - 30.7)
04:35	At AZ = -123, EL = -27 (Alpha = 124.4, Beta = - 30.7)
07:22	Stow switch to STOW AZ = -125.1, EL = -29.6 (Alpha = 124.3, Beta = - 27.5)
07:43	Alpha and Beta gimbals are locked
07:58	Wiggle test complete - system ready for STOW
08:40	Antenna Deployed Assembly begins to move to its stowed position
09:02	Deployed Assembly is STOWED
09:20	Ku-Band system is powered OFF

4.1.2 Vehicle Structural Modes

Vehicle structural modes constitute some primary components of the Orbiter's vibratory environment in the oscillatory region of the acceleration spectrum. In the absence of substantial transient acceleration events or crew exercise, these resonant frequencies dominate the spectrum below about 10 Hz. They establish the ambient oscillatory acceleration environment in this spectral region in that they are always present with varying degrees of intensity. Crew exercise and Orbiter thruster firings tend to excite these resonances, causing heightened acceleration levels which persist for a short period of time before damping down toward some baseline.

As evidenced by the red vertical streaks in the spectrograms on Appendix pages C-12 and C-13, and as documented in the STS-87 As-Flown Attitude Timeline, Columbia's thrusters imparted numerous impulsive accelerations in an attempt to track the wayward Spartan satellite from about MET 002/01:20 to about MET 002/12:00. Like sporadic pinging of a tuning fork, these firings excited the Orbiter's natural frequencies and provided the opportunity for examining the heightened response of these vehicle structural modes. Toward that end, spectral averaging was performed on Hanning-windowed PSDs calculated with the parameters shown in Table 11 for the period from MET 002/02:30 to MET 002/07:30.

Table 11. PSD Parameters for Satellite-Tracking Period

SAMS Sensor Head			Number of Points per PSD	Number of PSDs for Spectral Average	Effective Span (Hours)
Unit	TSH	Sample Rate (samples per second)			
F	A	50	1024	660	3.75
F	B	125	4096	344	3.13
G	B	250	8192	346	3.15

Note that the last column shows the aggregate span of the spectral average. This does not total 5 hours, as suggested by the MET span, because any candidate PSD period containing a substantial impulsive transient (like would be the case for a thruster firing) was ignored. The intent here was to examine the resonant ringing after these impulsive accelerations. Figures 9, 10, and 11 show the resultant PSDs. Once these were computed, the RMS accelerations were then derived from them via Parseval's relation to yield the results shown in Table 12.

The resonance at 3.5 Hz represents an Orbiter fuselage torsion mode and expectedly imparts most energy in the $Y_0 Z_0$-plane. The strongest structural mode resides at about 4.7 Hz and aligns primarily with the Z_0-axis. Note that structural modes can be hard to identify on plots of short periods of time, but are readily apparent when examining a long-duration spectrogram.

Table 12. Structural Mode RMS Accelerations Resulting from Satellite-Tracking Maneuvers

Frequency (Hz)	RMS Acceleration (μg_{RMS})								
	Unit F, TSH A			Unit F, TSH B			Unit G, TSH B		
	X_O	Y_O	Z_O	X_O	Y_O	Z_O	X_O	Y_O	Z_O
3.2	4.6	11.4	7.3	1.4	7.1	3.5	6.7	3.5	3.6
3.5	2.9	25.6	5.5	2.0	25.7	7.0	3.7	19.5	3.3
4.7	6.4	18.3	39.1	3.9	13.4	35.6	1.7	4.0	24.2
6.3	3.3	5.0	7.2	1.4	2.2	5.0	1.5	1.2	3.0

The spectrogram of Figure 12 represents an arbitrary 6-hour time frame where the structural modes quantified in Table 12 are indicated by the long horizontal ticks shown on the frequency axis. Of these, the mode at 3.2 Hz is the most obscure, while again we see that the 4.7 Hz mode is the most intense. The RMS accelerations shown in Table 12 were computed from a time span of repeated impulsive battering. In order to investigate the nominal behavior of the 4.7 Hz mode measured over a longer time frame, the RMS acceleration contributed by this mode was computed every 81 seconds for SAMS Unit F, TSH A data, and every 66 seconds for TSH B data from both SAMS Units F and G. This RMS acceleration tracking was performed for the 24-hour period starting at MET 010/00:00. The results for SAMS Unit F, TSH B are shown in Figure 13. The salient features of this plot are as follows:

- the sample rate, f_s, shown in small text in the upper left portion of the figure represents how often the RMS acceleration value was computed (one sample every 66 seconds at 0.02 samples per second),

- the alignment of this structural mode is reinforced by comparing the Z_0-axis data (blue trace) to those of the other two axes (red trace is X_0-axis, green trace is Y_0-axis); essentially, the X_0-and Y_0-axes' data represent ambient or background accelerations in this spectral region,

- the transition to crew wake occurs just before the 4-hour mark as seen by heightening of the blue trace (see also Appendix page C-44) and the transition to crew sleep occurs just before the 22-hour mark as seen by quieting of the blue trace (see also Appendix page C-47); as expected, crew movement tends to excite this mode,

- crew exercise periods (at around hours 4 to 6 and again at around hour 18) result in the highest measured RMS accelerations for this mode in this 24-hour period; in fact, when the third harmonic of the shoulder-sway frequency approaches 4.7 Hz (as seen at about MET 010/05:20 on Appendix page C-44 and at about MET 010/17:30 on Appendix page C-46), the resonant RMS acceleration level contributed by this mode alone approaches that of Vernier Reaction Control System (VCRS) thruster firings.

Results from similar RMS acceleration versus time plots for SAMS Unit F, TSH A and Unit G, TSH B mimic those gleaned from Figure 13. Table 13 summarizes the results for all three plots.

Table 13. 4.7 Hz Structural Mode Mean RMS Accelerations for MET 010/00:00 - 011/00:00

	RMS Acceleration (μg_{RMS})								
	Unit F, TSH A			Unit F, TSH B			Unit G, TSH B		
Frequency (Hz)	X_o	Y_o	Z_o	X_o	Y_o	Z_o	X_o	Y_o	Z_o
4.7	2.8	8.2	29.3	2.6	7.2	26.4	1.9	5.7	21.9

Comparing the shaded cells in Tables 12 and 13, note that the 4.7 Hz mode was somewhat higher in amplitude in the aftermath of the repeated thruster firings required for satellite-tracking maneuvers. In contrast to the steady, albeit nebulous, mode at 4.7 Hz, the apparent structural mode at about 3.2 Hz has been observed to shift in frequency. Most notable are the spectral shifts seen on the spectrogram of Appendix page B-50 at about MET 011/12:35, 011/13:53, 011/14:39, and 011/16:43. The cause of these frequency shifts is unknown at this time.

4.1.3 Deadband Collapse

The Orbiter's attitude with respect to its orbital path plays an important role in a number of operational concerns. Maintaining suitable orientation for links with communications satellites, minimizing damage by space debris, and keeping proper alignment to account for the orbital mechanics that dictate quasi-steady acceleration levels are three motivating factors for defining an attitude. Deadband is a term used to specify the allowable deviations (number of degrees and rotational rate of the Orbiter) from a desired attitude. The Orbiter's Reaction Control System is used to maintain a desired attitude, ensuring that the chosen deadband criteria are met. The Reaction Control System consists of the Primary Reaction Control System (PRCS) and the VRCS. The PRCS is typically used on orbit for pitch, roll, and yaw maneuvers, while the VRCS is used for fine adjustments of vehicle attitude. The Digital Auto Pilot (DAP) constantly monitors the Orbiter's orientation and governs the VRCS (or PRCS), commanding the proper sequence and direction of thruster firings required to return to attitude when a specified deadband limit is exceeded.

On occasion, the deadband is changed as more (or less) stringent pointing needs arise or as vehicle health issues evolve. When the deadband is changed from a higher value to a lower one, the allowable deviation from the nominal attitude decreases. This is referred to as a deadband collapse. There were numerous deadband collapses during the STS-87 mission, many of them imposed for jet temperature maintenance [16]. Table 14 is a partial list of deadband collapse times from this mission as recorded in the PIMS logbook or as indicated by examination of the acceleration data. For these times, the DAP was changing between the A3 (0.07° deadband) and the A12 (1.0° deadband) settings. Note, as indicated in the center column of this table, that most of these collapsed deadbands lasted for just a few minutes. However, there were some that lasted for nearly 10 minutes.

Table 14. Deadband Collapse Times

Approximate MET Start	Approximate Duration (minutes)	Appendix D Page
006/08:20:14	1.8	D-29
007/06:01:29	0.5	D-33
008/07:29:48	9.3	D-37
008/11:47:48	1.6	D-37
008/14:14:04	3.2	D-38
008/20:06:03	9.9	D-39
009/21:53:58	1.1	D-43
009/22:55:03	1.4	D-43
009/23:30:52	1.9	D-43

Table 15 gives a rudimentary accounting of VRCS thruster firing activity during time frames before and during two of the longer deadband collapses. The values shown in the "Number of VRCS Firings" column were retrieved from the operational downlink database maintained as part of MEWS. The values shown in this column were tallied such that simultaneous firings were counted as a single firing and, because the database is incomplete, these numbers represent a minimum value. For example, during the period MET 008/07:00:00-008/07:29:00, there were no fewer than 22 VRCS thruster firings.

Note from the shaded rows in Table 15 that, during the two periods of deadband collapse, the VRCS firing rate was a couple of orders of magnitude greater than during nominal periods. Qualitative examination of the spectrogram pages from Appendix D referenced in Table 14 reveals that the increased firing frequency of the VRCS during deadband collapse tends to have broadband spectral effects. Most noticeably, it excites the vehicle structural modes below about 10 Hz, and somewhat heightens the spectrum around the Ku-band antenna dither frequency (17 Hz) and its harmonics. Figure 14 provides a quantitative measure of the effects of the deadband collapse that started at about MET 008/07:29:48. The data for each of the four subplots in this figure start at MET 008/07:00. The upper-left plot is SAMS Unit F, TSH A (10 Hz) data, the upper-right plot is SAMS Unit F, TSH B (25 Hz) data, the lower-left plot is SAMS Unit G, TSH A (5 Hz) data, and the lower-right plot is SAMS Unit G, TSH B (100 Hz) data. Note that the ordinate scales for the four plots shown in this figure are different. Table 16 summarizes the acceleration magnitude disparity between a portion of the deadband collapse period (MET 008/07:31 to 008/07:37) and a period preceding this (MET 008/07:00 to 008/07:29).

Table 15. Deadband Collapse VRCS Firing Comparisons

MET	Duration (minutes)	Number of VRCS Firings	VRCS Firing Rate (firings per minute)
008/07:00:00 - 008/07:29:00	29.0	22	0.8
008/07:29:48 - 008/07:39:08	9.3	953	102.1
008/19:30:00 - 008/20:00:55	30.9	25	0.8
008/20:06:03 - 008/20:15:57	9.9	1699	171.6

Table 16. Acceleration Magnitude Comparison for Deadband Collapse

SAMS Unit	TSH	Sensor Cutoff Frequency (Hz)	MET	Acceleration Magnitude (μg)
F	A	10	before deadband collapse 008/07:00-008/07:29	35
			during deadband collapse 008/07:31-008/07:37	201
F	B	25	before deadband collapse 008/07:00-008/07:29	156
			during deadband collapse 008/07:31-008/07:37	627
G	A	5	before deadband collapse 008/07:00-008/07:29	26
			during deadband collapse 008/07:31-008/07:37	133
G	B	100	before deadband collapse 008/07:00-008/07:29	781
			during deadband collapse 008/07:31-008/07:37	809

The values of acceleration magnitude shown in the rightmost column of Table 16 represent the average for the time frame indicated. As expected, for each sensor the acceleration magnitude was greater during the deadband collapse period. The difference was more extreme for the lower frequency sensors (TSH A for both SAMS Units F and G). This is because below 10 Hz the acceleration spectrum of the Orbiter is dominated by vehicle structural modes, which are highly excitable by impulsive events such as thruster firings. While this is still a factor for the higher frequency sensors, the effect of the firings is overshadowed by vehicle subsystems and experimental equipment vibrations above 10 Hz. For these sensors, the measured acceleration magnitude difference mentioned above is smaller because vibrations caused by experimental equipment and vehicle subsystems (except for RCS) are not driven by these firings.

4.1.4 Water Dump Operations

The Orbiter Food, Water, and Waste Management Subsystem provides storage and dumping capabilities for potable and waste water [17]. Supply and waste water dumps are performed using nozzles on the port side of the Orbiter. Water dumps from these nozzles are expected to cause a steady acceleration of about 5.0×10^{-7} g in the Y_b-axis [18]. Figures 15 and 16 show the effect of a simultaneous supply water and waste water dump and of a supply water dump on the quasi-steady acceleration environment, as represented by OARE data. These water dump plots show contributions to the Y_b-axis and to the Z_b-axis. While the anticipated effects on the acceleration environment from water dumps is exclusively in the Y_b-axis, effects have been routinely observed in the Z_b-axis since STS-73/USML-2.

4.1.5 Orbiter Attitudes

A summary plot of the OARE data for the entire STS-87 mission is provided in acceleration versus time format, Figure 17, and in Quasi-Steady Three-Dimensional Histogram (QTH) format, Figure 18 [12]. Each plot format illustrates some unique aspects of the USMP-4 mission. Figure 17 clearly illustrates the sleep cycles of the crew through the periodic quieting of the data on all three axes. Peak-to-peak variations are on the order of 1×10^{-6} g for crew active periods and 0.2×10^{-6} g for crew sleep periods. Figure 18 illustrates that multiple attitudes were flown in support of separate USMP-4 payloads and the non-microgravity payloads, including Spartan.

As a result of the multiple attitudes flown to support the STS-87 mission, many of the attitudes are not as clearly observed by examining a QTH plot of the entire mission. This is because the QTH plot displays data related to an Orbiter attitude as a “percentage of time spent” relative to the total amount of OARE data under examination. For the QTH plot for the entire mission, this can result in an attitude’s contribution being somewhat “washed out,” if the time spent at that attitude was relatively short when compared to the entire length of the mission. The various attitudes of the STS-87 mission are more clearly observed by separating Figure 18 into two QTH images, one for non-microgravity periods (Figure 19) and one for microgravity periods (Figure 20). Figure 19 examines the first 96 hours of the STS-87 mission while Figure 20 examines the remaining 280 hours of OARE data. The additional attitudes observed in these two plots are annotated in the plots themselves. Note the variable trace in Figure 20 introduced by the solar inertial attitude in days 14/15. The respective quasi-steady acceleration magnitudes for each of these attitudes can be extracted from the plots.

4.1.6 Radiator Deployment

Radiator panels attached to the forward payload doors are part of the Active Thermal Control System which provides Orbiter heat rejection during a mission. The port and starboard side radiators can be deployed independently to accommodate the heat rejection requirements for a particular Orbiter attitude or mission. An electromechanical actuation system on the door unlatches and deploys the radiators when open and latches and stows the radiators when closed [19]. In deploying each radiator, six motor driven latches are unlocked and the deploy motor

moves the radiator to the desired position.

The deployment or stowage of either the port or starboard side radiators results in a general excitation of the Orbiter structural modes. In particular, the 6.3 Hz structural mode and its 2nd and 3rd harmonics are excited. Figure 21 combines PSDs for periods just prior to (red), during (blue), and just after (green) deployment of the port side radiator. The excitation of the 6.3 Hz structural mode and its harmonics is readily apparent, as is a spectral component around 9.5 Hz. Figure 22 is an acceleration vector magnitude versus time plot during deployment of the port side radiator. The increased magnitude around the 150-second mark of this plot illustrates the impact of the radiator deployment on the environment.

4.2 On-board Activities

Numerous objectives slated for this mission kept the Orbiter crew busy for the duration of their work periods. Vehicle maintenance, Spartan satellite deployment/retrieval, spacewalks, and microgravity science were some of the key responsibilities that consumed crew time. Crew movement on-board and in the payload bay translates to vibrational disturbances being introduced to the Orbiter's microgravity environment. The extent and character of the disturbances attributable to crew activity can best be examined in differential fashion. That is, comparison of the acceleration environment during times when the crew is active versus times when they are not active is desired. Generally, single shift crew sleep and Public Affairs Office (PAO) events offer extended periods of crew inactivity. For this mission, both of these scenarios took place and serve as contrast to the impact of nominal crew activity. On the other extreme, crew exercise can have a severe impact on the microgravity environment. On STS-87, an exercise vibration isolation device was used to minimize the effects on the sensitive USMP-4 experiments.

4.2.1 Crew Sleep Cycle

Table 17 shows the MET start and stop times of crew sleep taken from the mission replanned timeline. This table shows that the nominal scheduled sleep duration was eight hours, and sleep start times shifted forward in time as the mission progressed as dictated by landing and Spartan deployment constraints. As human nature has it, the start time for sleep can be planned, but the transition is certainly not instantaneous. On the other hand, the sleep stop time can be enforced with an alarm, which in this case was a daily wake-up song that was broadcast up to the crew. These facts are evidenced by examining the sleep start/stop times in the Appendix plot pages referenced in Table 17. For example, compare the transition of spectral levels (most evident below about 13 Hz) that occurs around MET 003/14:40 on page B-18 to the transition that occurs at around MET 003/22:00 on page B-19. These typify the effects seen when the crew transitions to sleep and to wake, respectively.

The spectrograms cited in Table 17 show an obvious quieting below about 13 Hz when the crew transitions from wake to sleep, however, they do not indicate with much precision how much quieter the acceleration environment becomes. In order to obtain an accounting of this detail, the RMS acceleration level contributed by the spectrum below 13 Hz was calculated approximately

every 66 seconds for a 96-hour span (MET 009/12:00 to 013/12:00) for SAMS TSH B on both Units F and G. Figure 23 shows the results of these calculations for Unit F. The four pairs of consecutive dashed/solid red lines indicate scheduled crew sleep start/stop times, respectively, for this 4-day time frame. Note again that actual reduction in acceleration levels typically lags scheduled sleep start times by at least several minutes, while increased excitation of the environment is coincident with the scheduled wake times owing to the daily wake-up song. For the plot shown in Figure 23, the mean RMS acceleration during the non-sleep times was 62 μg_{RMS}, while the mean RMS acceleration during the four sleep periods was 23 μg_{RMS}. Calculations for Unit G yield a mean RMS acceleration during non-sleep times of 55 μg_{RMS}, and a mean RMS acceleration during sleep periods of 29 μg_{RMS}.

Table 17. USMP-4 Replanned Timeline Crew Sleep Times

Start Sleep Period		End Sleep Period	
MET	**Appendix Page**	**MET**	**Appendix Page**
000/11:00	B-5	000/19:00	B-7
001/12:00	B-9,10	001/20:00	B-11
002/12:00	B-13,14	002/20:00	B-15
003/14:00	B-18	003/22:00	B-19
004/15:00	B-22	004/23:00	B-23
005/16:00	B-26	006/00:00	B-27,28
006/17:00	B-30	007/01:00	B-32
007/18:00	B-34,35	008/02:00	B-36
008/19:00	B-39	009/03:00	B-40
009/20:00	B-43	010/04:00	B-44
010/21:00	B-47	011/05:00	B-48
011/22:00	B-51	012/06:00	B-52,53
012/22:00	B-55	013/06:00	B-56,57
013/22:00	B-59	014/06:00	B-60,61
014/22:00	B-63	015/07:00	B-65

As might be expected, the crew may have to wake during a sleep period for one reason or another. It is quite possible that this is what happened at around MET 003/17:20, see spectrogram on Appendix page D-18. Note in this plot that there are 5 to 10 minutes of heightened spectral response, particularly below 10 Hz, starting just before MET 003/17:20. This period coincides with an entry in the PIMS mission logbook, which notes that the IDGE science team observed “their crystal rotate and move” at that time. The correlation implied here is not a definitive cause-and-effect identification, it is merely conjecture. The IDGE team's

concern about their crystal motion prompted an unsuccessful search (by Marshall Space Flight Center and Johnson Space Center controllers) for specific disturbance sources.

While the whole mission OARE acceleration versus time plot shown in Figure 17 clearly demonstrates the sleep cycles of the crew, QTH plots can be employed to examine the relative excursions in the OARE data during crew sleep versus crew active periods. Figure 24 is a QTH plot created using a concatenation of OARE data from all the USMP-4 crew sleep periods from MET 004/00:00:00 to the end of the mission. Similarly, Figure 25 is a QTH plot created using a concatenation of OARE data from all the crew active periods for the same period of time. A comparison of the figures clearly shows the effect of crew activity on the OARE data. Figure 24 indicates a tight clustering of the recorded OARE data during crew sleep, which permits a more straightforward extraction of the quasi-steady acceleration vector from the OARE data. The increased scatter observable in the data of Figure 25 demonstrates the impact of the crew and equipment on the quasi-steady acceleration environment. Note, the circular/oval shaped signature in Figure 24 is the result of the Orbiter being in a solar inertial attitude during one of the crew sleep periods.

4.2.2 PAO Events

While crew sleep clearly provides a certain measure of quieting as detailed earlier, there are other non-sleep times during a mission that afford similar effects on the acceleration environment. Most notably, PAO events offer at least a brief respite for the crew. During a typical PAO event, the crew is relatively motionless and gathered in front of a camera for audio and video communications with interested parties on the ground. This period of minimal movement mimics that of sleep from an acceleration disturbance perspective, albeit for a much shorter time span. PAO events normally last around 15 to 20 minutes, compared to the 8-hour sleep periods. For this mission, the crew participated in more than a half dozen PAO events; Table 18 lists six of these that show up prominently on the spectrograms on the Appendix plot pages listed in the table.

Table 18. PAO Events

Approximate MET Start	Duration (minutes)	Appendix Pages
003/07:44	19	B-, C-, D-, E-17
006/13:03	8	B-, C-, D-, E-30
007/14:53	15	B-, C-, D-, E-34
011/08:32	19	B-, C-, D-, E-49
012/14:49	34	B-, C-, D-, E-54
014/17:15	15	B-, C-, D-, E-62

The longer-than-normal PAO event that takes place starting at about MET 012/14:49 (see Appendix page B-54) exemplifies the quietude, especially below about 13 Hz or so, which can be achieved by minimizing crew movement. For person-intensive tasks, this restriction might be impractical or unfeasible, but situational awareness and planning may facilitate maximum usage of desirable acceleration environmental conditions at some time in the future of microgravity research.

The quasi-steady environment measured by OARE also exhibits a noticeable quieting during PAO events. Figure 26 shows the effect of the fifth PAO event listed in Table 18 on the quasi-steady acceleration environment. With the reduced crew activity, the quasi-steady acceleration environment variations are more pronounced, much like the effects observed for crew sleep periods. The variations in the OARE data during PAO events is typically 0.2×10^{-6} g peak-to-peak. Non-PAO time intervals demonstrate a peak-to-peak variation of 1×10^{-6} g.

4.2.3 Bicycle Ergometer Isolation

While crew sleep periods and PAO events provide quiet microgravity conditions, other crew activity is routinely observed to have a negative effect on the microgravity environment. Crew members are expected to exercise to maintain physical conditioning. On STS-87, aerobic exercise was achieved using a bicycle ergometer. During the first few days of the mission, the ergometer was mounted to the Orbiter with each of three configurations of an ergometer vibration isolation system called the Passive Cycle Isolation System (PCIS). During mission planning, the mission management team requested that the PIMS team provide analysis of the SAMS Unit F, TSH A data collected during these initial days of crew exercise to assist them in assessing the vibration isolation performance of the PCIS. Two types of analysis were employed to quantify the differences measured by the SAMS among the three PCIS configurations and a hardmount configuration: (1) Δg_{RMS} derived from interval RMS acceleration versus time, and (2) cumulative RMS acceleration versus frequency.

The Δg_{RMS} derived from interval RMS acceleration versus time analysis was aimed at quantifying the change in the RMS acceleration level for two distinct periods: a non-exercise baseline period and the exercise period of interest. Care was taken to ensure that no strong, non-exercise related disturbances below 10 Hz were present for one period and not for the other. A spectrogram plot spanning both the baseline and the exercise periods served as the basis for this check. From this spectrogram, periods were identified as baseline and as exercise. Once these periods were selected, a 0.5-second interval RMS acceleration versus time curve was plotted for the same time span covered by the spectrogram. Based on this plot, the difference in the median of the RMS acceleration values between the baseline and exercise periods was calculated. This was done for the three (XYZ) orthogonal Orbiter structural axes and for the overall RMS acceleration calculated from the root-sum-of-squares (RSS) of the XYZ RMS acceleration values. The results were compiled in near real-time in tabular form on a PIMS WWW page.

After the Δg_{RMS} values were calculated, the cumulative RMS acceleration versus frequency curves for both the baseline and exercise periods were plotted. These served to quantify the contributions of spectral components at and below a given frequency to the overall RMS acceleration level for the periods of interest.

Commander Kevin Kregel was the only crew member to exercise in all of the ergometer configurations. Configuration #1 used stiff PCIS mounts on the front of the ergometer and stiff mounts at the seat connection; #2 used soft front and stiff seat connections; and #3 used stiff front and soft seat mounts. Based on analyses of Kregel's early exercise (see Table 19 below), several observations were made. Overall, the PCIS configuration #3 was better than either of the first two configurations. For the X_0-axis only, the PCIS configuration #2 was the best. For the Y_0-axis only, the PCIS configuration #1 was the best. For the Z_0-axis, the hardmount was the best. The differences among the three PCIS configurations were marginal in all cases.

Table 19. Δg_{RMS} Comparison of Commander's Exercise

Ergometer Configuration	Axis	Δg_{RMS}
PCIS Configuration #1 Stiff Front/Stiff Seat	RSS	9.206×10^{-5}
	X_O	2.227×10^{-5}
	Y_O	5.293×10^{-5}
	Z_O	7.010×10^{-5}
PCIS Configuration #2 Soft Front/Stiff Seat	RSS	1.245×10^{-4}
	X_O	1.027×10^{-5}
	Y_O	7.006×10^{-5}
	Z_O	1.053×10^{-4}
PCIS Configuration #3 Stiff Front/Soft Seat	RSS	8.410×10^{-5}
	X_O	2.405×10^{-5}
	Y_O	5.619×10^{-5}
	Z_O	5.093×10^{-5}
Hardmount	RSS	2.401×10^{-4}
	X_O	1.478×10^{-5}
	Y_O	2.495×10^{-4}
	Z_O	4.096×10^{-5}

Based on the analysis provided by PIMS, the PCIS configuration to be used for the USMP-4 timeframe was uplinked to the crew as part of the Flight Day 5 Payload Summary,

> RECOMMENDED PCIS CONFIGURATION: It appears that the differences among the three configurations are marginal. However, after analyzing the Δg_{RMS} (g_{RMS} exercise - g_{RMS} background) values for the three configurations, the final configuration was found to have the overall lowest value. Therefore, the Mission Scientist recommends the final configuration #3 as the optimum PCIS configuration for [Flight Days] 5-14.

The real-time PCIS data analysis relied exclusively on the SAMS Unit F, TSH A data which had the temperature/acceleration data problem mentioned earlier. This analysis, however, was done in a differential fashion, whereby the Δg_{RMS} between baseline and exercise periods was the decisive quantity. Assuming that the anomalous low-frequency component varied only slightly over the span of the baseline and exercise periods, then this analysis should not have been significantly affected.

4.3 Payload Operations

4.3.1 IDGE-Related Disturbances

Early in the mission, following activation of the USMP-4 experiments, a set of acceleration disturbances clustered around 56 Hz was noticed in the real-time spectrogram displays of SAMS Unit G, TSH B. See, for example, the pronounced red horizontal streaks at this frequency in the spectrograms of Appendix D. The CHeX team expressed concern about these disturbances because of their experiment susceptibility to vibrations around 55 Hz. During the first few days of the mission, an investigation was conducted by consulting with the various experiment teams, Spacelab-MPESS support staff, and Orbiter subsystem personnel to ascertain the source of these disturbances. In discussions with IDGE personnel, it was discovered that there were seven cooling fans within the IDGE apparatus. One of the fans had its speed controlled according to a measured internal IDGE temperature.

The spectrogram on Appendix page D-65 shows the SAMS Unit G, TSH B data during the IDGE experiment deactivation time on MET day 015. In addition to the 56 Hz traces, the variable trace between 35 and 40 Hz and a 74 Hz disturbance cease at the time of the IDGE power-off at about MET 015/09:45. When the IDGE and SAMS units were returned to NASA Lewis Research Center after de-integration from the Orbiter, a vibration assessment was performed with the IDGE flight apparatus and SAMS Unit G, TSH B. The data acquired by SAMS for this test are shown in Figure 27. This test confirmed that the variable 35 to 40 Hz trace, the traces around 56 Hz, and the 74 Hz disturbance were all related to IDGE fans.

During the ground testing of the IDGE hardware, another as-yet-unidentified disturbance evident in the SAMS data was potentially assigned to IDGE. This disturbance was manifested as a persistent spectral peak at 21 Hz (1260 rpm if a rotational source) and can be seen to start and stop in the bench test SAMS data shown in Figure 27. A similar disturbance was seen in the mission data. It was tightly controlled in frequency and spanned the time frame from approximately MET 000/20:39 (see Appendix page B-7) to MET 014/15:30 (see Appendix page

B-62) with only two brief pauses. The first intermission started at about MET 001/05:19 and lasted just under 7 minutes (see Appendix page B-8). The second started at about MET 013/09:58 and lasted just over 15 minutes (see Appendix page B-57). To quantify this disturbance, its RMS acceleration was computed every 33 seconds for the 24-hour period starting at MET 004/00:00 for TSH B on both SAMS Units F and G. The physical separation of these two heads and their cutoff frequencies enabled a comparison of the measured impact of this disturbance at two different locations in the Orbiter's payload bay. Figure 28 shows the RMS acceleration versus time for the frequency range from 20.8 to 21.1 Hz for SAMS Unit F, TSH B measurements. As seen, the intensity of this disturbance is somewhat variable; similar analyses of SAMS Unit G, TSH B data lead to the results summarized in Table 20. The RMS values indicate that this disturbance is relatively close in intensity at the two different sensor locations.

Table 20. RMS Accelerations from 21 Hz Disturbance for MET 004/00:00 - 005/00:00

	RMS Acceleration (μg_{RMS})	
	Unit F, TSH B	**Unit G, TSH B**
Minimum	3.1	3.9
Mean	12.4	14.6
Maximum	48.8	68.2

4.3.2 SAMS Hard Drive Disturbance

The spectrograms most often referred to in this report are those included in the appendices; these plots display data up to the filter cutoff frequency for the SAMS data. When characterizing the microgravity environment of the Orbiter, it is useful to also examine spectrograms that show data out to the Nyquist frequency, even though the acceleration energy represented by the plot between the cutoff and Nyquist frequencies is suppressed by filtering [12]. Such spectrograms are included on the report CD-ROM. While studying the SAMS Unit G, TSH B Nyquist frequency spectrograms, a strong, persistent 120 Hz disturbance was noticed. Subsequent discussions with the SAMS engineering team and evaluation of groundtest data led to the determination that the 120 Hz disturbance was caused by the 7200 rpm rotation of the SAMS computer hard disk drives used to record data on orbit.

4.3.3 Orbiter Cabin and Airlock Depressurization

In preparation for the two EVAs conducted during the STS-87 mission, the crew cabin and the airlock had to be depressurized to various degrees. In preparation for both EVAs, the cabin was depressurized from a nominal 14.7 psi to 10.2 psi. Prior to egress, the airlock was depressurized from 10.2 psi to the vacuum of space. This airlock depressurization was performed in two steps, from 10.2 psi to 5.5 psi and from 5.5 psi to vacuum. The air removed from the Orbiter during depressurization was vented through a relief valve located on the port side of the Orbiter. This relief valve is located very near the valves used for conducting supply water and waste water

dumps. This was the first mission where the effects of cabin depressurization and airlock depressurization on the microgravity acceleration environment were measured and recorded.

The effects of cabin depressurization and airlock depressurization are most evident in the quasi-steady acceleration environment. The OARE Y_b-axis and the OARE Z_b-axis data shown in Figures 29 and 30 indicate that the magnitude of the cabin depressurization can be as large as 10 μg. The OARE Y_b-axis and the OARE Z_b-axis data shown in Figures 31 and 32 indicate the magnitude of the airlock depressurization can be as large as 5 μg.

Figure 33 illustrates the two step process involved in performing the airlock depressurization. The red trace in Figure 33 is the differential pressure between the airlock and the payload bay as indicated by data retrieved from the MEWS system. The change in the differential pressure approximately 23 minutes into the plot causes a corresponding change in the quasi-steady acceleration environment of about 5 μg. When 5.5 psi is reached, the venting is stopped for about 5 minutes. The next change in pressure results in further venting that also affects the quasi-steady acceleration environment.

4.3.4 EVA Operations

As NASA prepares to build the International Space Station in collaboration with its international partners, successful completion of EVA missions becomes critical. Designers and mission planners are developing the equipment and procedures for constructing the space station and, while a good deal of testing can be done on the ground, certain tests must be performed on orbit. Lessons learned from a series of EVA tests will serve to increase the experience base of hardware developers, flight controllers, and the astronauts doing the spacewalks [20]. During the STS-87 mission, astronauts Winston Scott and Takao Doi performed two EVAs. Grappling and berthing of the wayward Spartan satellite consumed much of the time on the first of these. The second was focused on evaluation of equipment and procedures that will be used during construction and maintenance of the International Space Station. This spacewalk was intended to accomplish all of the primary objectives originally planned as part of the STS-80 mission in November 1996 that were not achieved due to a stuck airlock hatch [21].

For convenience, the first EVA, which took place from about MET 005/04:30 to 005/11:50 will be referred to as EVA #1, and the one that took place from about MET 013/13:20 to 013/18:15 will be referred to as EVA #2 in the remainder of this report. A cursory examination of the SAMS data collected during these times shows that these EVAs tended to excite the acceleration spectrum below about 50 Hz. This increased excitation can be seen in a relative manner by comparing Appendix D Figures 22 (during EVA #1) to 23 (after EVA #1) for SAMS Unit G, TSH B on pages D-25 and D-26. In order to quantify this comparison and to gain a better understanding of the effects that an EVA activity has on the Orbiter's acceleration environment, the RMS accelerations for a number of frequency bands were calculated as a function of time.

The RMS acceleration for each of the frequency bands shown in Table 21 was computed every 32.768 seconds from the SAMS Unit G, TSH B data for the period MET 005/06:30 to 005/15:30,

which spans most of EVA #1 and a few hours thereafter; and for the period MET 013/13:00 to 013/22:00, which spans most of EVA #2 and a few hours following. The RMS levels shown in the "During EVA" columns represent the median values during part of the EVA (MET 005/07:30 to 005/10:30 for EVA #1, and MET 013/13:20 to 013/16:20 for EVA #2), while the "After EVA" columns show the median values after the EVA (MET 005/12:30 to 005/15:30 for EVA #1, and MET 013/19:00 to 013/22:00 for EVA #2). Note that for each band the levels during the EVAs were higher, although only marginally so above about 50 Hz. The RMS acceleration levels for the 0-10, 10-20, and 30-40 Hz bands for this sensor are appreciably lower after the EVAs. For example, a plot of the RMS acceleration versus time for the first band (0 to 10 Hz) is shown in Figure 34. The red segment of the trace indicates the "During EVA #1" time frame considered for Table 21, while the blue segment indicates the "After EVA #1" span. Note from the figure the obvious disparity in RMS levels for this frequency band.

Table 21. EVA RMS Acceleration Comparison (SAMS Unit G, TSH B)

Frequency Range (Hz)	RMS Acceleration (μg_{RMS})			
	During EVA #1	After EVA #1	During EVA #2	After EVA #2
0 - 10	110	45	98	41
10 - 20	259	156	295	163
20 - 30	110	68	138	58
30 - 40	202	122	197	98
40 - 50	108	69	97	62
50 - 60	138	137	213	195
60 - 70	91	89	99	95
70 - 80	84	83	90	87
80 - 90	102	98	88	81
90 - 100	77	71	90	85

Table 22. EVA #1 RMS Acceleration Comparison (SAMS Unit F, TSH A and B)

Frequency Range (Hz)	RMS Acceleration (μg_{RMS})			
	Unit F, TSH A		Unit F, TSH B	
	During EVA	After EVA	During EVA	After EVA
0 - 10	116	48	121	51
10 - 20			267	105

Table 23. EVA #2 RMS Acceleration Comparison (SAMS Unit F, TSH A and B)

Frequency Range(Hz)	RMS Acceleration (μg_{RMS})			
	Unit F, TSH A		Unit F, TSH B	
	During EVA	After EVA	During EVA	After EVA
0 - 10	116	52	121	55
10 - 20			318	185

SAMS Unit F, TSH A and B data were analyzed as described above, with the exception that the analysis was limited by the lowpass filter cutoff frequencies of these heads (10 Hz for TSH A, and 25 Hz for TSH B). The results shown in Tables 22 and 23 for Unit F are similar to those obtained for Unit G.

To further investigate the sources of disturbance that may have contributed to the measured accelerations during the two EVAs, Orbiter thruster firing activity was analyzed. The MEWS software enabled access to a record, albeit incomplete, of Columbia's Reaction Control System thruster firing times. The firing count shown in the right-hand column of Table 24 gives the minimum number of times that the VRCS jets were fired. Simultaneous firings were counted as one. The PRCS thrusters were not fired during either EVA according to the MEWS data.

Table 24. Orbiter VRCS Thruster Firing Activity During EVAs

MET	VRCS Thruster Firing Count
005/08:00 - 005/11:00 (during EVA #1)	154
005/12:00 - 005/15:00 (after EVA #1)	640
013/13:40 - 013/16:40 (during EVA #2)	414
013/19:00 - 013/22:00 (after EVA #2)	66

For EVA #1, these data indicate that the increased excitation observed during the spacewalk is not attributable to thruster firings. The same implication cannot be gleaned from the firing count numbers for EVA #2 taken alone, however, when considered in conjunction with those of EVA #1, we infer that the thruster firings did not play a defining role in heightening the acceleration spectra in some preferential manner during the EVAs. The nature of the work being done during these spacewalks may help to explain the increased acceleration levels. It stands to reason that cumbersome space suits and "construction" work requires greater forces be exerted by the astronauts than nominal crew compartment activities. Also, during the EVAs the astronauts were closer to the SAMS sensors; spacewalk disturbances originated in the Orbiter's cargo bay, where the SAMS heads were mounted, instead of the middeck or flight deck, where the crew was the remainder of the mission.

4.4 Unknown Disturbance Sources

4.4.1 Twin Disturbances at 12 to 15 Hz

An unidentified pair of disturbances shows up as two closely spaced spectral peaks, most clearly seen in the spectrograms of Appendix B. These twin disturbances tend to track each other in the frequency domain, and gradually increase in frequency from around 12 Hz early in the mission to over 15 Hz on MET day 11. They exhibit sharp spectral transitions on occasion. For example, see Appendix pages B-31 and B-32 until about MET 007/01:30, Appendix pages B-35 and B-36 until about MET 008/01:40, and Appendix page B-47 at about MET 010/22:50. These disturbances are hard to discern from about MET 008/06:30 (Appendix page B-37) to about MET 008/18:00 (Appendix page B-38), and apparently cease sometime around MET 011/04:30 (Appendix page B-48).

4.4.2 Unknown 11.35 Hz Disturbance

An unidentified disturbance at 11.35 Hz, along with its 2nd harmonic at 22.70 Hz, is visible occasionally in the Appendix B spectrograms. The first occurrence of this disturbance was at approximately MET 009/14:30:00 and the last occurrence was at approximately MET 010/09:00:00. There exist eleven occurrences of this disturbance, the maximum duration being about 15 minutes. Typical durations seem to be approximately 5 minutes in length.

Figure 35 is a plot of RMS acceleration versus time for the narrow frequency band 11.25 Hz to 11.45 Hz. The intent of this analysis was to compare the signal in this frequency band when the 11.35 Hz signal was active versus when it was inactive. The elevated levels from the 0 to 10 minute mark and from the 90 to 100 minute mark represent intervals when the 11.35 Hz signal was present and clearly illustrate the change in signal. Appendix page B-43 shows the spectrogram representation of this condition from MET 009/22:00 to 010/00:00.

5. Summary

The OARE and two SAMS units were used to measure and record the microgravity environment of the Orbiter Columbia during the STS-87 mission in November-December 1997. Data from the two SAMS units were telemetered to the ground during the mission and data plots were displayed for USMP-4 investigators in near real-time using the World Wide Web. During SAMS data processing after the mission, it was determined that there was a problem with temperature / acceleration signals on SAMS Unit F, TSH A. The effects of this problem can be removed from the data in some types of analyses. Plots generated using OARE data telemetered to the ground were provided to the investigators approximately twelve hours after data recording using the World Wide Web.

Disturbances in the microgravity environment as recorded by these instruments are grouped by source type in this report: Orbiter systems, on-board activities, payload operations, and unknown sources. The environment related to the Ku-band antenna dither, Orbiter structural modes, attitude deadband

collapses, water dump operations, crew sleep, and crew exercise was comparable to the effects of these sources on previous Orbiter missions. RMS acceleration levels for the Ku-band dither disturbance (16.93 to 17.13 Hz) were about 1.9×10^{-4} g_{RMS} during USMP-4. Average RMS acceleration levels for the 4.7 Hz Orbiter structural mode ranged from 2×10^{-6} g_{RMS} for the least affected X_0-axis to 3×10^{-5} g_{RMS} for the most affected Z_0-axis. Attitude deadband collapses necessitated by VRCS jet conditions tended to increase the VRCS jet firing rate from approximately one firing per minute for the standard deadband (1.0°) to greater than 100 firings per minute for the collapsed deadband (0.07°). Disturbances related to operations of the IDGE fans and SAMS hard drives that were not observed on previous missions are detailed in the text.

The effects of EVAs and related Orbiter cabin depressurization on the microgravity environment are reported. The exact cause of heightened SAMS-recorded acceleration spectral levels during EVAs is not known, although the nature and location of the work being done during the STS-87 spacewalks may help to explain the increased levels. The effects of the cabin depressurizations performed to prepare the spacewalking astronauts for their EVAs were best seen in the OARE data as excursions from the background acceleration levels of as much as 1×10^{-5} g.

The attached CD-ROM version of this report contains the text and figures of this hard-copy along with Appendix plots and supplementary plots representing the entire mission. These spectrograms are for each of the four SAMS sensor heads that recorded data during the mission. The plots are useful in identifying relative acceleration levels and the approximate start and stop times of disturbances.

6. References

[1] Rogers, M. J. B. and R. DeLombard, Summary Report of Mission Acceleration Measurements for STS-62. NASA Technical Memorandum 106773, November 1994.

[2] Rogers, M. J. B., K. Hrovat, M. Moskowitz, K. McPherson, and R. DeLombard, Summary Report of Mission Acceleration Measurements for STS-75. NASA Technical Memorandum 107359, November 1996.

[3] DeLombard, R. and B. D. Finley, Space Acceleration Measurement System Description and Operations on the First Spacelab Life Sciences Mission. NASA Technical Memorandum 105301, November 1991.

[4] DeLombard, R., B. D. Finley, and C. R. Baugher, Development of and Flight Results from the Space Acceleration Measurement System (SAMS). NASA Technical Memorandum 105652, January 1992.

[5] Baugher, C. R., G. L. Martin, and R. DeLombard, Low-frequency Vibration Environment for Five Shuttle Missions. NASA Technical Memorandum 106059, March 1993.

[6] Rogers, M. J. B., C. R. Baugher, R. C. Blanchard, R. DeLombard, W. W. Durgin, D. H. Matthiesen, W. Neupert, and P. Roussel, A Comparison of Low-gravity Measurements On-board Columbia During STS-40. Microgravity Science and Technology VI/3 (1993) 207.

[7] Rogers, M. J. B. and R. DeLombard, Summary Report of Mission Acceleration Measurements for STS-73. NASA Technical Memorandum 107269, July 1996.

[8] Blanchard, R. C., M. K. Hendrix, J. C. Fox, D. J. Thomas, and J. Y. Nicholson, Orbital Acceleration Research Experiment. J. Spacecraft and Rockets 24 (1987) 504.

[9] Blanchard, R. C., J. Y. Nicholson, and J. R. Ritter, STS-40 Orbital Acceleration Research Experiment Flight Results During a Typical Sleep Period. NASA Technical Memorandum 104209, January 1992.

[10] Blanchard, R. C., J. Y. Nicholson, and J. R. Ritter, Preliminary OARE Absolute Acceleration Measurements on STS-50. NASA Technical Memorandum 107724, February 1993.

[11] Blanchard, R. C., J. Y. Nicholson, J. R. Ritter, and K. T. Larman, OARE Flight Maneuvers and Calibration Measurements on STS-58. NASA Technical Memorandum 109093, April 1994.

[12] Rogers, M. J. B., K. Hrovat, K. McPherson, M. Moskowitz, and T. Reckart, Accelerometer Data and Presentation Techniques. NASA Technical Memorandum 113173, September 1997.

[13] DeLombard, R., K. McPherson, M. Moskowitz, and K. Hrovat, Comparison Tools for Assessing the Microgravity Environment of Missions, Carriers and Conditions. NASA Technical Memorandum 107446, April 1997.

[14] Personal communication with Martin O'Hare, Ku-Band Subsystem Engineer, Boeing North American, Johnson Space Center.

[15] Personal communication with Richard LaBrode, Instrumentation and Communication Officer (INCO), United Space Alliance, Johnson Space Center.

[16] STS-87 Space Shuttle Mission Report, NSTS-37418, Johnson Space Center, Houston, TX, February 1998.

[17] Shuttle Operational Data Book, Volume 1, JSC-08934, Rev. E, Johnson Space Center, Houston, TX, January 1988.

[18] Rogers, M. J. B., B. P. Matisak, and J. I. Alexander, Venting Force Contributions—Quasi-steady Accelerations on STS-50. Microgravity Science and Technology VII/4 (1995) 293.

[19] http://shuttle.nasa.gov/reference/shutref/structure/baydoors.html

[20] http://shuttle.nasa.gov/sts-80/orbit/eva/edftov.html

[21] http://shuttle.nasa.gov/sts-87/orbit/payloads/#EVA

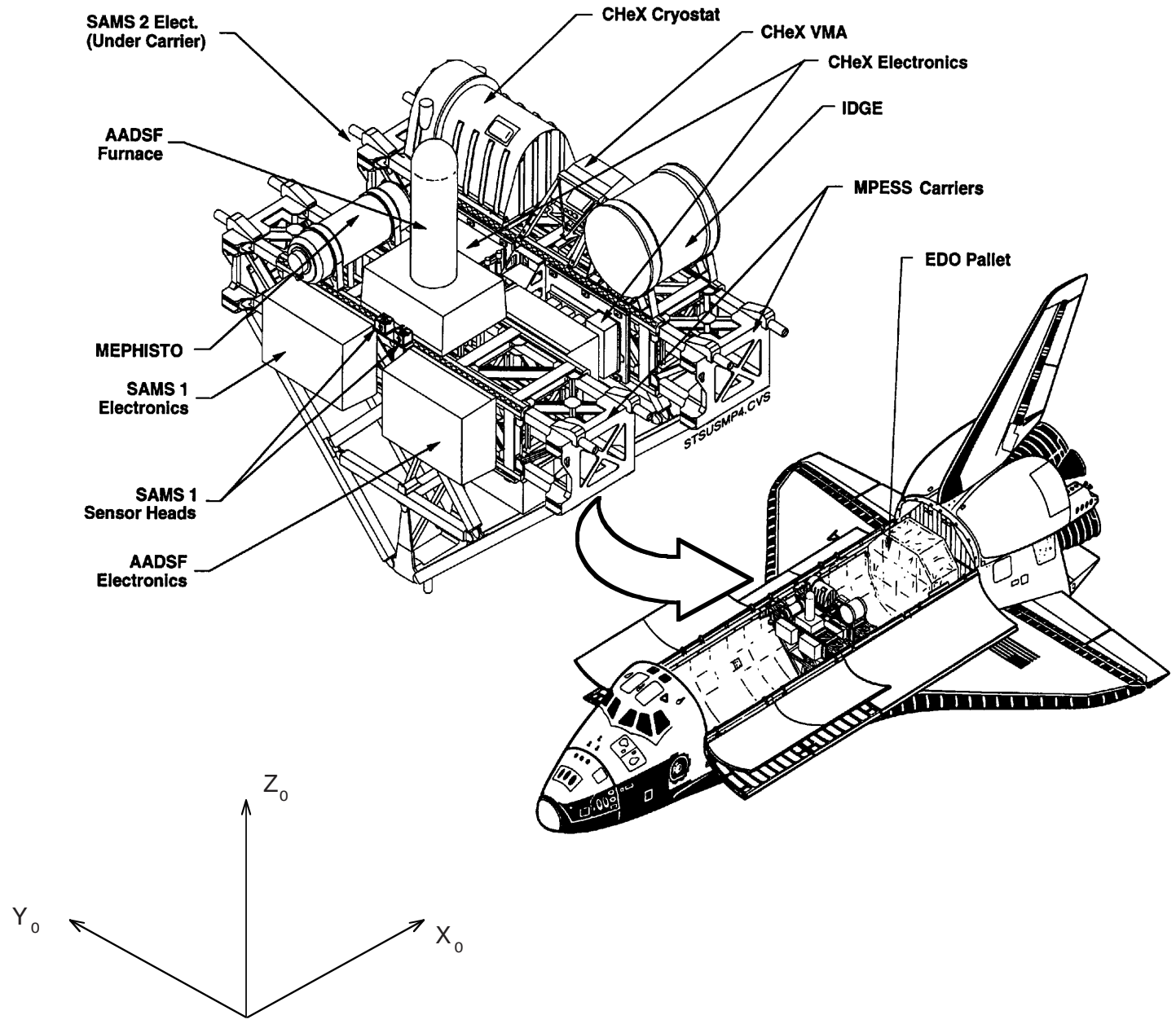

Figure 1. MPESS Layout and Approximate Payload Bay Location of USMP-4.

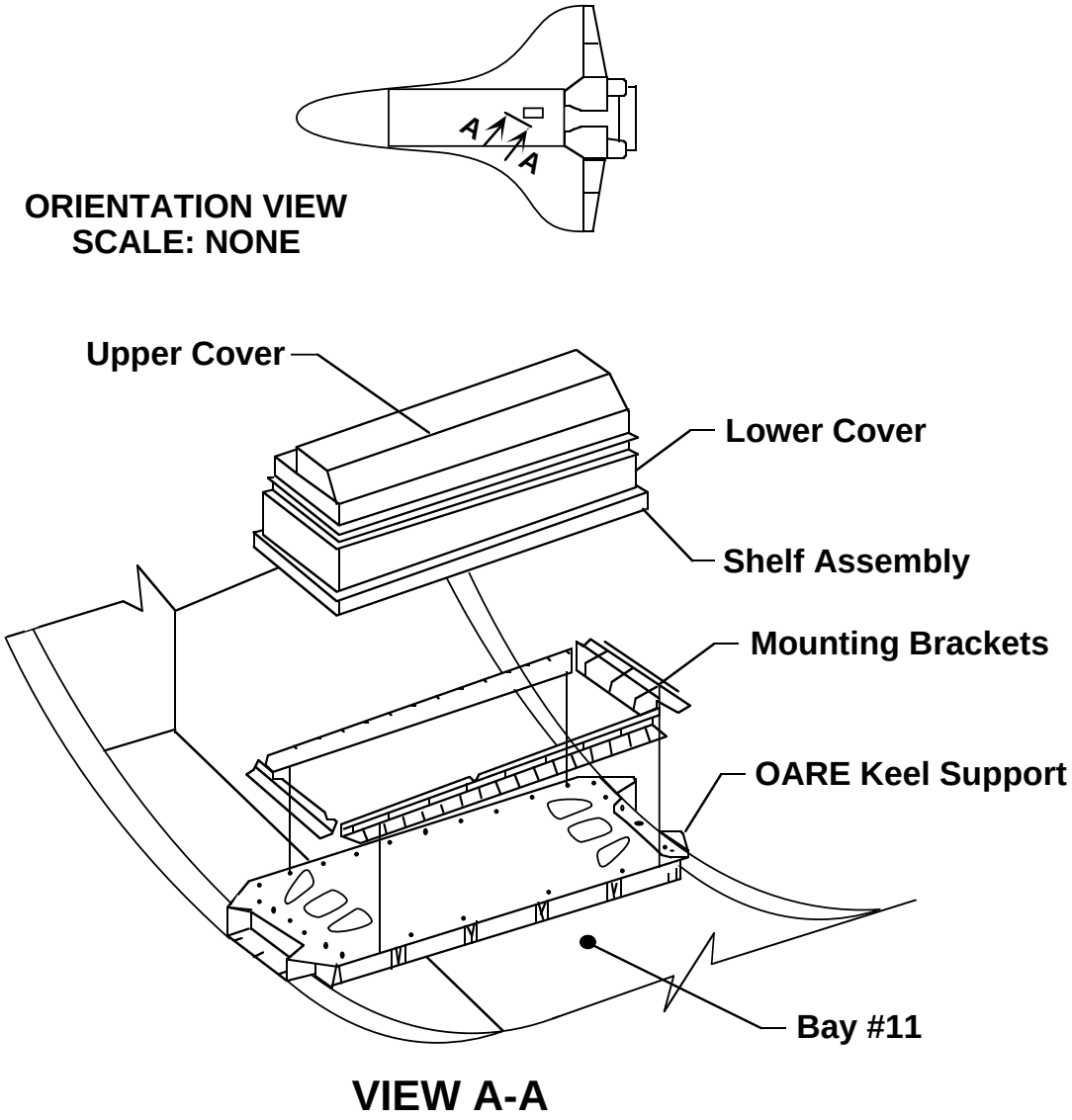

Figure 2. OARE Instrument Location for USMP-4.

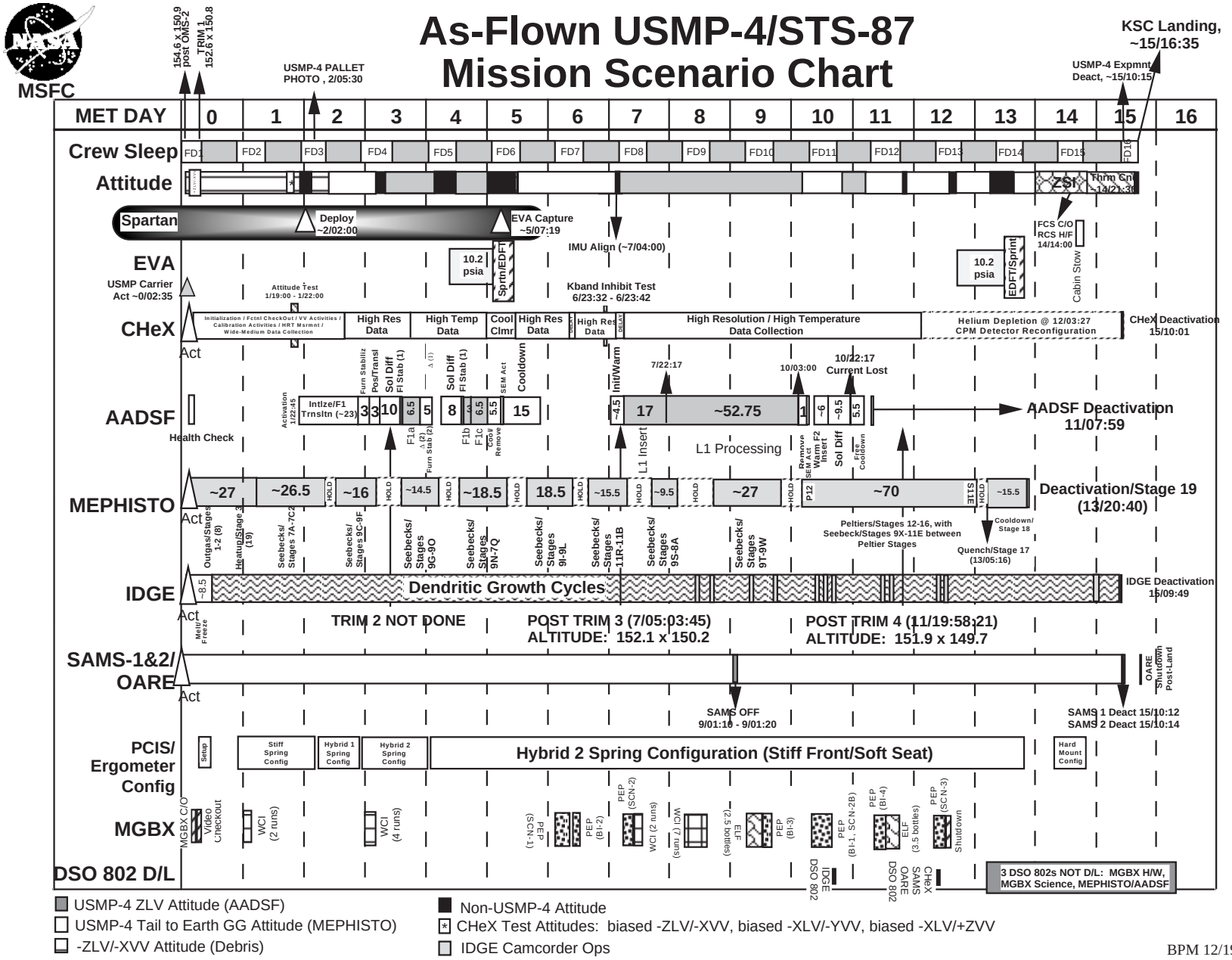

Figure 3. As-Flown Scenario.

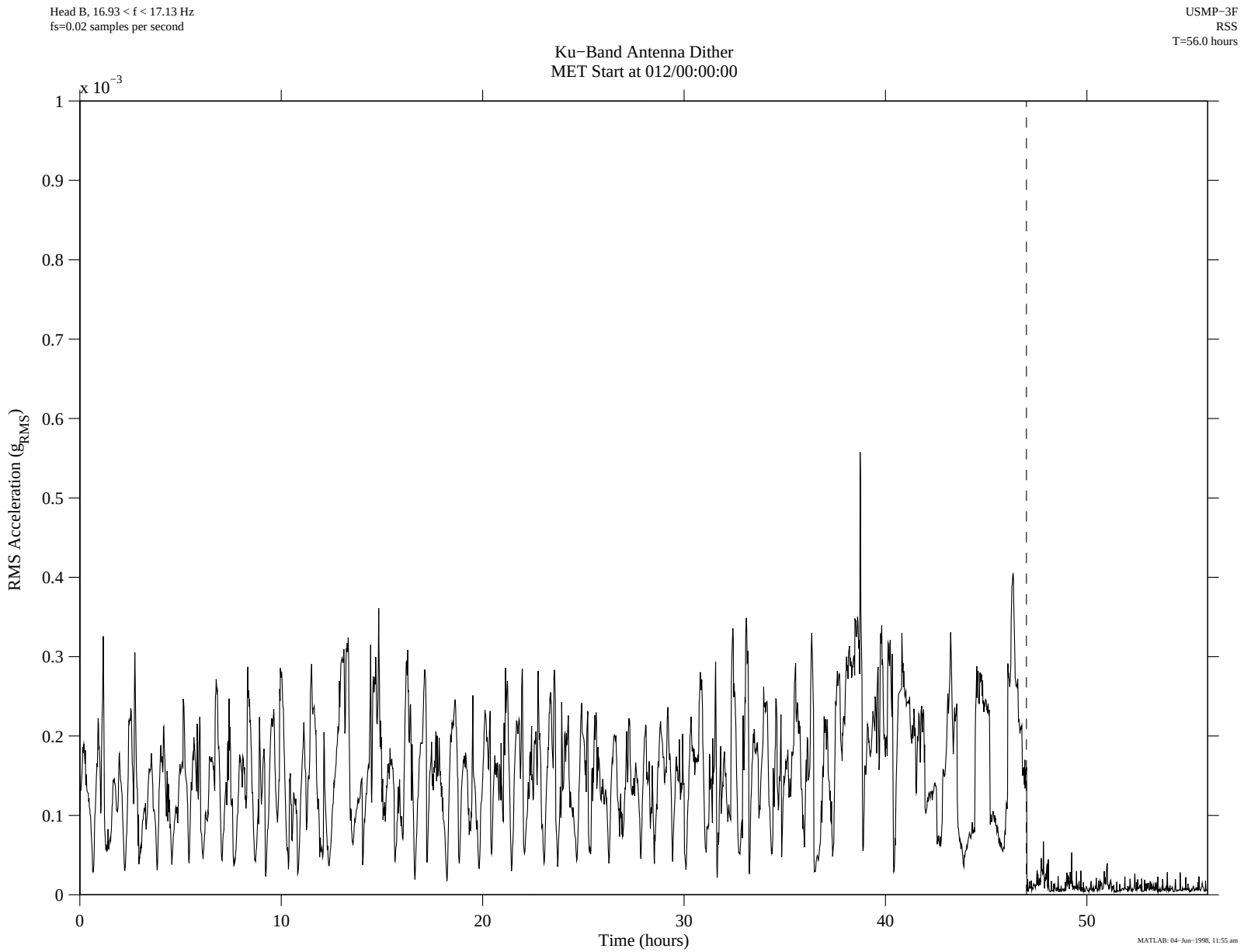

Figure 4. Ku-Band Antenna Dither Cessation (USMP-3).

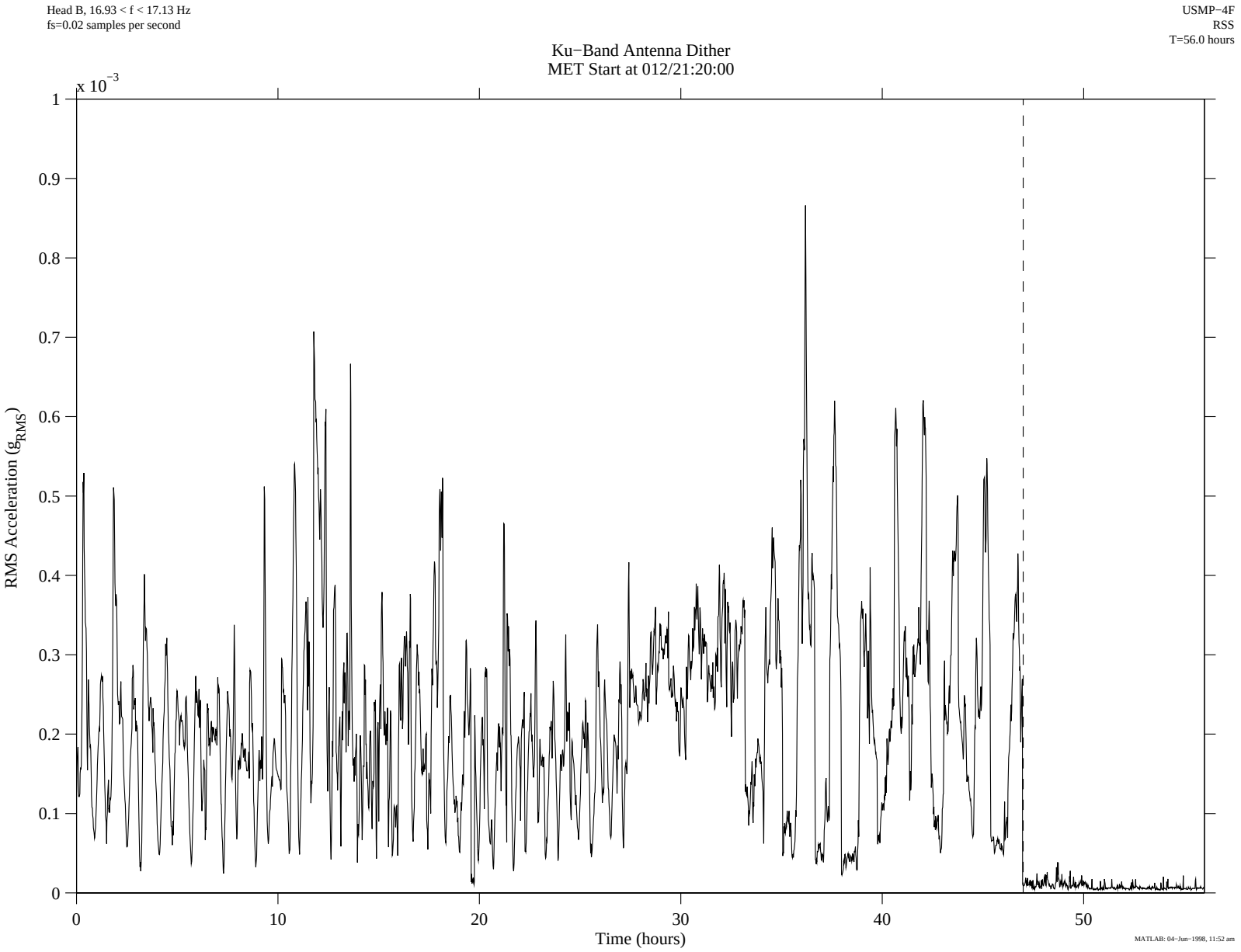

Figure 5. Ku-Band Antenna Dither Cessation (USMP-4).

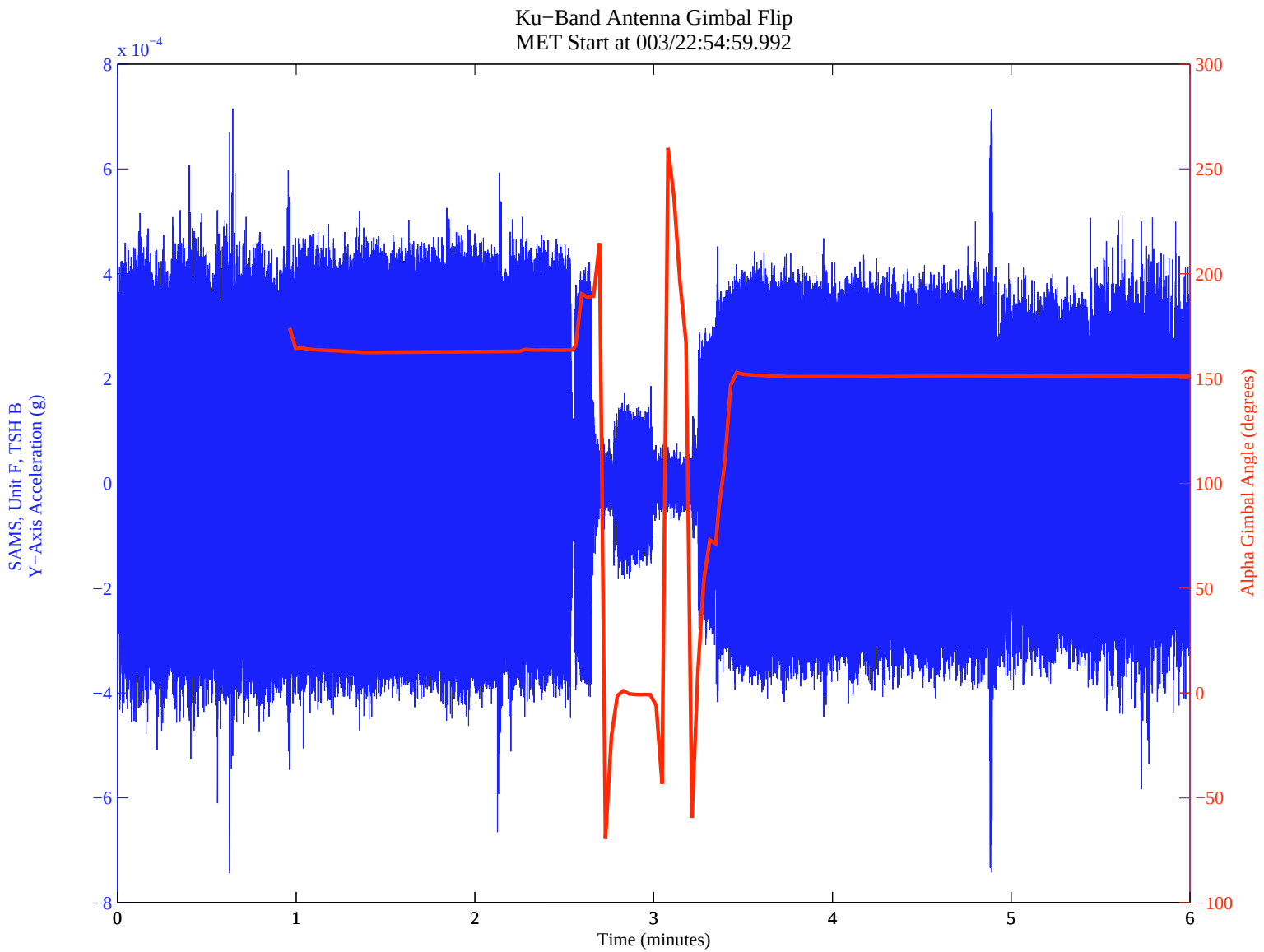

Figure 6. Ku-Band Antenna Gimbal Flip, Acceleration/Alpha Gimbal Angle Overlay.

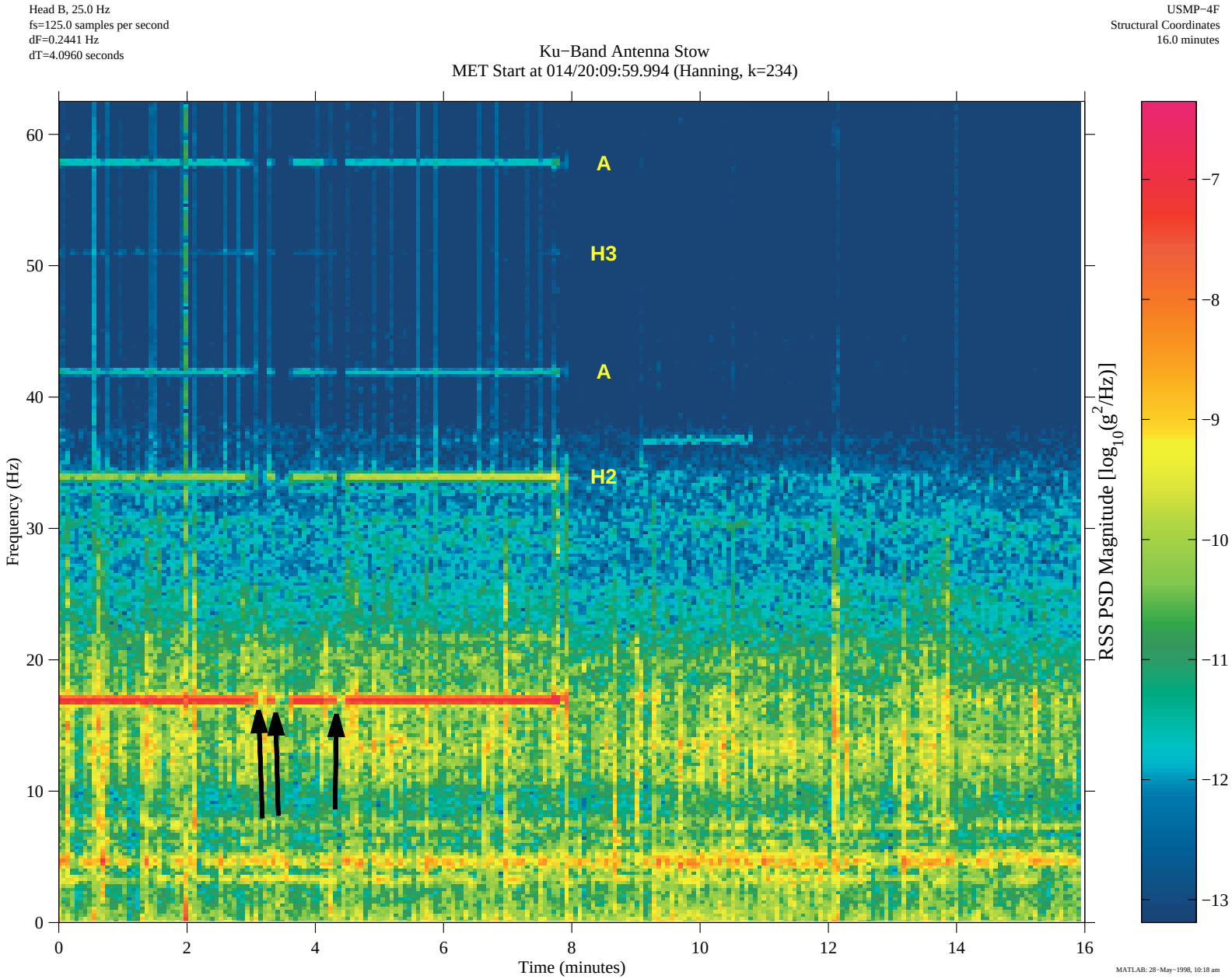

Figure 7. Ku-Band Antenna Stow Spectrogram.

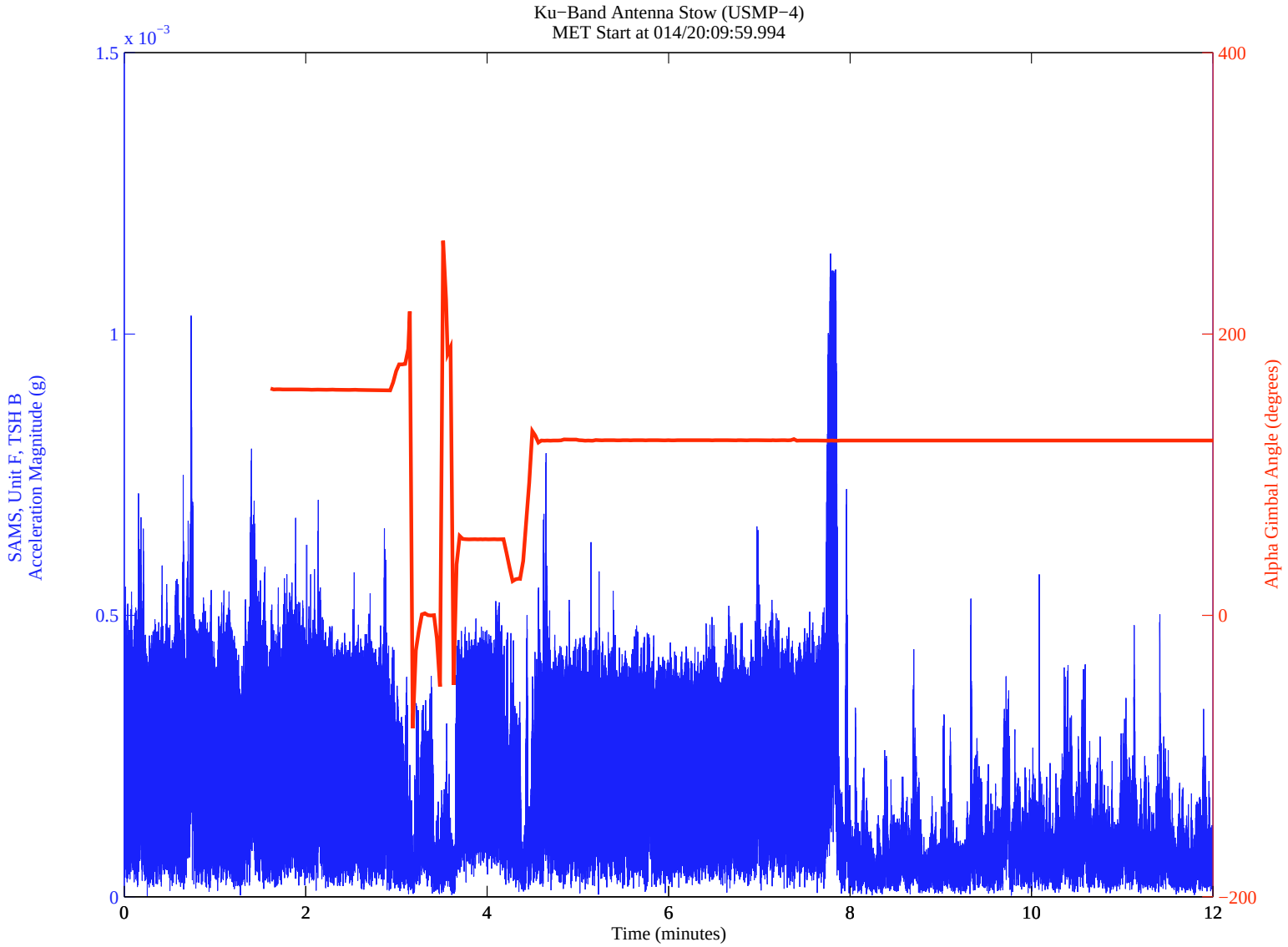

Figure 8. Ku-Band Antenna Stow, Acceleration/Alpha Gimbal Angle Overlay.

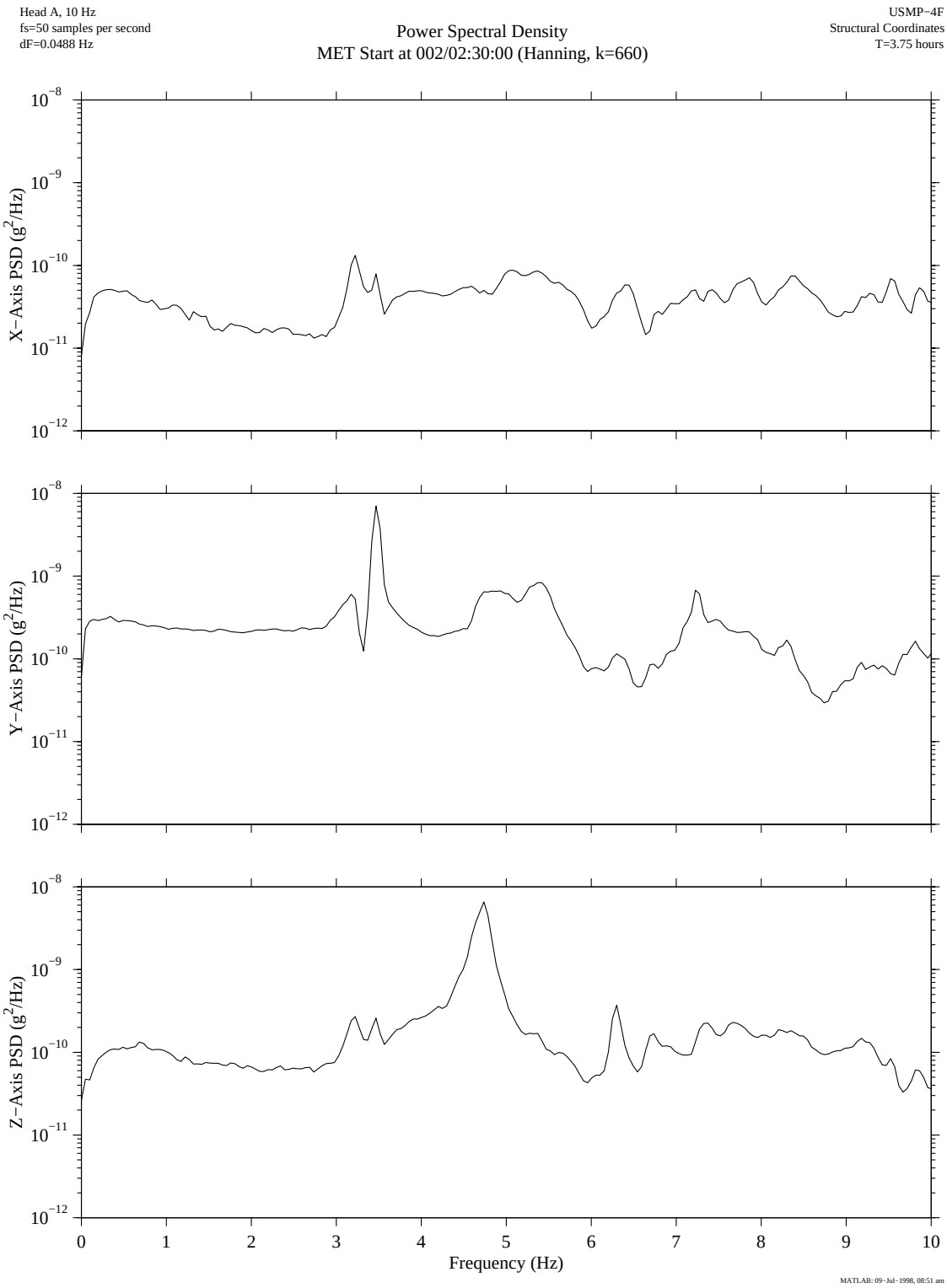

Figure 9. Structural Response to Satellite-Tracking Maneuvers (SAMS Unit F, TSH A).

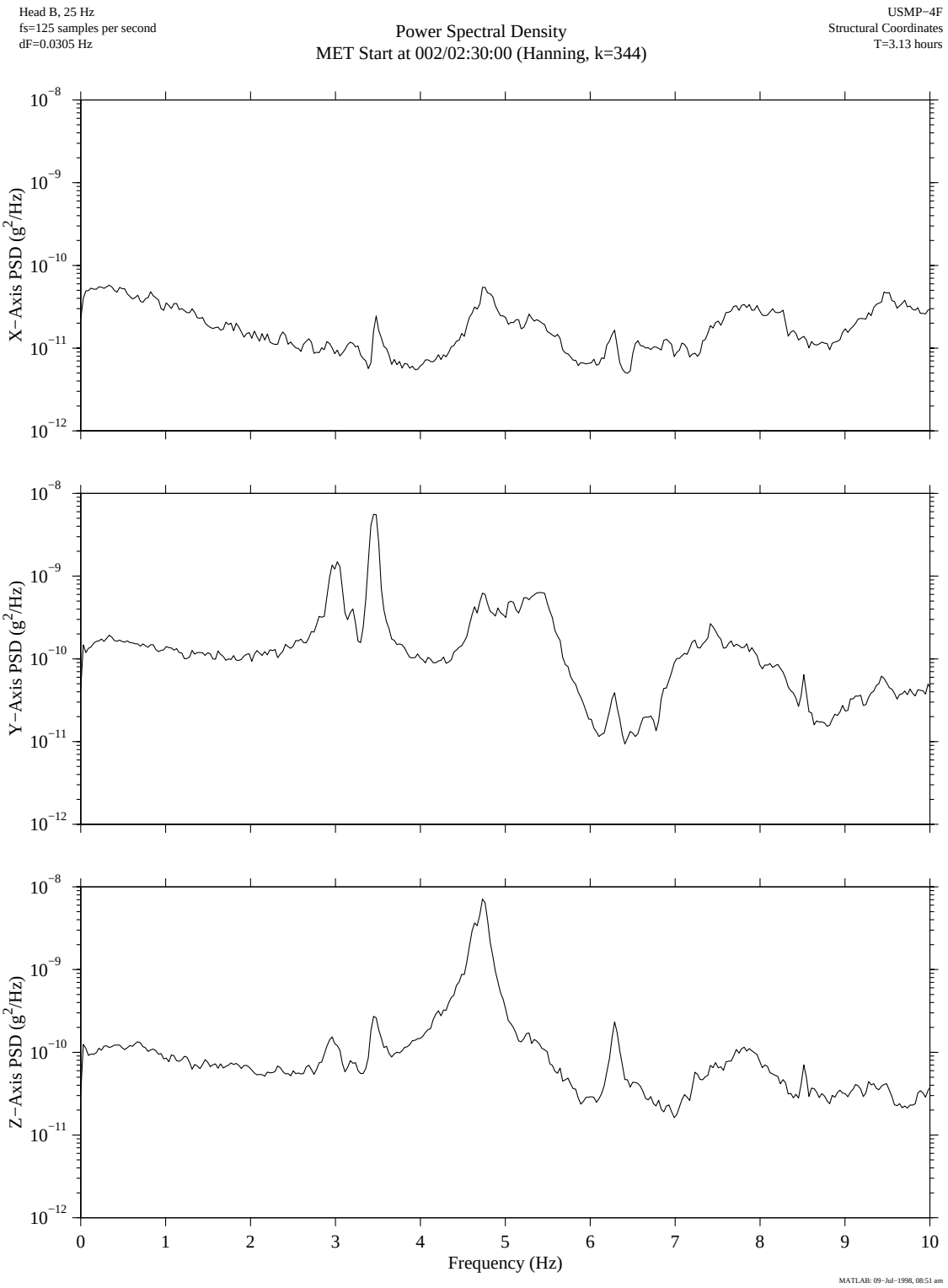

Figure 10. Structural Response to Satellite-Tracking Maneuvers (SAMS Unit F, TSH B).

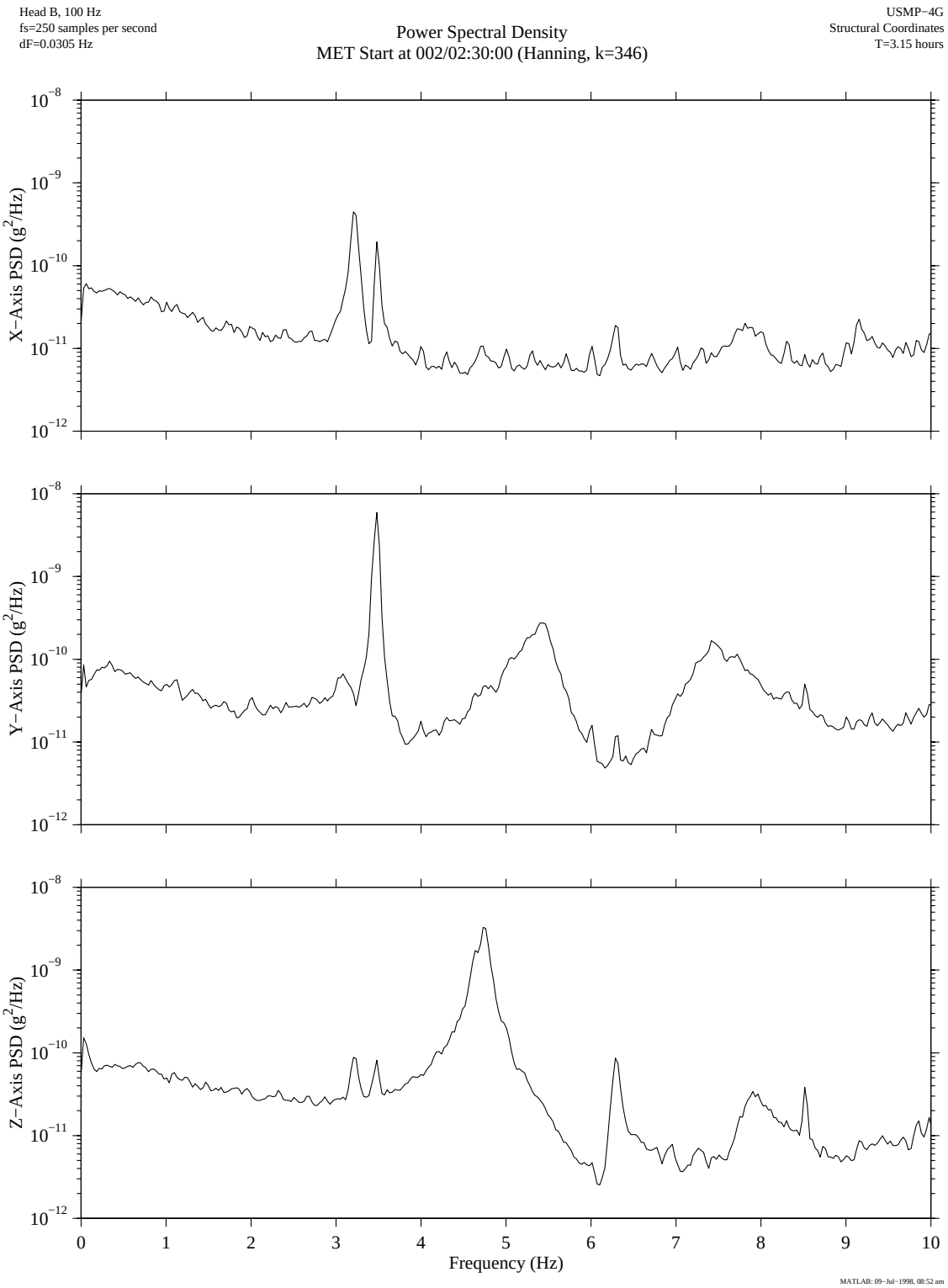

Figure 11. Structural Response to Satellite-Tracking Maneuvers (SAMS Unit G, TSH B).

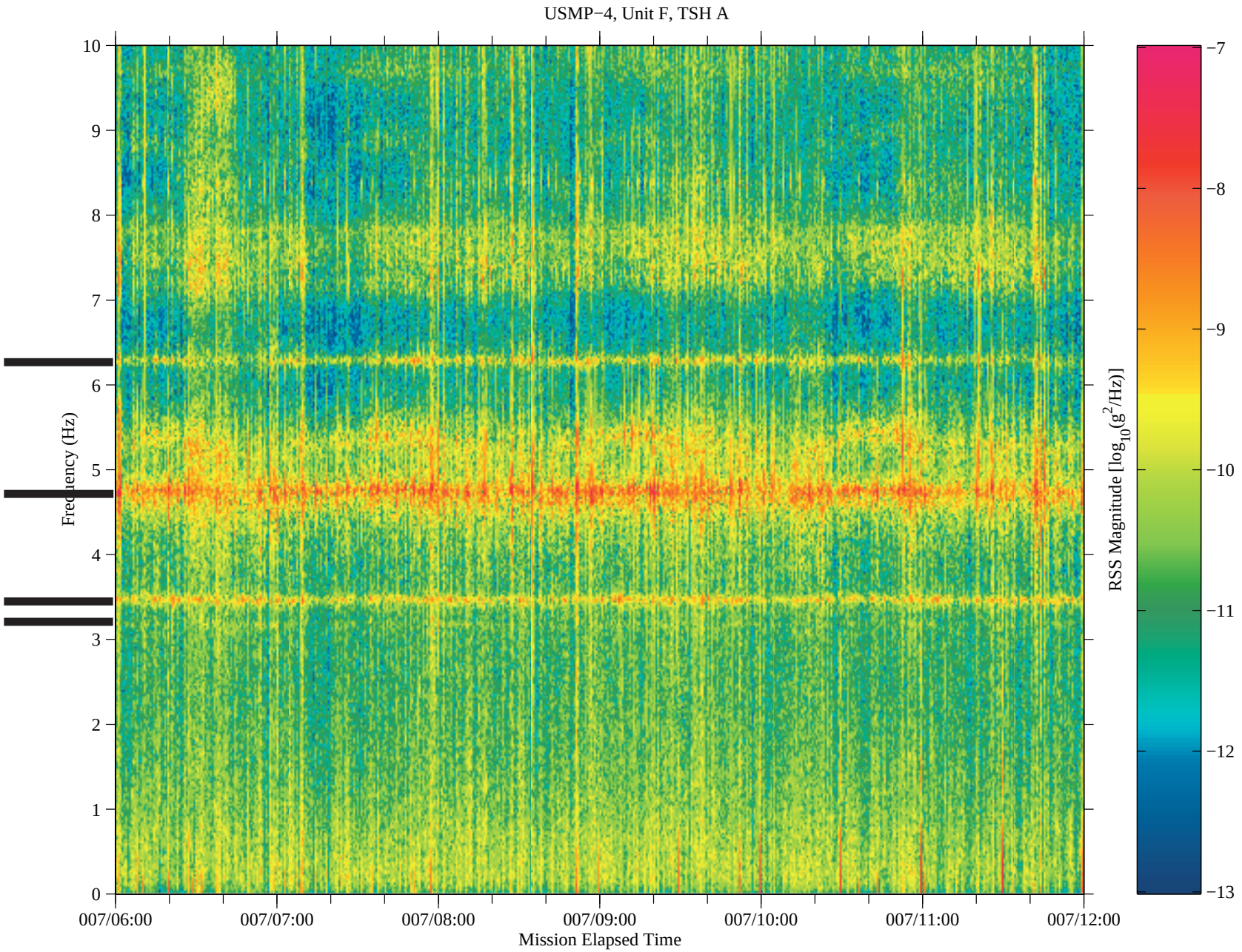

Figure 12. Structural Modes Spectrogram.

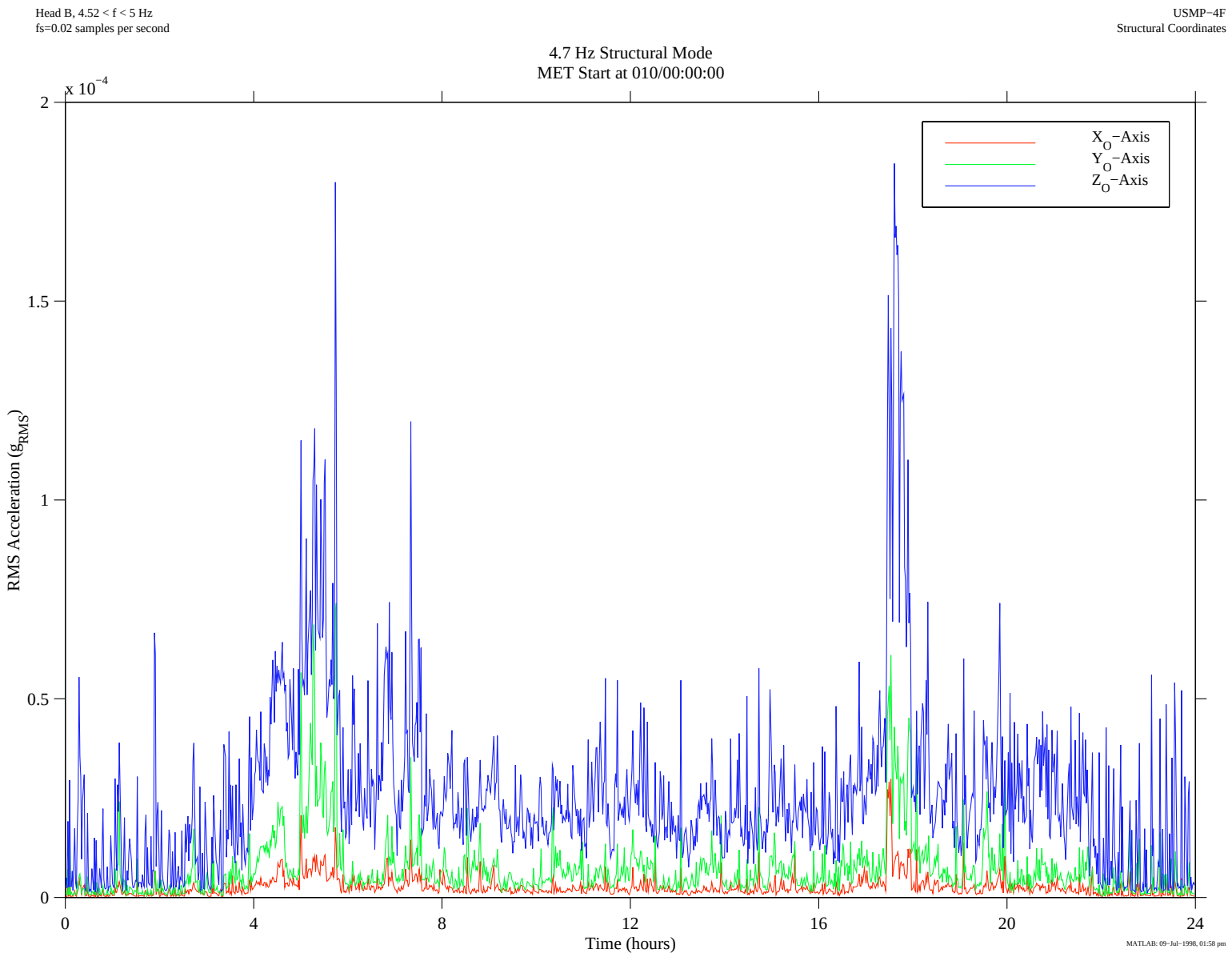

Figure 13. Structural Mode (4.7 Hz) XYZ RMS Acceleration Versus Time.

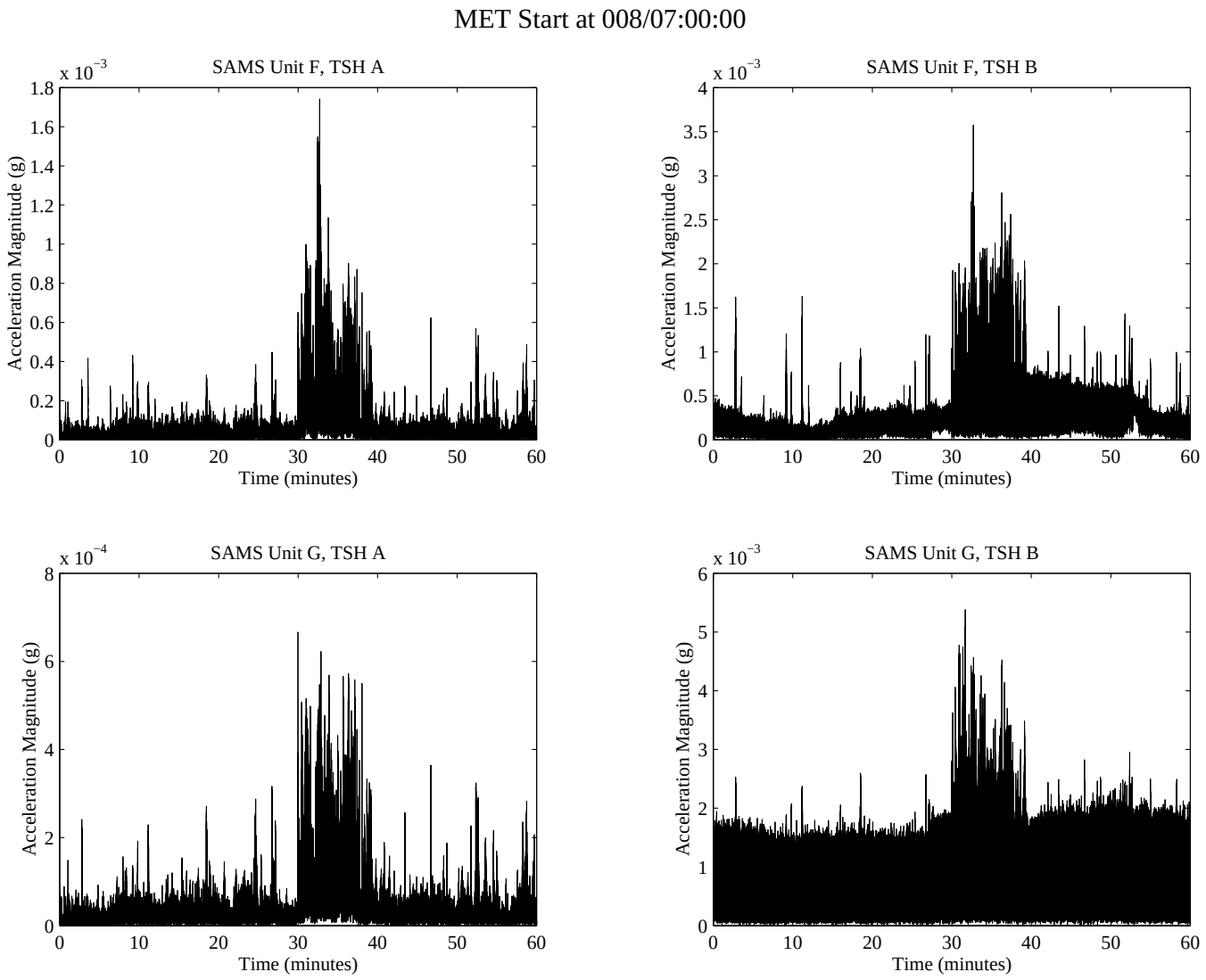

Figure 14. Heightened Acceleration Magnitude During Deadband Collapse.

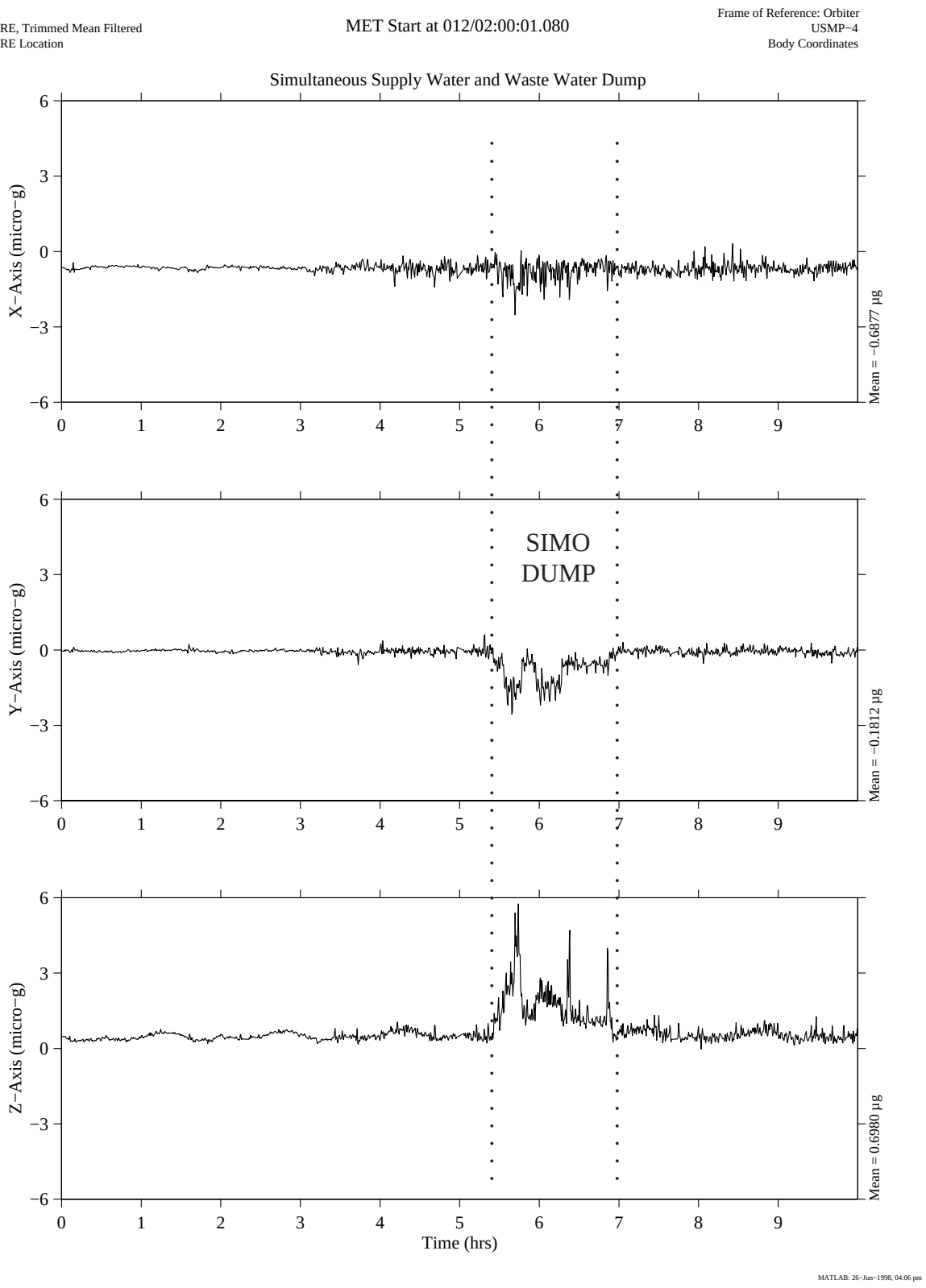

Figure 15. OARE Data Collected During a Simultaneous Supply and Waste Water Dump. MET Start at 012/02:00.

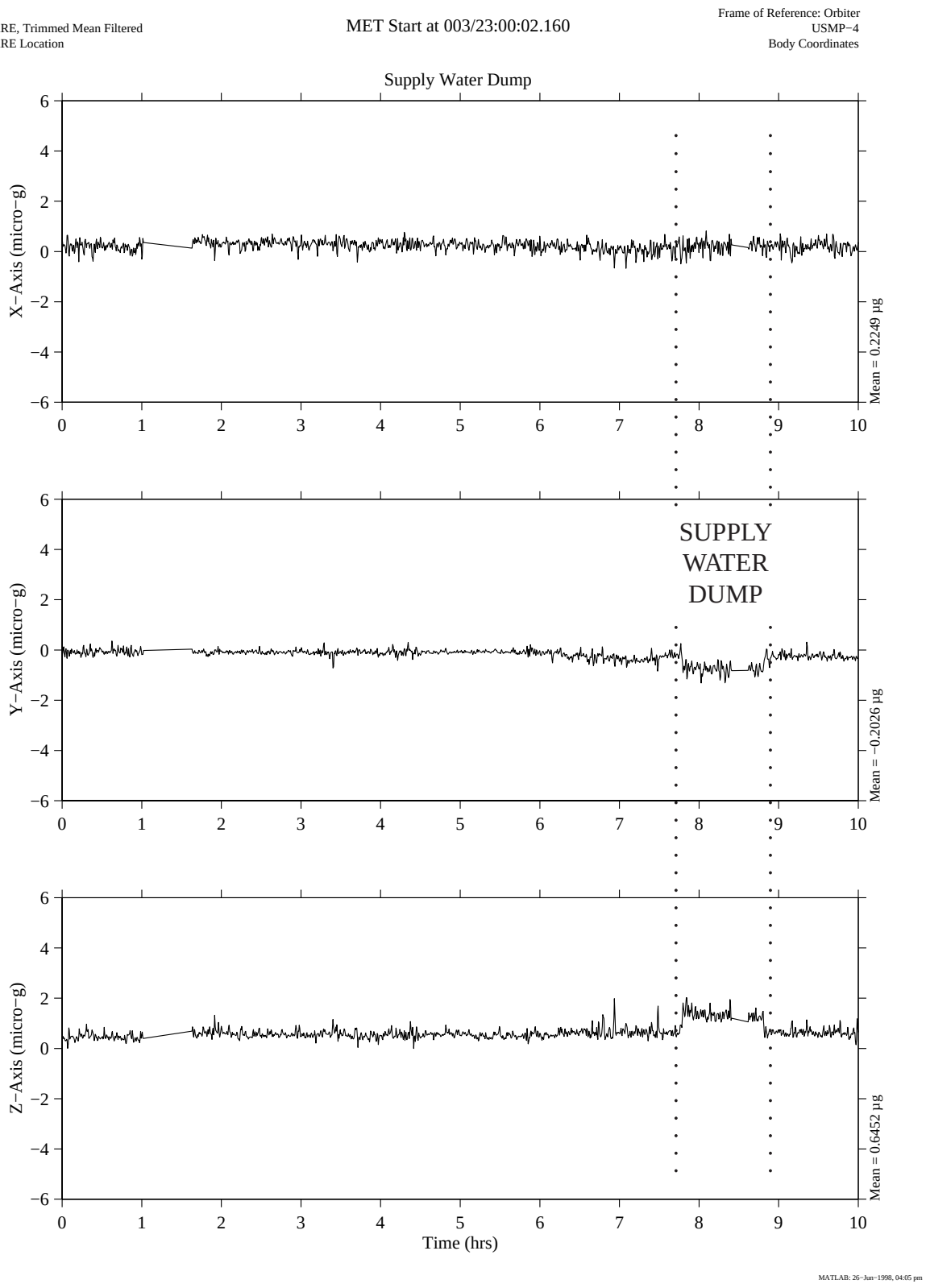

Figure 16. OARE Data Collected During a Supply Water Dump Starting at Approximately MET 004/07:00.

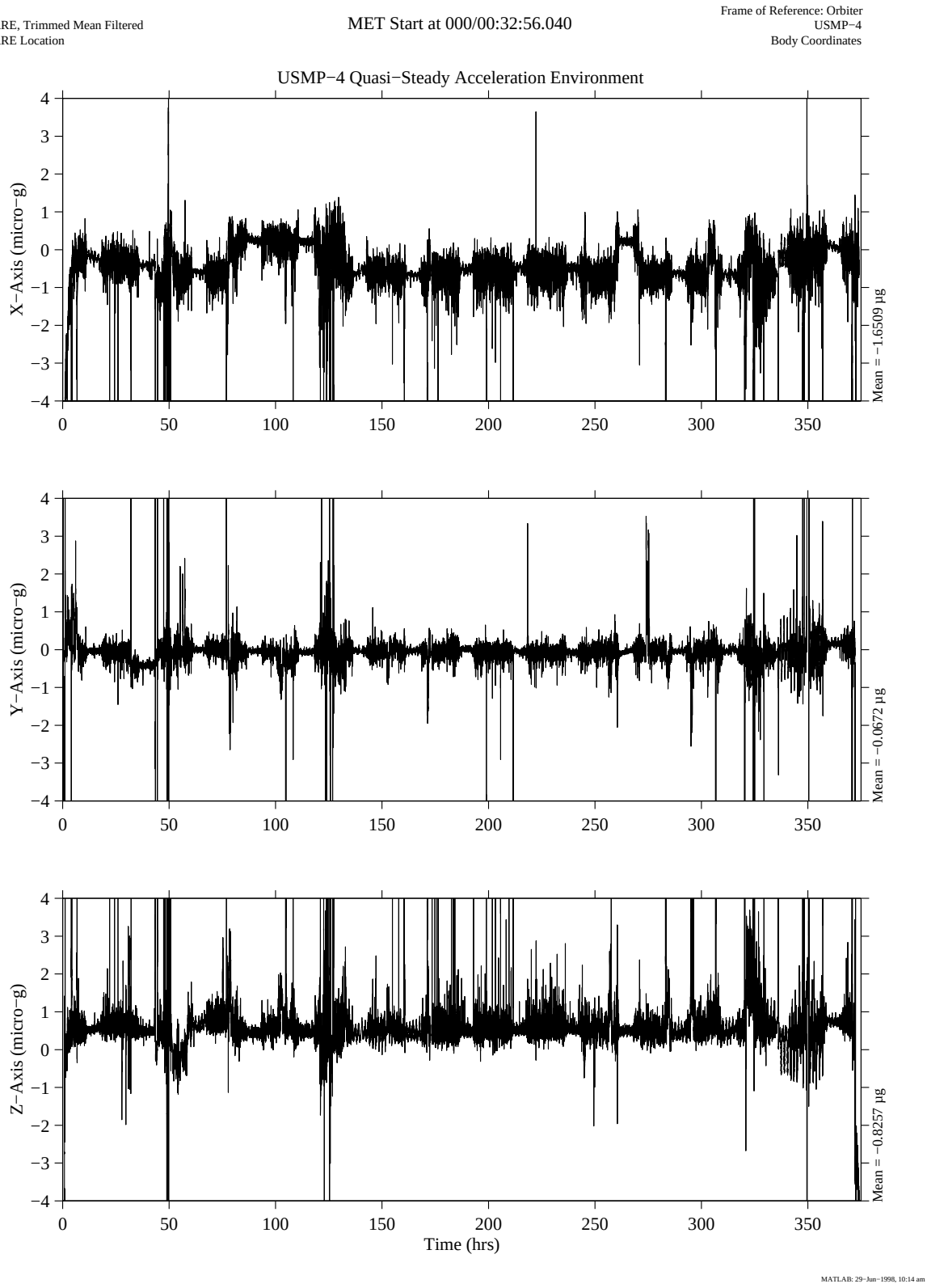

Figure 17. Trimmean Filtered OARE Data Versus Time for the STS-87 Mission.

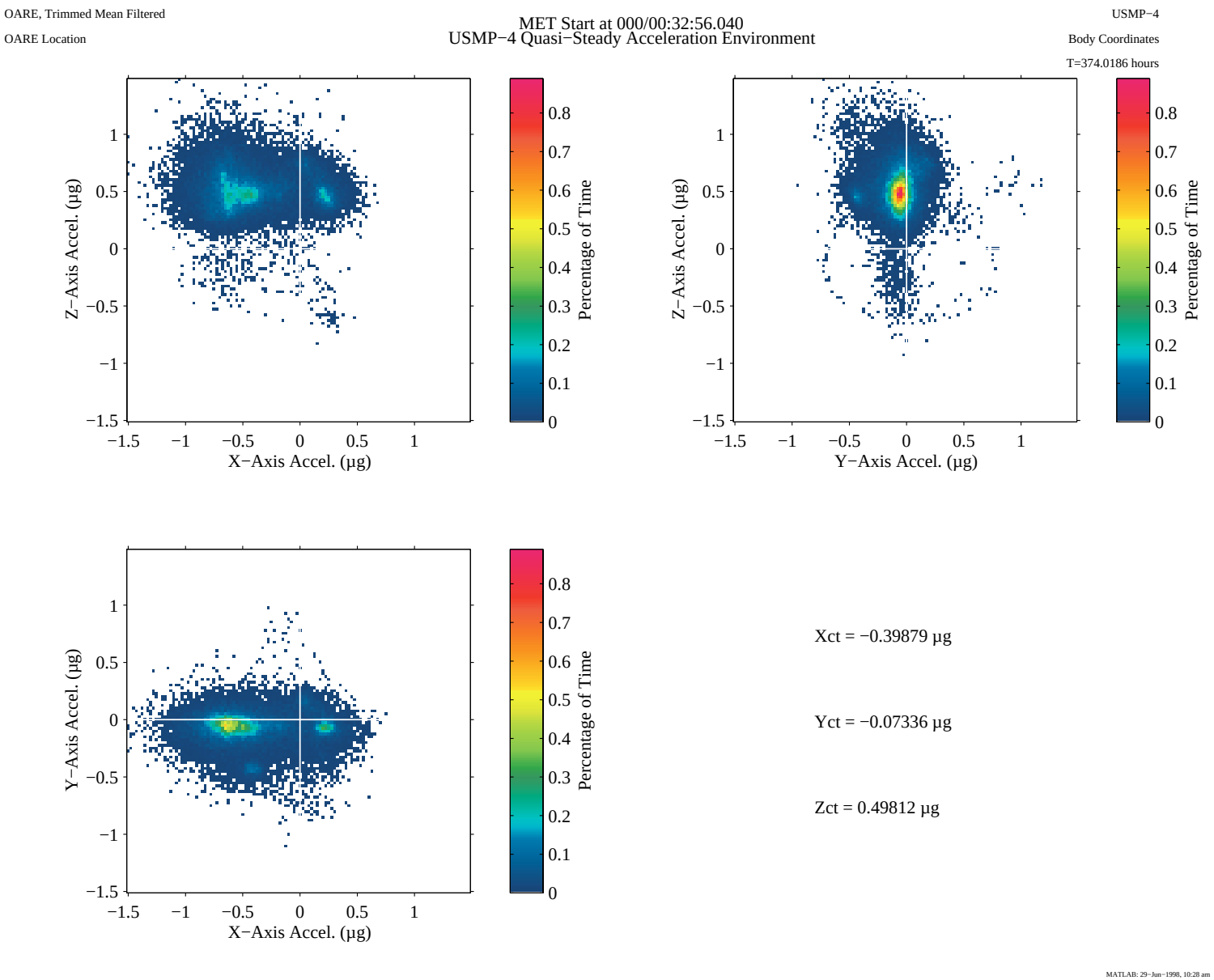

Figure 18. Quasi-Steady Three-Dimensional Histogram of Trimmean Filtered OARE Data for the STS-87 Mission.

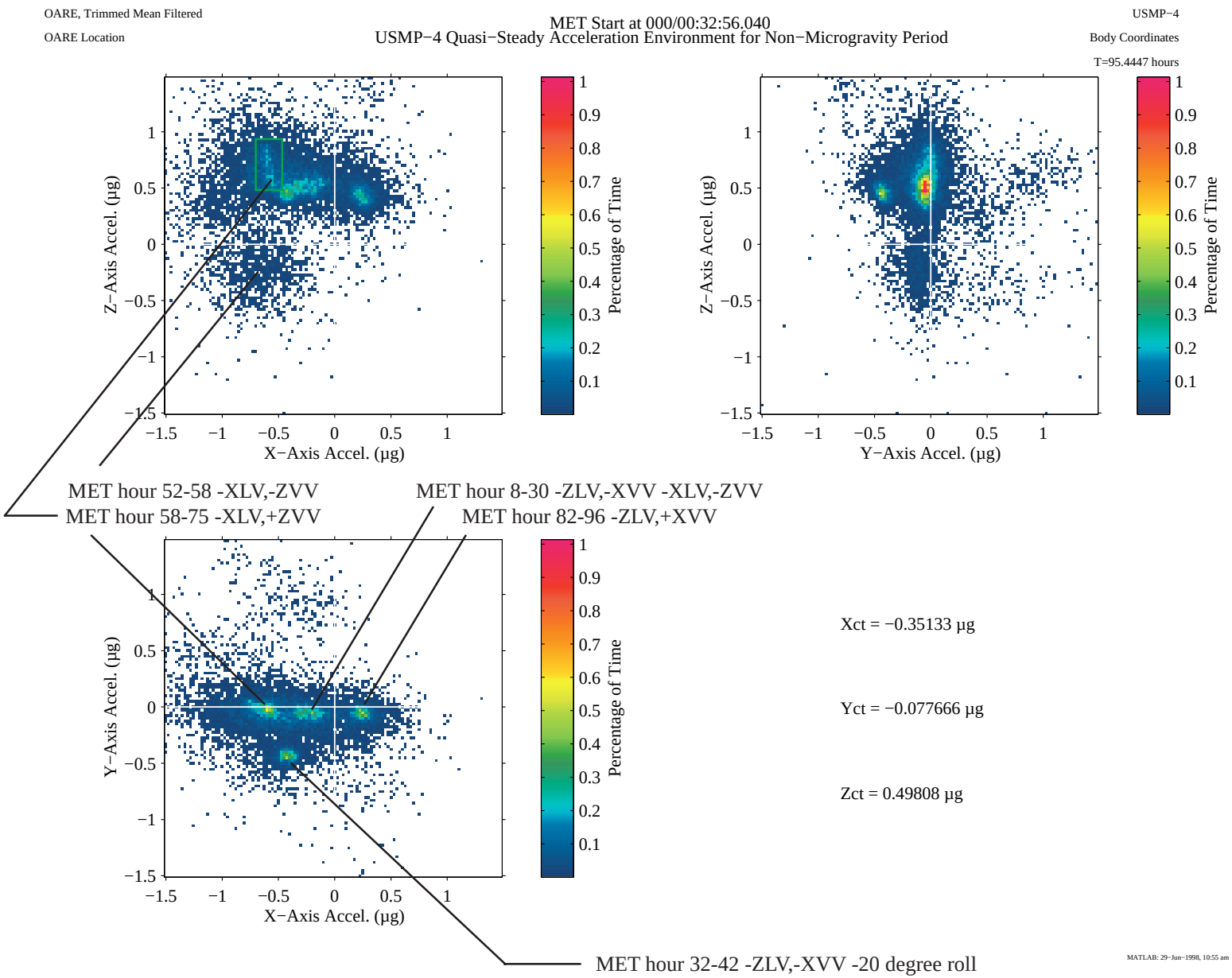

Figure 19. Quasi-Steady Three-Dimensional Histogram of the Non-Microgravity Period for the STS-87 Mission.

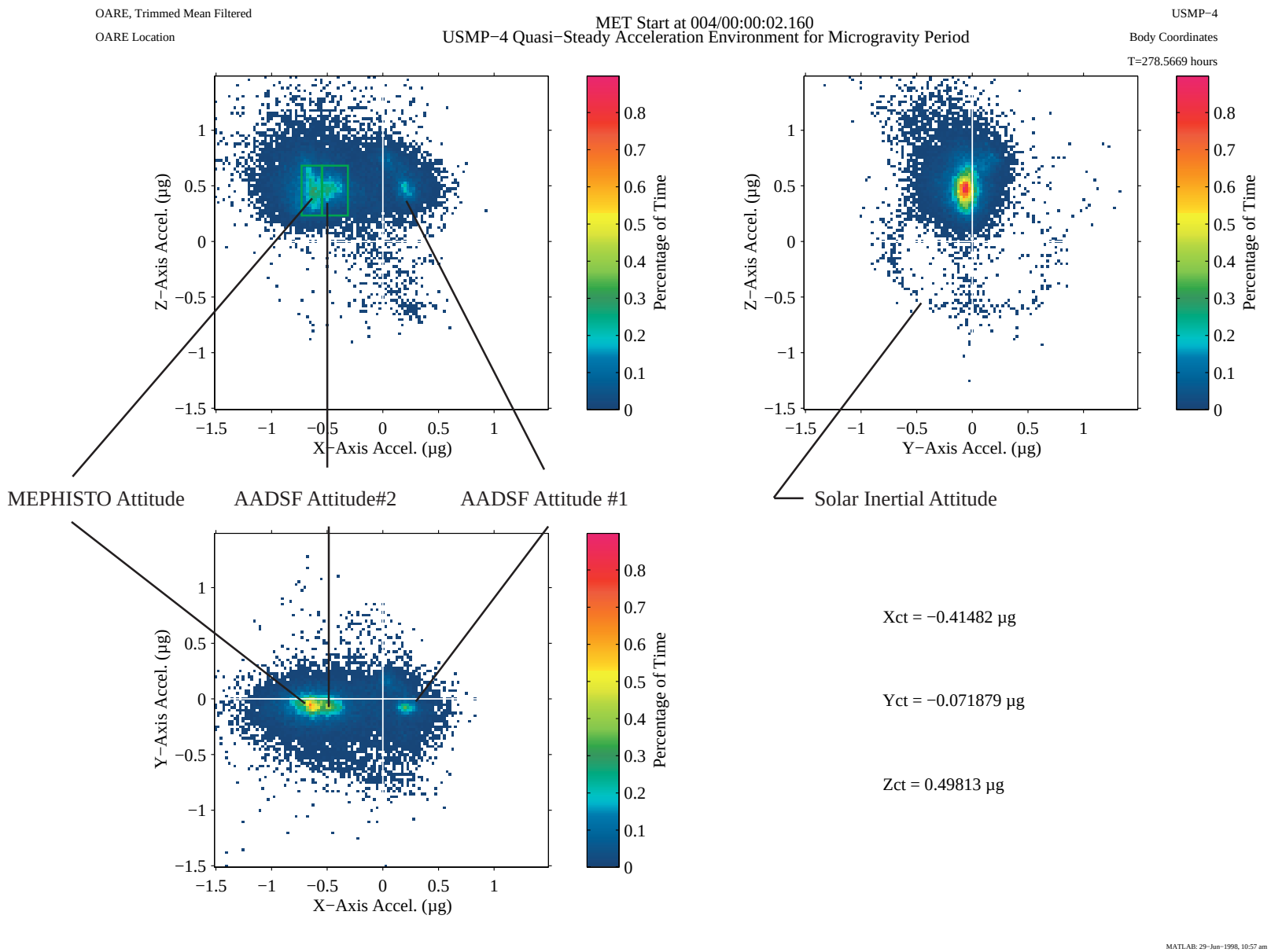

Figure 20. Quasi-Steady Three-Dimensional Histogram of the Microgravity Period for the STS-87 Mission.

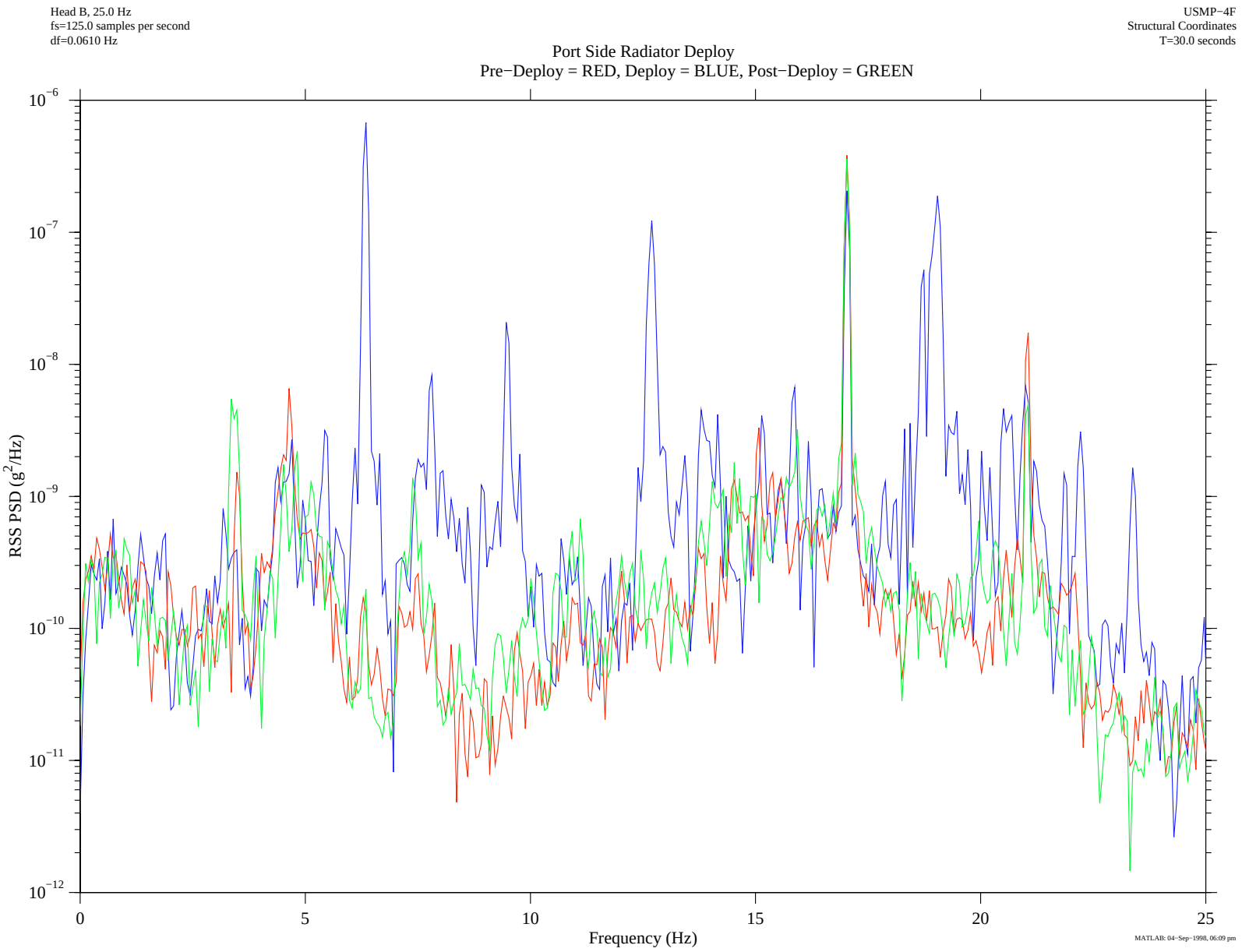

Figure 21. Port Side Radiator Deploy PSD.

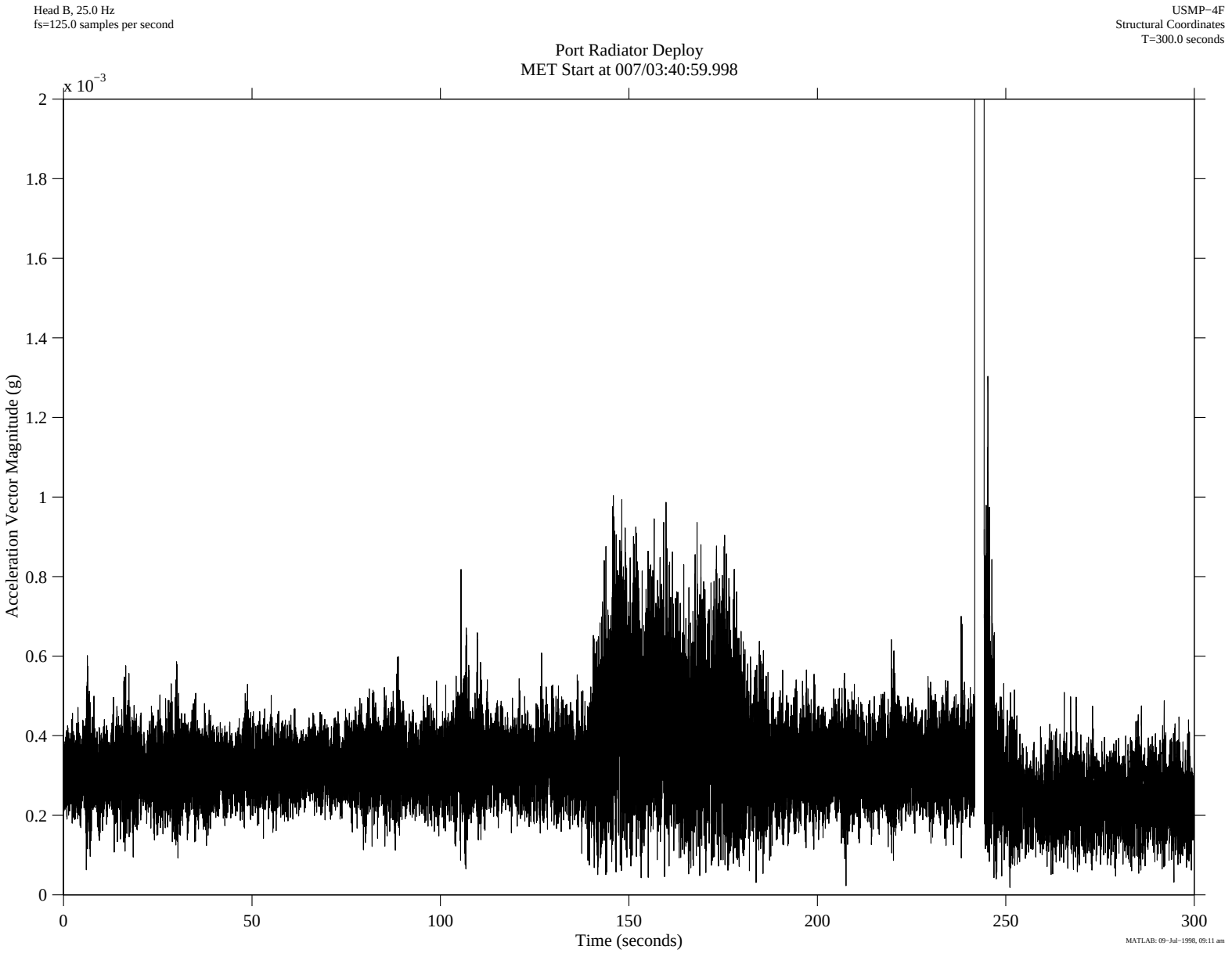

Figure 22. Port Radiator Deploy.

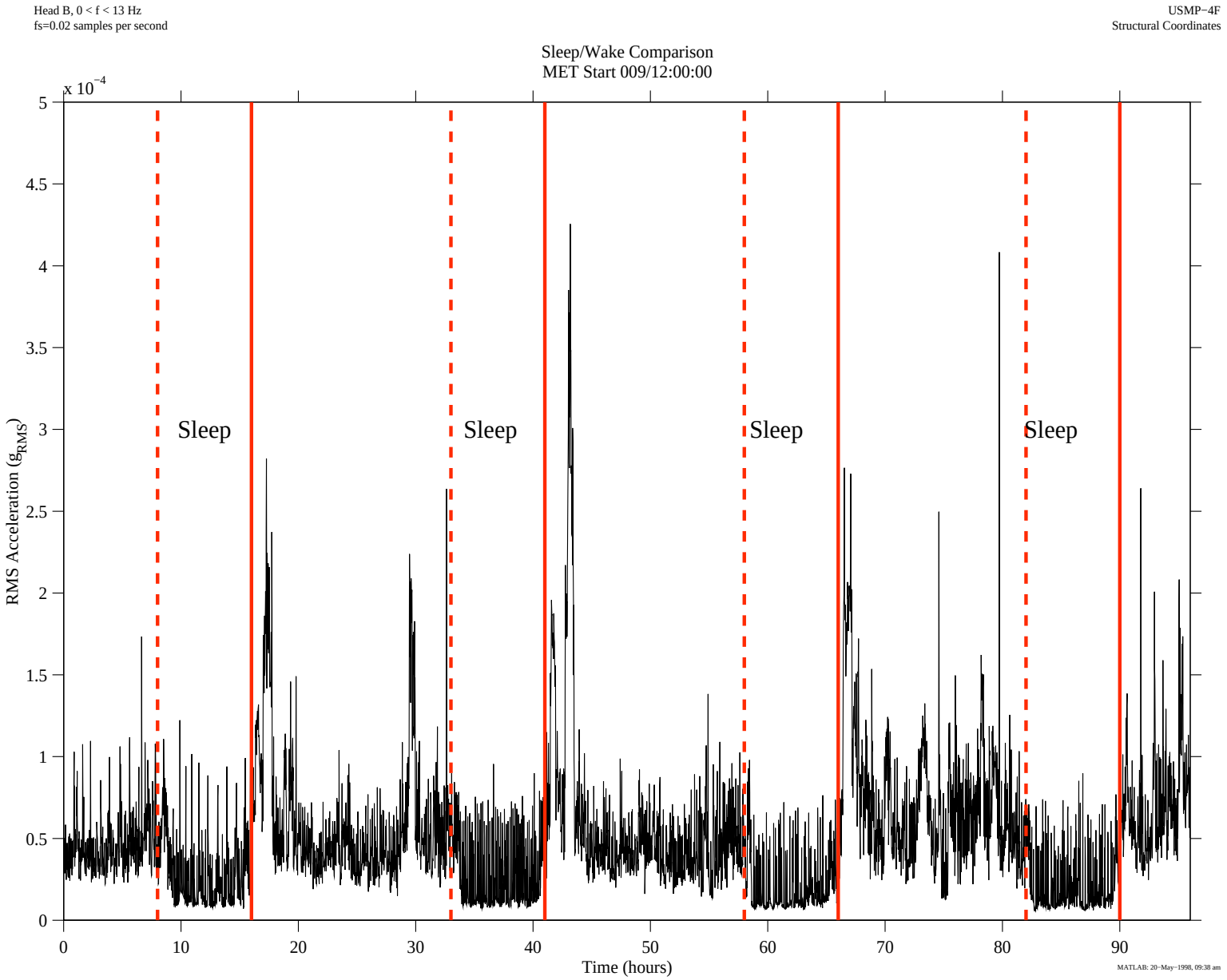

Figure 23. Sleep/Wake RMS Acceleration Comparison.

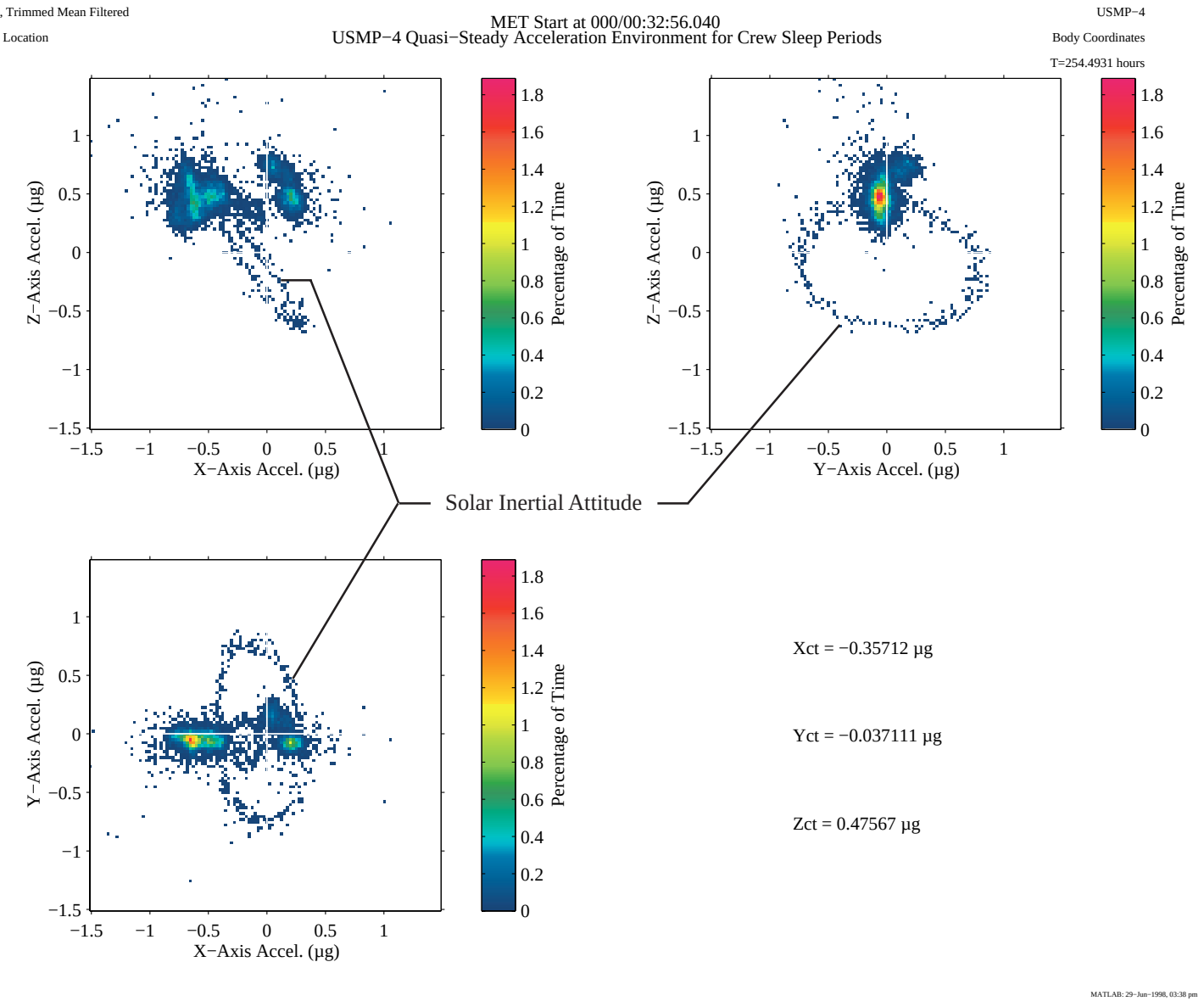

Figure 24. Quasi-Steady Three-Dimensional Histogram for Crew Sleep Periods During the STS-87 Mission.

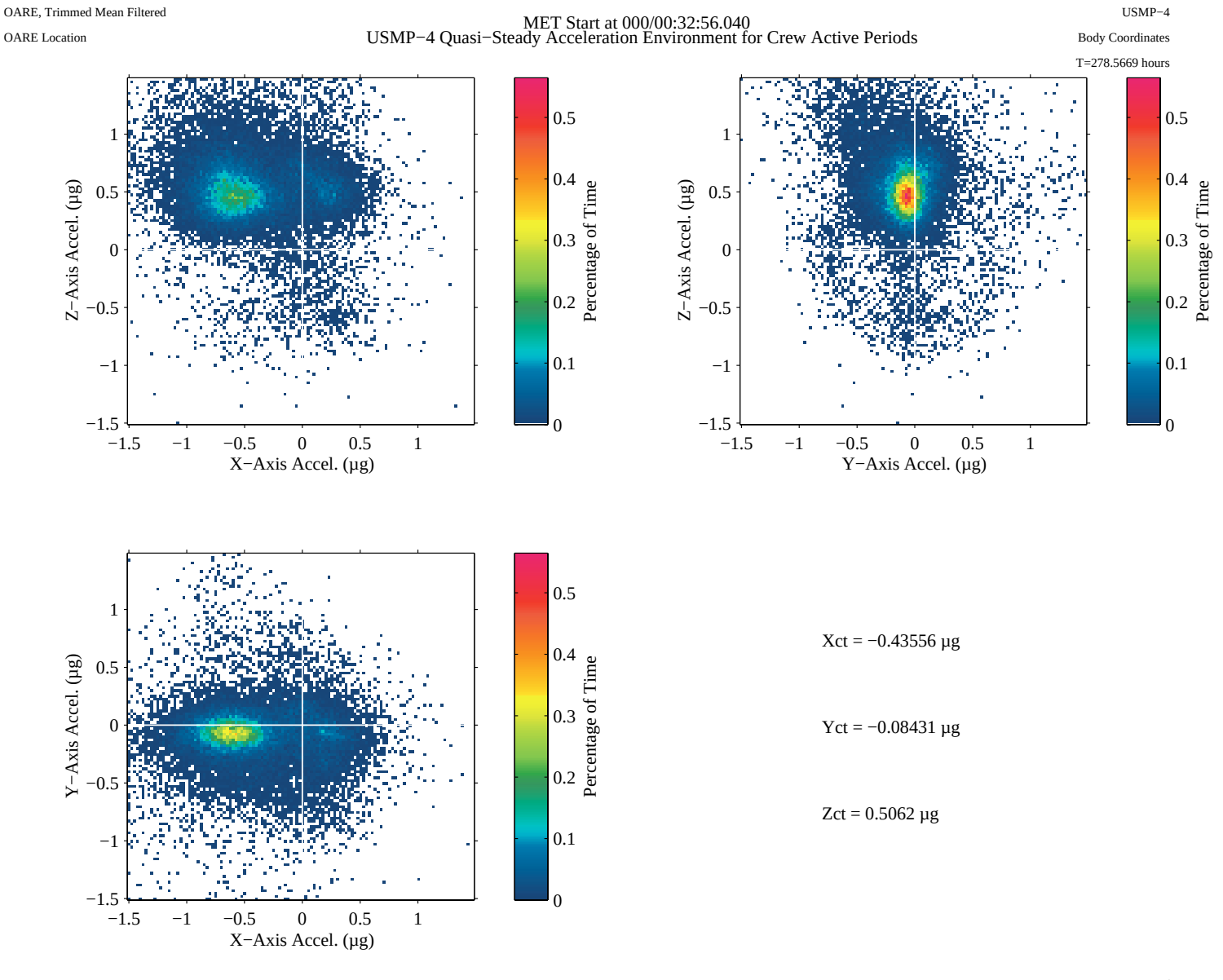

Figure 25. Quasi-Steady Three-Dimensional Histogram for Crew Active Periods During the STS-87 Mission.

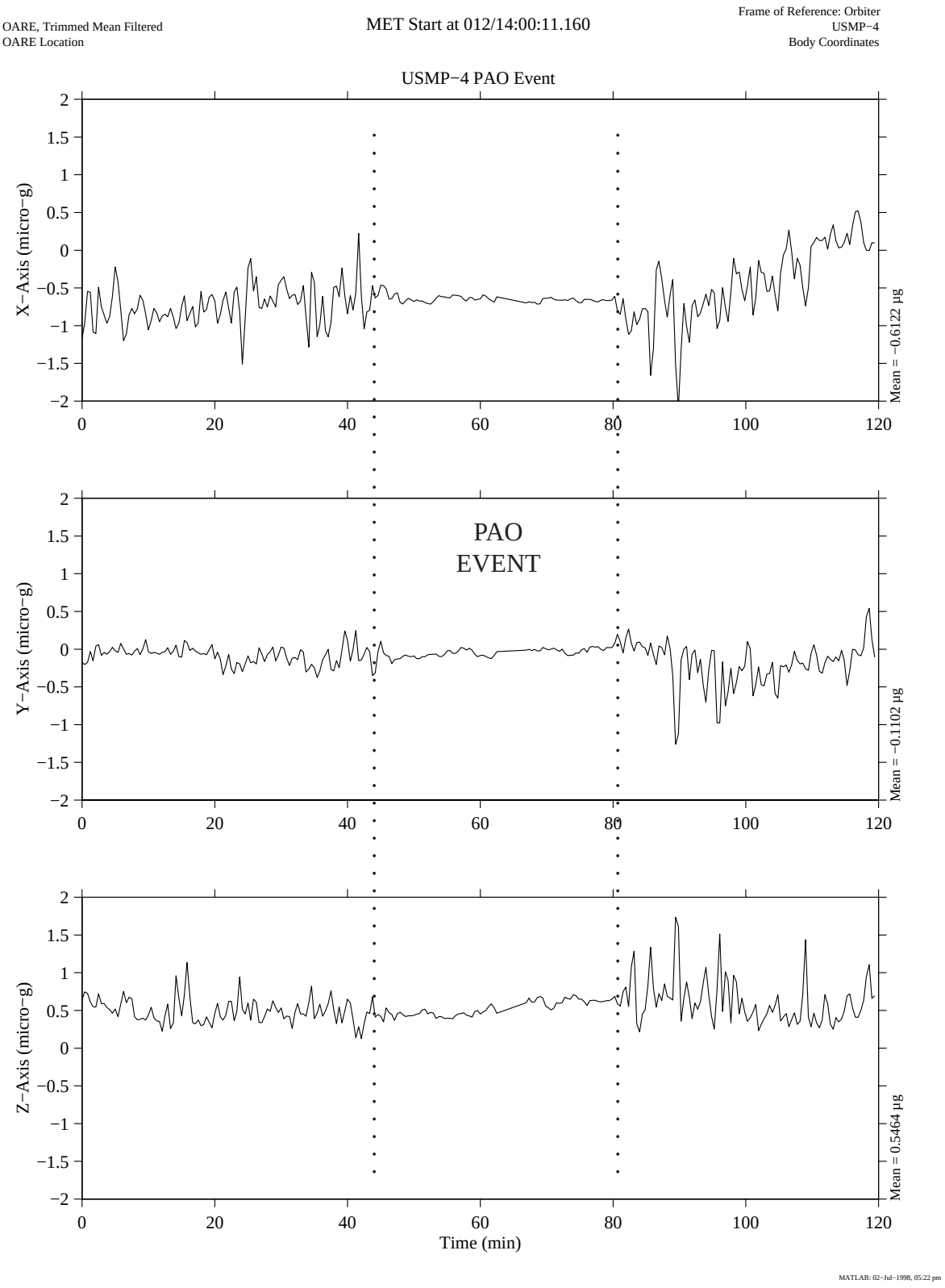

Figure 26. Trimmean Filter OARE Data During an STS-87 PAO Event.

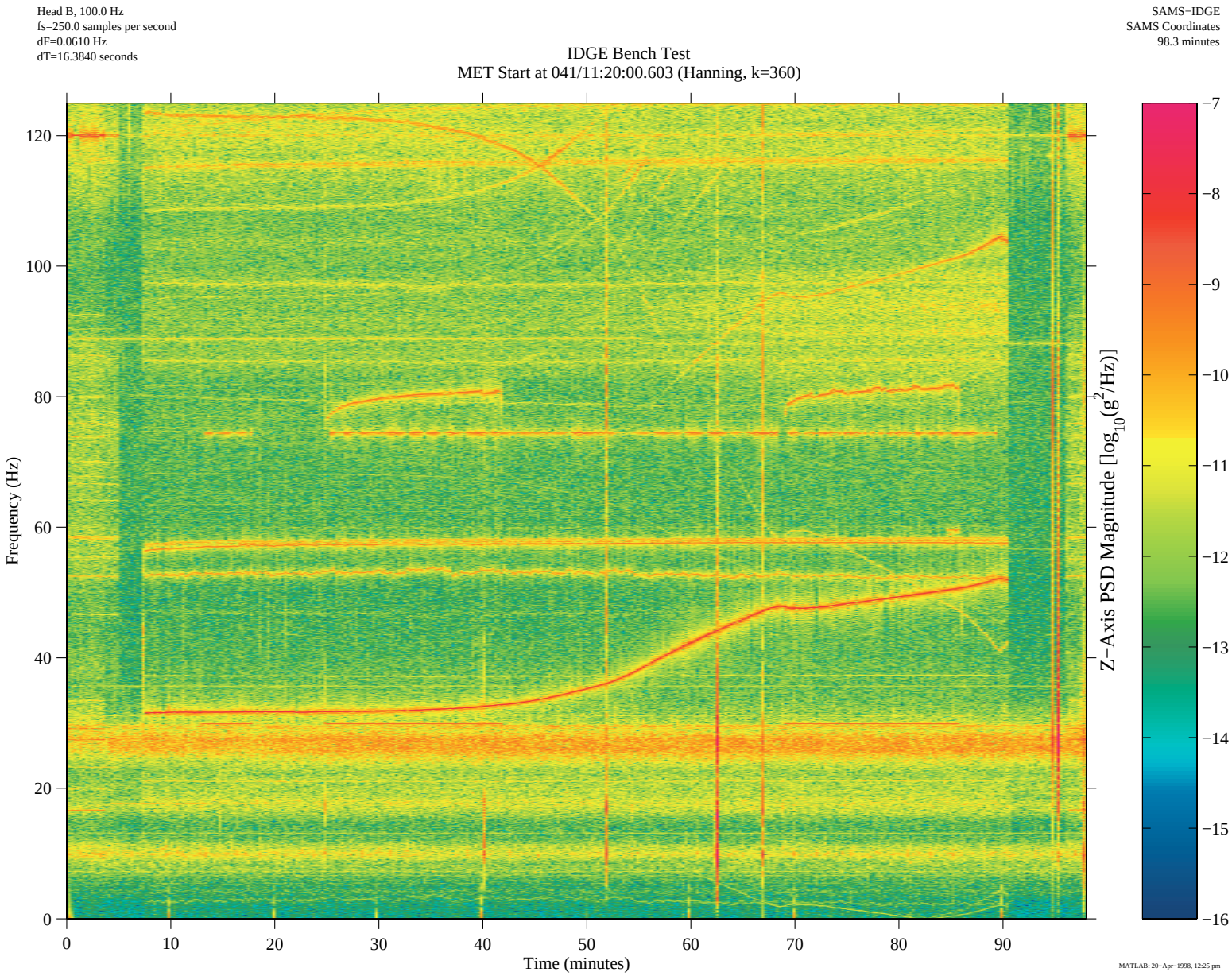

Figure 27. Spectrogram for SAMS/IDGE Bench Test.

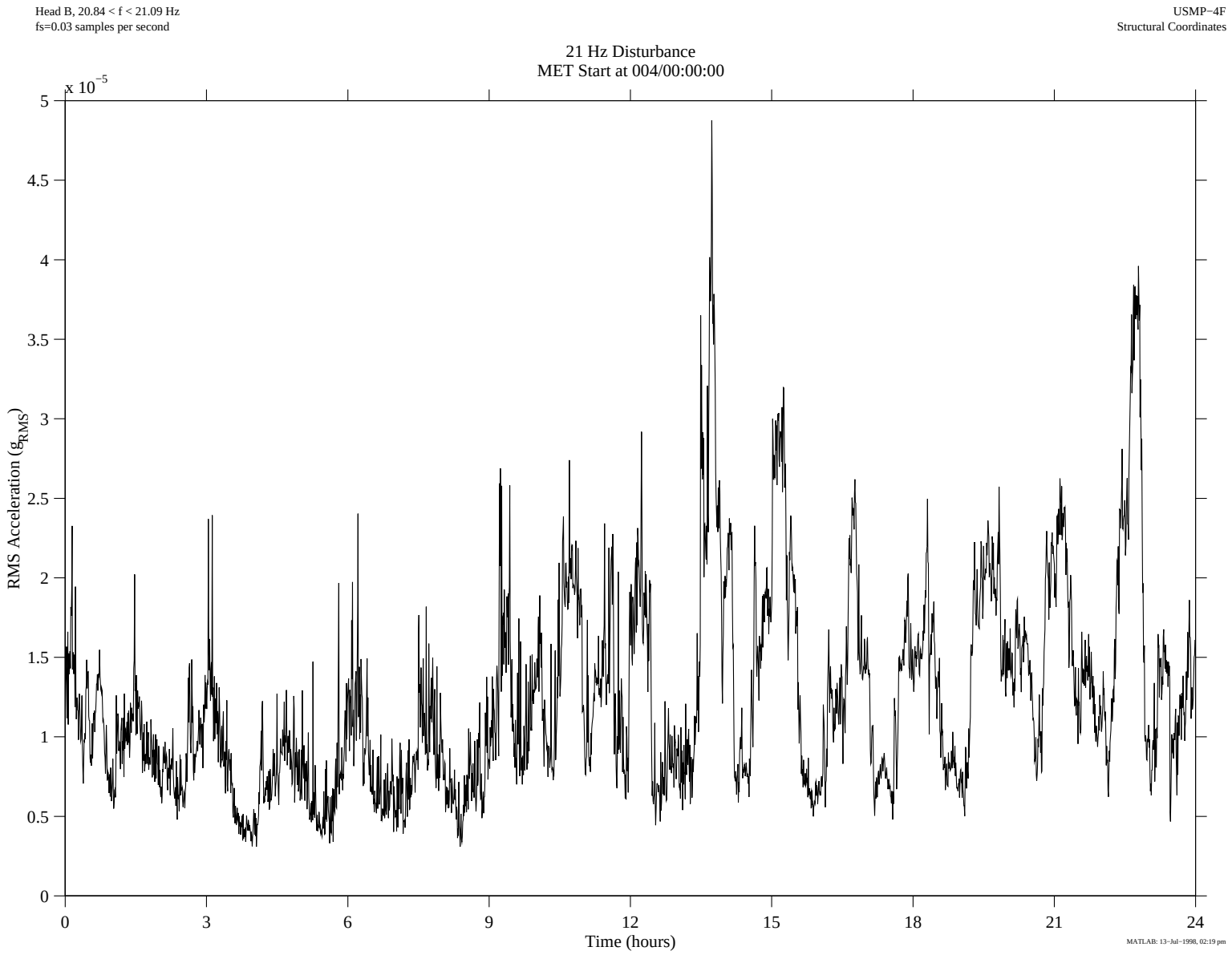

Figure 28. RMS Acceleration Versus Time for 21 Hz Disturbance.

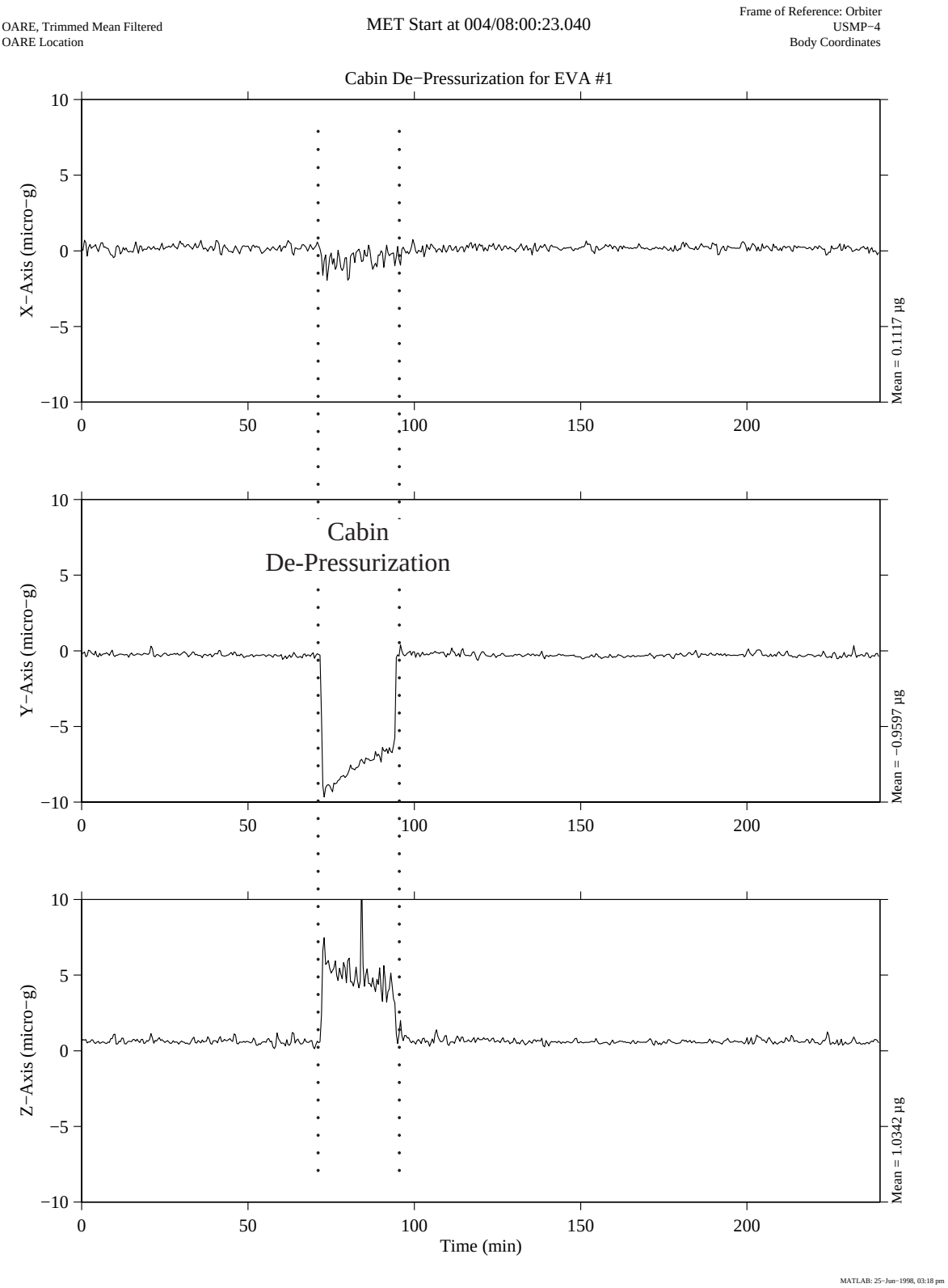

Figure 29. Cabin De-Pressurization in Preparation for EVA #1.

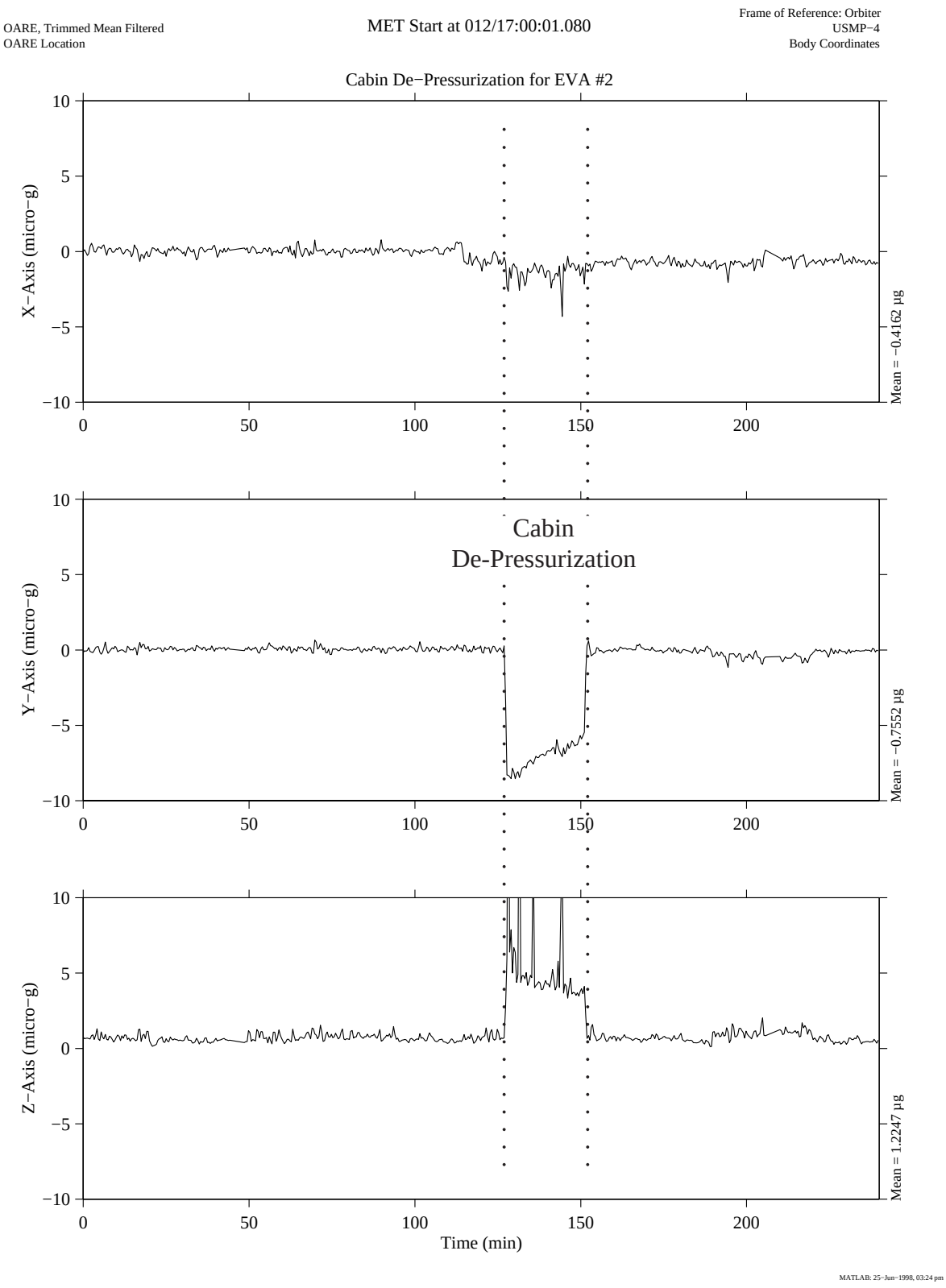

Figure 30. Cabin De-Pressurization in Preparation for EVA #2.

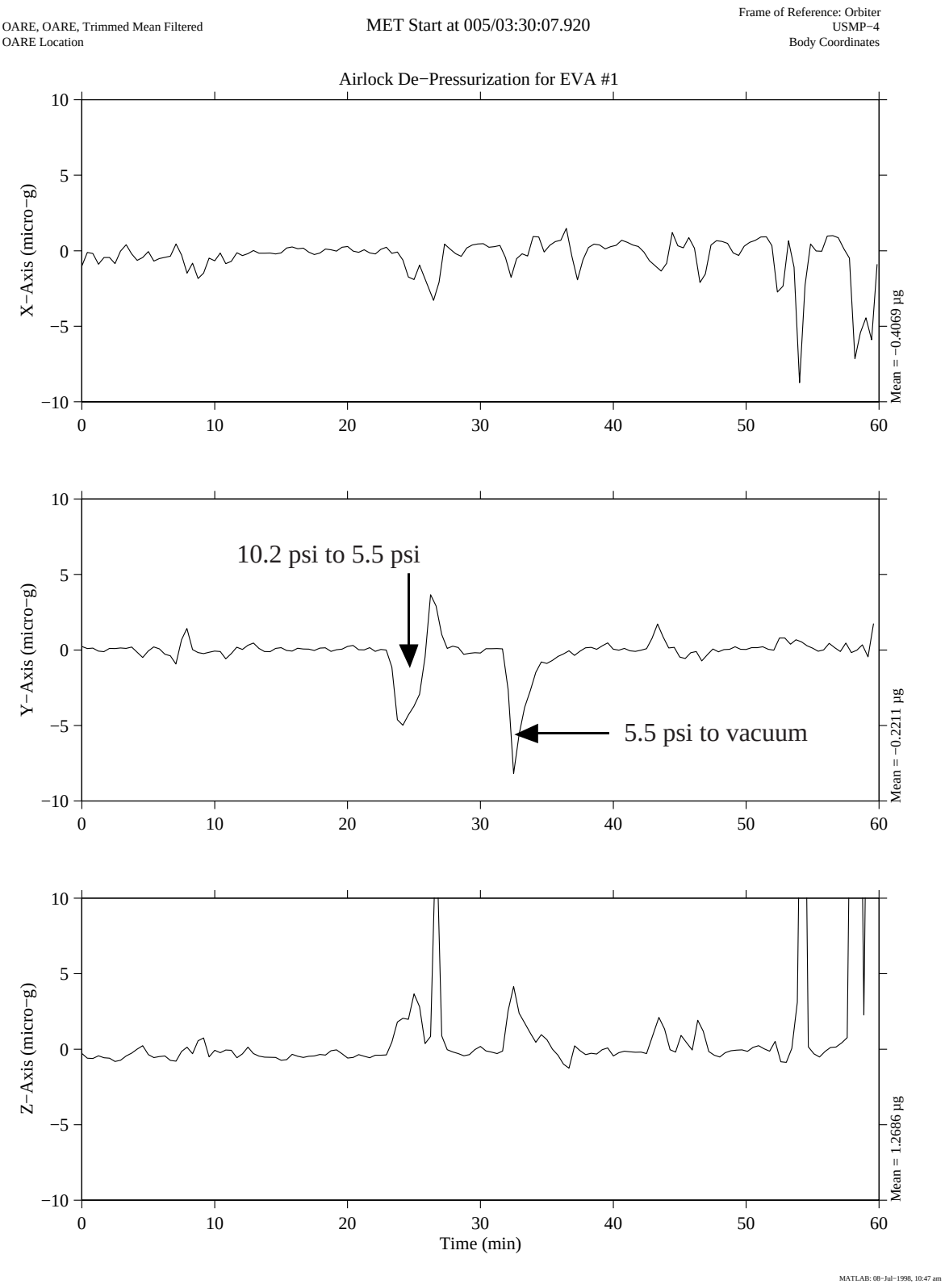

Figure 31. Airlock De-Pressurization in Preparation for EVA #1.

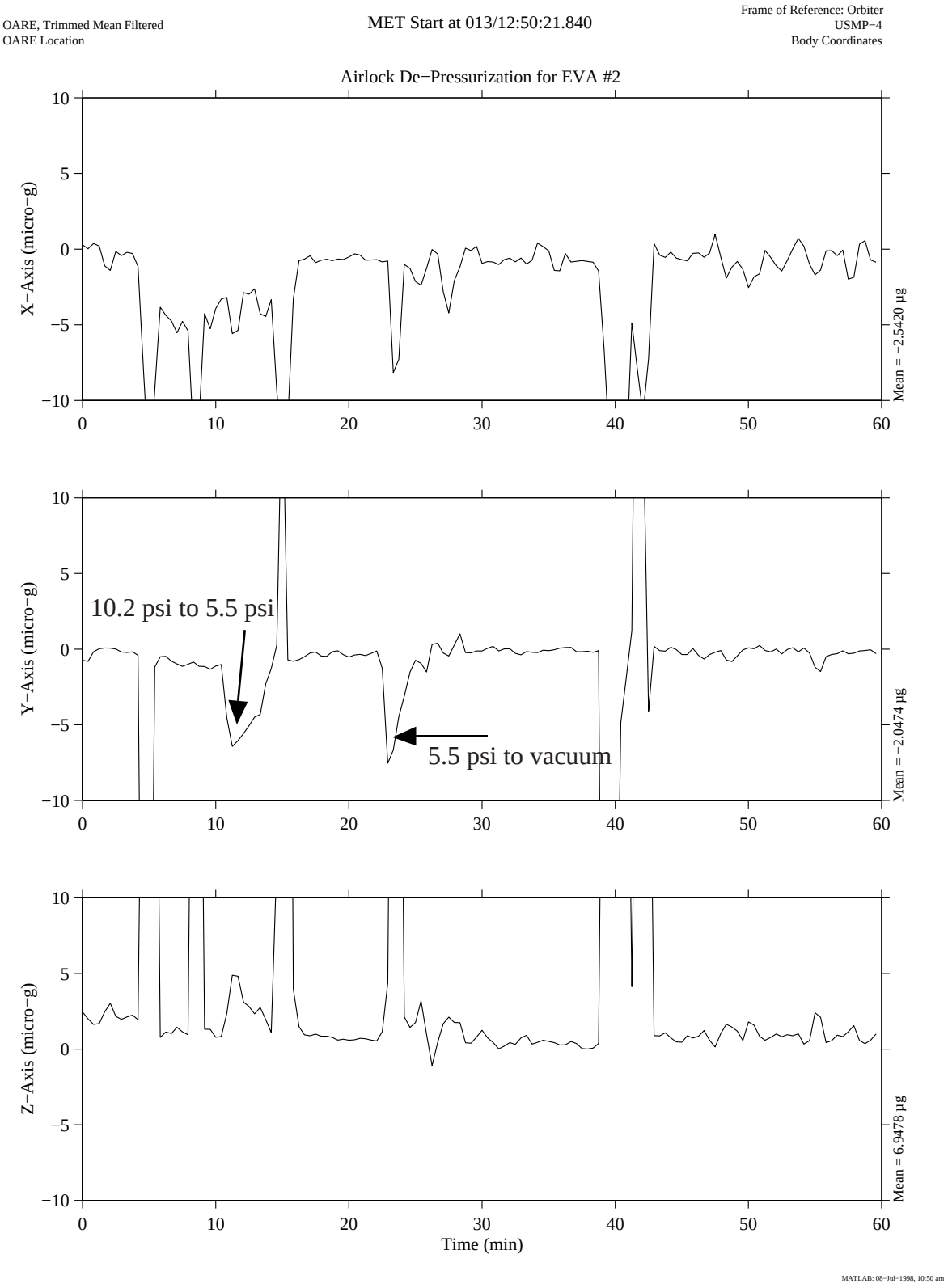

Figure 32. Airlock De-Pressurization in Preparation for EVA #2.

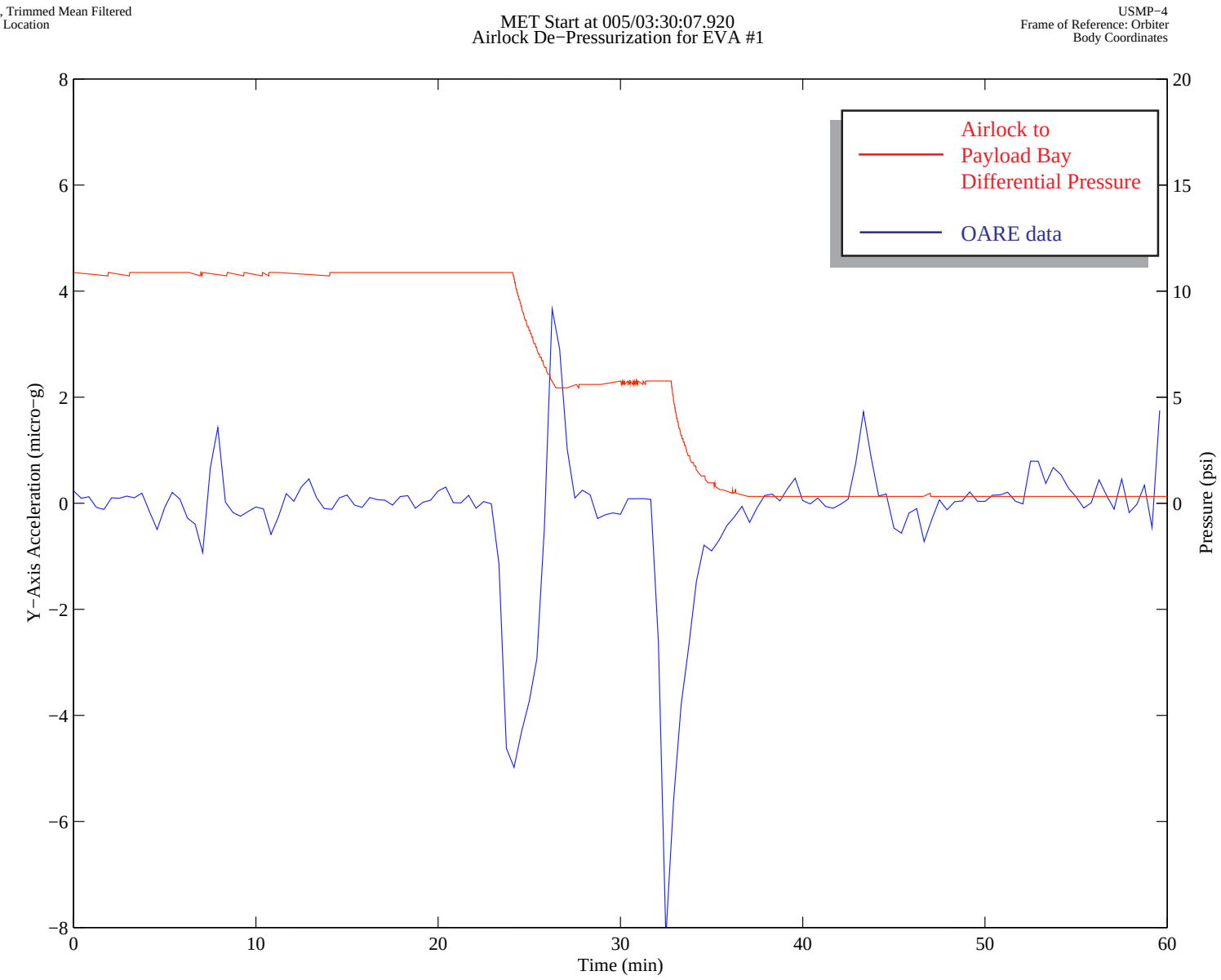

Figure 33. Airlock De-Pressurization for EVA #1 from STS-87.

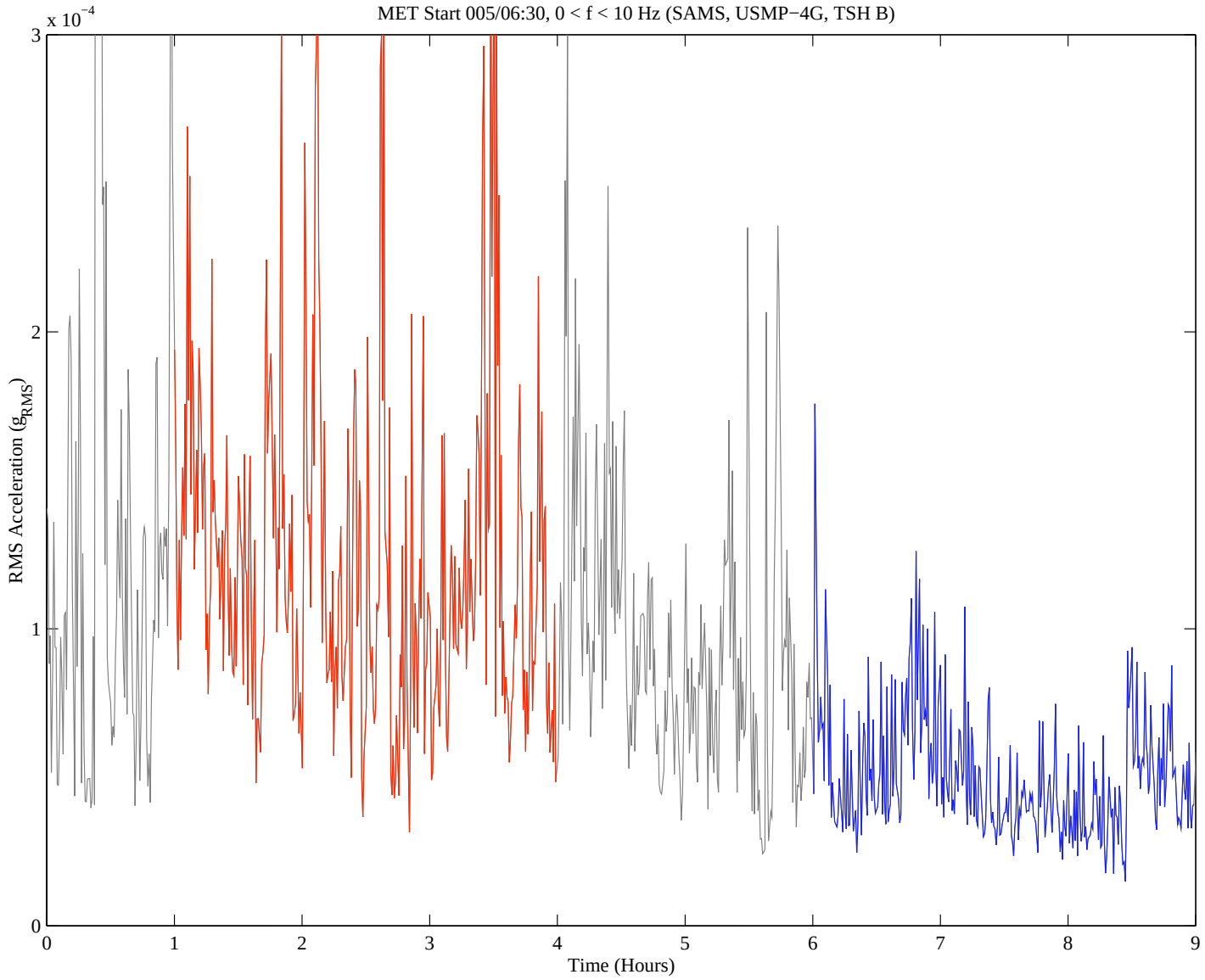

Figure 34. RMS Acceleration Versus Time During /After EVA #1.

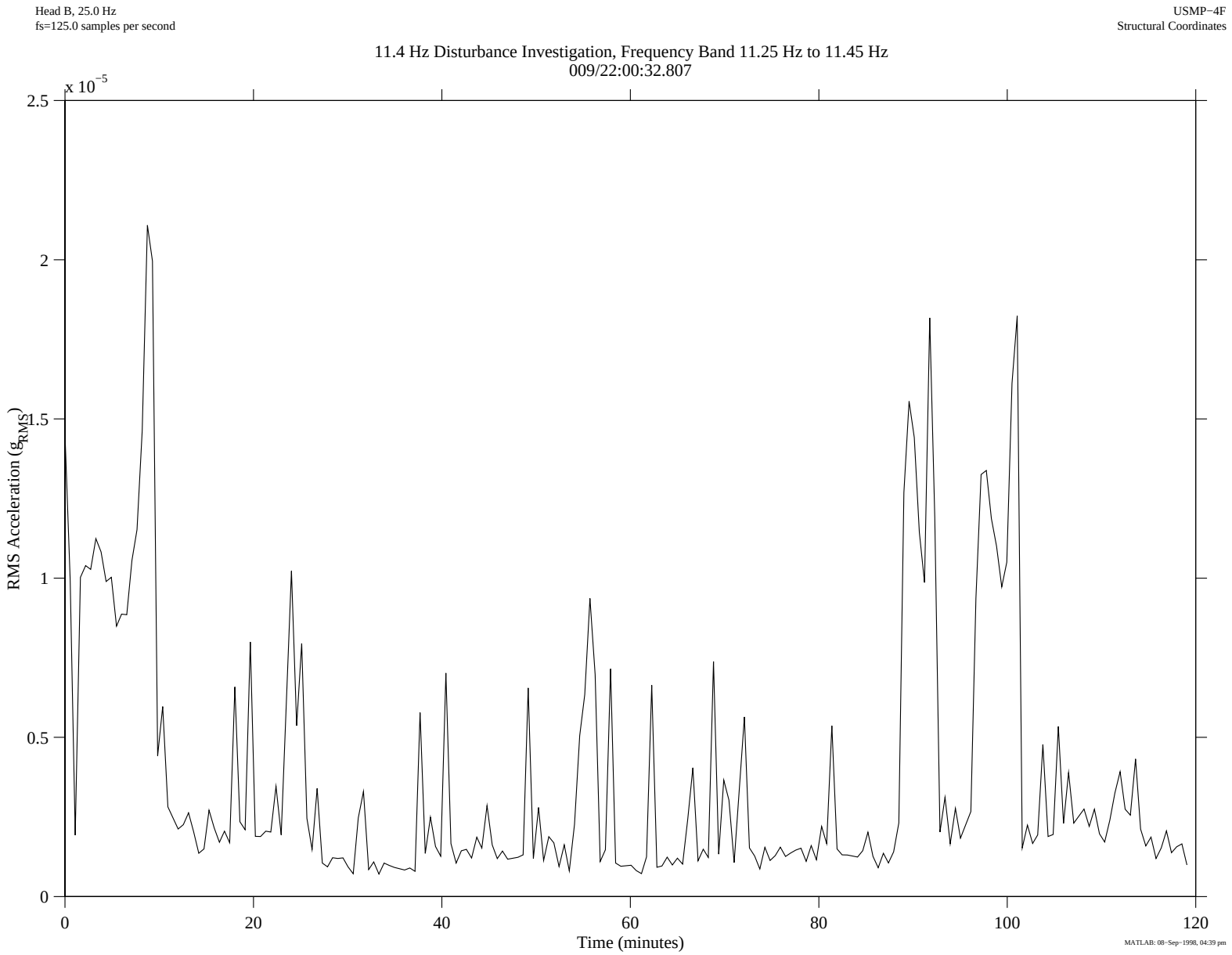

Figure 35. 11.35 Hz Disturbance Investigation, Frequency Band 11.25 Hz to 11.45 Hz.

Appendix A: Accessing Acceleration Data Via the Internet

SAMS and OARE data are available over the Internet from the NASA Lewis Research Center file server "beech.lerc.nasa.gov". Acceleration data files are arranged in a tree-like structure. Data are first separated based upon accelerometer and then by mission. For SAMS data files, the data are further subdivided based upon some portion of the mission, sensor head, year (for Mir data), day, and finally type of data file (acceleration, temperature, or gain). The following figure illustrates this structure.

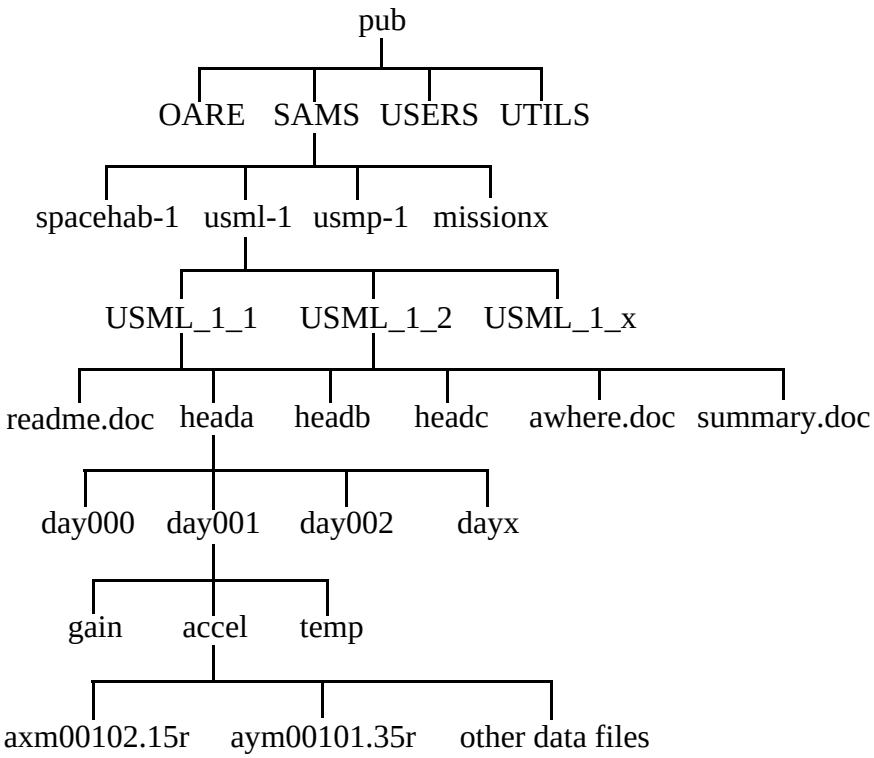

The SAMS data files (located at the bottom of the tree structure) are named based upon the contents of the file. For example, a file named "axm00102.15r" would contain TSH A data for the X-axis for day 001, hour 02, file 1 of 5. The readme.doc file gives a complete explanation of the file naming convention.

OARE data files also follow a tree-like structure, but with different branches. The data are first divided based upon mission, and then are divided by type of data. The OARE tree structure looks like this:

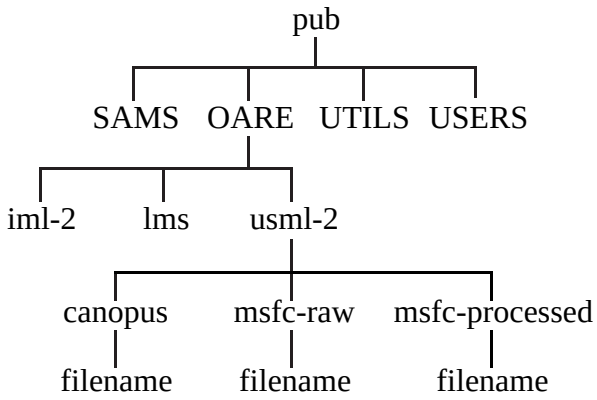

Files under the canopus directory are trimmean filter data, computed by Canopus Systems, Inc. Files under the msfc-raw directory contain the telemetry data files provided to PIMS by the Marshall Space Flight Center Payload Operations Control Center data reduction group. Files under the msfc-processed directory are raw files containing binary floating point values, listing the MET (in hours), and the x, y, and z axis acceleration in micro-g's. See the readme files under the canopus directory for complete data descriptions.

Data access tools for different computer platforms (MS-DOS, Macintosh, SunOS, and MS-Windows) are available in the /pub/UTILS directory.

The beech file server can be accessed via anonymous File Transfer Protocol (ftp), as follows:

1) Open a connection to "beech.lerc.nasa.gov"
2) Login as userid "anonymous"
3) Enter your e-mail address as the password
4) Change directory to pub
5) List the files and directories in the /pub directory
6) Change directory to the accelerometer of interest
7) Change directory to the mission of interest
8) Use the data file structures (described above) to locate the desired files
9) Enable binary file transfers
10) Transfer the desired files

If you encounter difficulty in accessing the data using the file server, send an electronic mail message to "pims@lerc.nasa.gov". Please describe the nature of the difficulty and also give a description of the hardware and software you are using to access the file server.

Appendix B: SAMS Color Spectrograms for Unit F, TSH B

The PIMS group has processed SAMS data from STS-87, Unit F, TSH B to produce the plots shown here. These data were collected at 125 samples per second, and a 25 Hz low pass filter was applied to the data by the SAMS unit prior to digitization. Prior to plot production, the raw SAMS data were compensated for gain changes, and then demeaned. Demeaning was accomplished by analyzing individual sections with a nominal length of 30 minutes. Users who are interested in further details for either of these operations are encouraged to contact the PIMS group.

Color spectrograms are used to show how the microgravity environment varies in intensity with respect to both the time and frequency domains. These spectrograms are provided as an overview of the frequency characteristics of the SAMS data during the mission. Each spectrogram is a composite of six hour's worth of data. The time resolution used to compute the spectrograms seen here is 16.4 seconds. This corresponds to a frequency resolution of 0.06 Hz.

In order to produce the spectrogram image, PSDs were computed for successive time intervals (the length of the interval is equal to the time resolution). For the PSD computation, a Hanning window was applied. In order to combine all three axes into a single plot to show an overall level, a vector magnitude (VM) operation was performed. Stated mathematically:

$$VM_k = \sqrt{PSD_{x_k}^2 + PSD_{y_k}^2 + PSD_{z_k}^2} .$$

By imaging the base 10 logarithm ($\log_{10}$) magnitude as a color and stacking successive PSDs from left to right, variations of PSD magnitude and frequency are shown as a function of time. Colors are assigned to discrete magnitude ranges, so that there are 207 colors assigned to the entire range of magnitudes shown.

The colorbar limits are chosen in order to minimize saturation in a given set of spectrogram plots. Data which fall outside of these limits will be imaged as either the highest or lowest magnitude, depending on which side they have saturated. If an area of interest seems to be saturated, care should be taken because the actual values may lie above or below the color mapping shown on the plot.

Due to the nature of spectrograms, care should be taken to not merely read a color's numeric value as being the "amount" of acceleration that is present at a given frequency. In order to get this type of information, the PSDs must be integrated between two frequencies. These frequencies (lower and upper) form the band of interest. The result of this integration is the g_{RMS} acceleration level in the $\left[f_{lower}, f_{upper}\right]$ band. The PIMS group is able to provide this type of analysis on a per-request basis.

Plot gaps (if any exist) are shown by either white or dark blue areas on the page. If a plot gap exists for an entire plot (or series of successive plots), a comment is placed on the page to let the user know there is a gap in the data. These "no data available" comments will not show exact times for which the data are not available, but will only indicate missing plots.

Appendix C: SAMS Color Spectrograms for Unit F, TSH A

The PIMS group has processed SAMS data from STS-87, Unit F, TSH A to produce the plots shown here. These data were collected at 50 samples per second, and a 10 Hz low pass filter was applied to the data by the SAMS unit prior to digitization. Prior to plot production, the raw SAMS data were compensated for gain changes, and then demeaned. Demeaning was accomplished by analyzing individual sections with a nominal length of 30 minutes. Users who are interested in further details for either of these operations are encouraged to contact the PIMS group.

Color spectrograms are used to show how the microgravity environment varies in intensity with respect to both the time and frequency domains. These spectrograms are provided as an overview of the frequency characteristics of the SAMS data during the mission. Each spectrogram is a composite of six hour's worth of data. The time resolution used to compute the spectrograms seen here is 40.96 seconds. This corresponds to a frequency resolution of 0.02 Hz.

In order to produce the spectrogram image, PSDs were computed for successive time intervals (the length of the interval is equal to the time resolution). For the PSD computation, a Hanning window was applied. In order to combine all three axes into a single plot to show an overall level, a vector magnitude (VM) operation was performed. Stated mathematically:

$$VM_k = \sqrt{PSD_{x_k}^2 + PSD_{y_k}^2 + PSD_{z_k}^2} .$$

By imaging the base 10 logarithm ($\log_{10}$) magnitude as a color and stacking successive PSDs from left to right, variations of PSD magnitude and frequency are shown as a function of time. Colors are assigned to discrete magnitude ranges, so that there are 207 colors assigned to the entire range of magnitudes shown.

The colorbar limits are chosen in order to minimize saturation in a given set of spectrogram plots. Data which fall outside of these limits will be imaged as either the highest or lowest magnitude, depending on which side they have saturated. If an area of interest seems to be saturated, care should be taken because the actual values may lie above or below the color mapping shown on the plot.

Due to the nature of spectrograms, care should be taken to not merely read a color's numeric value as being the "amount" of acceleration that is present at a given frequency. In order to get this type of information, the PSDs must be integrated between two frequencies. These frequencies (lower and upper) form the band of interest. The result of this integration is the g_{RMS} acceleration level in the $\left[f_{lower}, f_{upper}\right]$ band. The PIMS group is able to provide this type of analysis on a per-request basis.

Plot gaps (if any exist) are shown by either white or dark blue areas on the page. If a plot gap exists for an entire plot (or series of successive plots), a comment is placed on the page to let the user know there is a gap in the data. These "no data available" comments will not show exact times for which the data are not available, but will only indicate missing plots.

Appendix D: SAMS Color Spectrograms for Unit G, TSH B

The PIMS group has processed SAMS data from STS-87, Unit G, TSH B to produce the plots shown here. These data were collected at 250 samples per second, and a 100 Hz low pass filter was applied to the data by the SAMS unit prior to digitization. Prior to plot production, the raw SAMS data were compensated for gain changes, and then demeaned. Demeaning was accomplished by analyzing individual sections with a nominal length of 30 minutes. Users who are interested in further details for either of these operations are encouraged to contact the PIMS group.

Color spectrograms are used to show how the microgravity environment varies in intensity with respect to both the time and frequency domains. These spectrograms are provided as an overview of the frequency characteristics of the SAMS data during the mission. Each spectrogram is a composite of six hour's worth of data. The time resolution used to compute the spectrograms seen here is 16.4 seconds. This corresponds to a frequency resolution of 0.06 Hz.

In order to produce the spectrogram image, PSDs were computed for successive time intervals (the length of the interval is equal to the time resolution). For the PSD computation, a Hanning window was applied. In order to combine all three axes into a single plot to show an overall level, a vector magnitude (VM) operation was performed. Stated mathematically:

$$VM_k = \sqrt{PSD_{x_k}^2 + PSD_{y_k}^2 + PSD_{z_k}^2} .$$

By imaging the base 10 logarithm ($\log_{10}$) magnitude as a color and stacking successive PSDs from left to right, variations of PSD magnitude and frequency are shown as a function of time. Colors are assigned to discrete magnitude ranges, so that there are 207 colors assigned to the entire range of magnitudes shown.

The colorbar limits are chosen in order to minimize saturation in a given set of spectrogram plots. Data which fall outside of these limits will be imaged as either the highest or lowest magnitude, depending on which side they have saturated. If an area of interest seems to be saturated, care should be taken because the actual values may lie above or below the color mapping shown on the plot.

Due to the nature of spectrograms, care should be taken to not merely read a color's numeric value as being the "amount" of acceleration that is present at a given frequency. In order to get this type of information, the PSDs must be integrated between two frequencies. These frequencies (lower and upper) form the band of interest. The result of this integration is the g_{RMS} acceleration level in the $\left[f_{lower}, f_{upper}\right]$ band. The PIMS group is able to provide this type of analysis on a per-request basis.

Plot gaps (if any exist) are shown by either white or dark blue areas on the page. If a plot gap exists for an entire plot (or series of successive plots), a comment is placed on the page to let the user know there is a gap in the data. These "no data available" comments will not show exact times for which the data are not available, but will only indicate missing plots.

Appendix E: SAMS Color Spectrograms for Unit G, TSH A

The PIMS group has processed SAMS data from STS-87, Unit G, TSH A to produce the plots shown here. These data were collected at 50 samples per second, and a 5 Hz low pass filter was applied to the data by the SAMS unit prior to digitization. Prior to plot production, the raw SAMS data were compensated for gain changes, and then demeaned. Demeaning was accomplished by analyzing individual sections with a nominal length of 30 minutes. Users who are interested in further details for either of these operations are encouraged to contact the PIMS group.

Color spectrograms are used to show how the microgravity environment varies in intensity with respect to both the time and frequency domains. These spectrograms are provided as an overview of the frequency characteristics of the SAMS data during the mission. Each spectrogram is a composite of six hour's worth of data. The time resolution used to compute the spectrograms seen here is 40.96 seconds. This corresponds to a frequency resolution of 0.02 Hz.

In order to produce the spectrogram image, PSDs were computed for successive time intervals (the length of the interval is equal to the time resolution). For the PSD computation, a Hanning window was applied. In order to combine all three axes into a single plot to show an overall level, a vector magnitude (VM) operation was performed. Stated mathematically:

$$VM_k = \sqrt{PSD_{x_k}^2 + PSD_{y_k}^2 + PSD_{z_k}^2} .$$

By imaging the base 10 logarithm ($\log_{10}$) magnitude as a color and stacking successive PSDs from left to right, variations of PSD magnitude and frequency are shown as a function of time. Colors are assigned to discrete magnitude ranges, so that there are 207 colors assigned to the entire range of magnitudes shown.

The colorbar limits are chosen in order to minimize saturation in a given set of spectrogram plots. Data which fall outside of these limits will be imaged as either the highest or lowest magnitude, depending on which side they have saturated. If an area of interest seems to be saturated, care should be taken because the actual values may lie above or below the color mapping shown on the plot.

Due to the nature of spectrograms, care should be taken to not merely read a color's numeric value as being the "amount" of acceleration that is present at a given frequency. In order to get this type of information, the PSDs must be integrated between two frequencies. These frequencies (lower and upper) form the band of interest. The result of this integration is the g_{RMS} acceleration level in the $\left[f_{lower}, f_{upper}\right]$ band. The PIMS group is able to provide this type of analysis on a per-request basis.

Plot gaps (if any exist) are shown by either white or dark blue areas on the page. If a plot gap exists for an entire plot (or series of successive plots), a comment is placed on the page to let the user know there is a gap in the data. These "no data available" comments will not show exact times for which the data are not available, but will only indicate missing plots.

Appendix F: PIMS USMP-4 Logbook

During the STS-87 mission, members of the PIMS team monitored mission events using voice communication loops and video downlink. Items that were of interest because of the potential impact on the microgravity environment were recorded in the PIMS logbook. An electronic copy of the logbook is included in the CD-ROM version of this report.

Appendix G: User Comments Sheet

We would like you to give us some feedback so that we may improve the Mission Summary Reports. Please answer the following questions and give us your comments.

1. Do the Mission Summary Reports fulfill your requirements for acceleration and mission information?
_____Yes _____No If not why not?

Comments:

_____

_____

2. Is there additional information which you feel should be included in the Mission Summary Reports?
_____Yes _____No If so what is it?

Comments:

_____

_____

3. Is there information in these reports which you feel is not necessary or useful?

_____Yes _____No If so, what is it?

Comments:

_____

_____

4. Do you have internet access via: (____)ftp (____)WWW (____)gopher (____)other? Have you already accessed SAMS data or information electronically?

_____Yes _____No

Comments:

_____

_____

Completed by: Name:_____ Telephone_____

Address:_____ Facsimile_____

_____ E-mail addr_____

Return this sheet to:
PIMS Project Manager
NASA Lewis Research Center
21000 Brookpark Road MS 500-216
Cleveland, OH 44135

or
FAX to PIMS Project: 216-433-8660
e-mail to: pims@lerc.nasa.gov.

Appendix H: Contents of CD-ROM

Format

Supplementary Spectrogram Folder

Adobe Acrobat Reader Files

- Macintosh 3.01 Installer
- Windows 3.0 / 3.1.exe
- Sun Solaris 3.0 / 3.1.tar.gz
- Silicon Graphics 3.0.tar.gz

README.DOC